Comparing different methods of measuring particle size for pharmaceutical excipients

Jiawen Wang

Master thesis in Pharmaceutical Technology - KLGM05

LUND UNIVERSITY

Supervisor: Kyrre Thalberg
Examiner: Marie Wahlgren

Department of Food Technology Engineering and Nutrition
Faculty of Engineering, LTH
Lund University
Sweden

Acknowledgements

My master's life will come to an end as time flies like an arrow. It began in the pandemic autumn of 2020 and ended in the enthusiastic midsummer of 2022. It has been a short journey for the previous two years, but I have eventually found what I want to devote to this area in the future. The topic of the thesis work is a crucial chance for me, therefore I would like to convey my sincere appreciation to everyone who helped and supported me during the diploma work.

First and foremost, I am deeply indebted to my supervisor, Kyrre Thalberg, who has led me with his constant encouragement and patience through the entire process of selecting a thesis topic, conducting experiments, and producing the final report. During the past six months, he has spent much time teaching me how to conduct meticulous research and provided me with inspiring advice in scientific studies, assisting me in becoming a good researcher and presenting the thesis in the best possible way, as well as making me more rigorous, sedate, and tenacious in the future when faced with challenges.

I would also like to express my gratitude to Hans Bolinsson, who gave me every demo of applied instruments and helped me with technological issues. Without his consistent and illuminating instruction, the thesis would not have reached its present form. I also want to give my heartfelt thanks to my examiner, Marie Wahlgren, who was always concerned about the progress of my thesis, and whose smile always brightened my mood.

Above all, I want to express my gratitude to my family, who have watched me grow from a swaddled newborn to the present day, teaching me integrity, sincerity in dealing with people, and giving steadfast support for my studies all the time. Last but not least, I need to thank my boyfriend, Chunyu Zhang, who held my umbrella in the wind and rain, drove me to school and picked me up, and remained up late with me as I wrote my paper. With him, I aspire to run to a brighter future.

Goodbye, dear teachers in the department!
Goodbye, close friends in Lund!
Best wishes to all of you, see you around.

Abstract

In pharmaceutical science, particle size is one of the most fundamental parameters of materials, but different particle-sizing analysis methods lack a uniform standard for measuring irregular particle size, making it difficult to compare the accuracy and applicability of different particle-sizing analysis methods. Experiments on excipients used in pharmaceuticals are carried out in this paper by laser diffraction analysis (Malvern wet and dry), dynamic image analysis (Qicpic), and microscopic methods (Qicpic, SEM, and light microscopy) to determine the applicability and limitations of each method, as well as to clarify their advantages and disadvantages.

On the one hand, the shape of the excipients is determined using the 2D and 3D images acquired from Qicpic and SEM; sphericity, aspect ratio, D50, and D90 are employed as indicators to assess the accuracy and adaptability of Qicpic and Malvern analyses based on different testing principles. On the other hand, D10, D50, D90, percentage of fine particles, weighted residues are used in the Malvern methods to evaluate the difference between Malvern dry and wet applied to pure excipients and blend powders, as well as their stability with particle size distribution curves. Furthermore, while doing a wet analysis on lactose carriers, the effect of ultrasonication speed on particle size distribution and the accuracy of the Malvern wet analysis using the Fraunhofer or Mie theories, need to be considered. In addition, light microscopy was used to examine particle behavior during sonication. Finally, the particle size analysis methods are categorized for different sizes of particles and different shapes of particles.

Table of contents

1. Introduction

1.1 Aim

The aim of the study is to evaluate different methods to determine particle size and its distributions of pharmaceutical original excipients and mixtures by investigating d10, d50, d90 values, the span and the shape information. The advantages and disadvantages of the different particle-sizing methods are elucidated as well.

1.2 Objectives

Five grades of lactoses, three grades of cellets, one cellulose microcrystalline and three grades of sodium bicarbonate are selected to measure particle size using Malvern Mastersizer, wet measurement as well as dry measurement, Sympatec Qicpic, Scanning Electron Microscope (SEM) and light microscope. Among them, lactoses containing coarse and fine are always applied in inhalation products to alter the flow property of dry powders; cellets and cellulose microcrystalline are soluble in water, and are often used as a tablet filler or disintegrant to increase the release rate of the drug; sodium bicarbonate is commonly acted as a source of carbon dioxide for effervescent tablets and to maintain pH in pharmaceutical formulations. 5 blends of dry powder consisting of different sizes of particles are produced by the Turbula mixer. These blended powders are analyzed by the same methodology to evaluate the particle size of mixed dry powders. Overall, the results from different analytical methods are compared for pure excipients and blends.

1.3 Expected result

Some materials with easy structure/shape should give a good correlation of results between different methods, while others may be challenging to measure, such as very fine powders. Determining particle size is critical, which could ultimately impact the physical performance of the formulation and final drug product as well as the subsequent pharmacological effects of the drug. Through different methods of measuring the particle size for different excipients and mixtures, recommendations about methods of different samples can be derived based on these results.

2. Theory: the principle of each method

2.1 The introduction of particle size

Powders with different particle sizes have different physico-chemical properties, such as bioavailability, dissolution rate, in vivo deposition rate, physicochemical stability, flow properties, etc. Particle size is therefore a key factor for achieving optimal formulation and manufacturing safe and effective medicines.

Particle size includes two aspects, one is dimension of the single particle and the other is particle size distribution. In pharmaceutical systems, particles are almost rarely homogeneous spheres. They not only have irregular shapes but also different surface roughness, which leads to different densities, electrical conductivity or refractive index. In order to compare particles with complex shapes more easily, the equivalent diameter is constructed as the diameter of a sphere with the same volume of the particle, and there are other useful diameters for 2D measurement such as the perimeter diameter and projected area diameter as shown in **Figure 1**. Therefore, depending on the different equivalent methods, one particle might have several equivalent diameters. That's the reason why obtained results from different particle size analysis methods are different. (Shekunov et al., 2007)

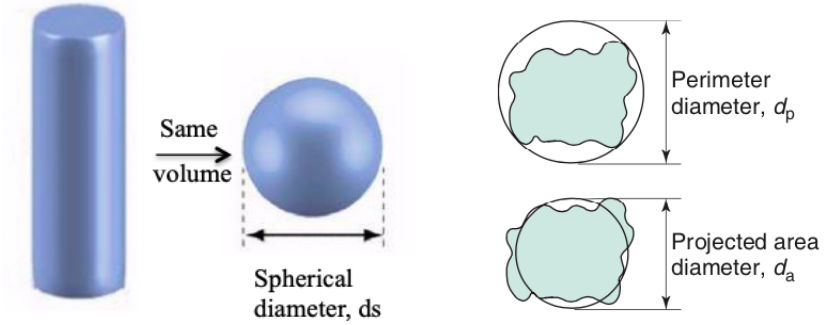

Figure 1. Different constructed diameters used for comparison of the particle size (Shekunov et al., 2007)

Particle size distribution (PSD) represents the distribution of groups of different particle sizes in the powder, and reflects the polydispersity of particle size. In pharmaceutical science, most particle populations are polydisperse or heterodisperse, and the frequency distribution curve of particle size is illustrated by a histogram. Distribution curves can be divided into symmetrical normal or log-normal distribution, asymmetric positive or negatively skewed distribution, and multimodal distribution according to the percentage of different size fractions.

Usually, the three measurement points on the distribution curve and the span are used to characterize the powder. The three-points refer to the particle size when the cumulative distribution of particles is 10%, 50% and 90%, and its values can be written as D10, D50, D90 respectively. Span is used to represent the width of dispersion of particle distribution, whose calculation equation is shown below. The smaller the value is, the smaller the degree of broadness is, indicating that the particle size distribution is more narrow. (Merkus, 2009)

$$\text{Span} = \frac{D90 - D10}{D50}$$

It should be noted that average particle sizes can be based either on the number, or the surface area, or volume(mass) of the particles. The former is the arithmetic mean diameter that can be obtained by dividing one particle with a specific parameter by the total number of particles. The two latter are the critical mean particle diameters in the laser diffraction method, denoted as D[3,2] and D[4,3], respectively. (Shekunov et al., 2007) The equations are as follows:

$$D[3,2] = \frac{\Sigma d^3}{\Sigma d^2}$$

$$D[4,3] = \frac{\Sigma d^4}{\Sigma d^3}$$

Different kinds of methods are performed in size analysis, such as sieve methods, sedimentation methods, microscope methods, electrozone sensing methods, laser diffraction methods and dynamic light scattering methods. Among them, microscope methods can be divided into light microscopy, scanning electron microscope (SEM) and transmission electron microscope. Light microscopy, SEM and laser diffraction are applied to measure selected pure samples and blends in this report and principles of these analytical methods for particle size will be explained in detail in the following part.

2.2 Particle size in pharmaceutical industry and product performance

In the pharmaceutical industry, drug particles ranging from nanometers to millimeters can exist in the form of dry powders, semisolid dispersions and suspended in liquids. Different particle size ranges will make different dosage forms and routes of administration achieve desired properties to affect its efficiency and safety.

2.2.1 Respiratory Drug Delivery

Respiratory Drug Delivery is to make drugs and excipients into aerosol particles, which are inhaled into the mouth (or nasal cavity) through the device, and gradually settle into the bronchi and alveoli to achieve the effect of targeted therapy. Only a small drug dose is required, because the drug reaches the target to the maximum extent and exerts the drug effect directly, which minimizes the deposition of the drug in other tissues and reduces the side effects (Shekunov et al., 2007). The properties of inhaled drugs mainly depend on the shape of the particles, the particle size distribution (PSD) and the dispersion properties of the powder. Particles with elongated shapes result in lower particle clearance rate. (Shekunov, 2005) Different particle sizes of inhaled drugs will cause different deposition patterns, for example the coarse ones will fall on the mucosal surface of the respiratory tract, and the fine ones may reach the bronchioles and alveoli. In general, particles with a mass median aerodynamic diameter (MMAD) of 1-5μm can be deposited in the bronchial and alveolar regions. (Crowder et al., 2002)

In inhaled drugs, PSD determines particle-particle interactions, inhaled dose and quality uniformity, while higher fine particle fraction (FPF) increases dissolution rate and bioavailability (Edwards et al., 1997). More recent attention in the public has focused on formulations for dry powder inhalers (DPI) (**Figure 2**), which are usually mixed with a drug and a lactose carrier, stored in capsules, blisters or small powder reservoirs. It has become the most common type of inhaler in the market due to its high inhalation efficiency, high drug loading capacity, low amounts of excipients, no propellant, good stability, and easy-to-use.

Small amounts of fine lactose are known to improve the dry powder delivery to the lungs. They can saturate the high-energy sites (such as bumps or crevices) on the surface of the carrier and/or increases the adhesion of the formulations and the corresponding fluidization energy and may also form aggregates with the drug particles that are easier to separate from the carrier during the inhalation, improving the dispersibility of the inhaled drug powder (Shur et al., 2008).

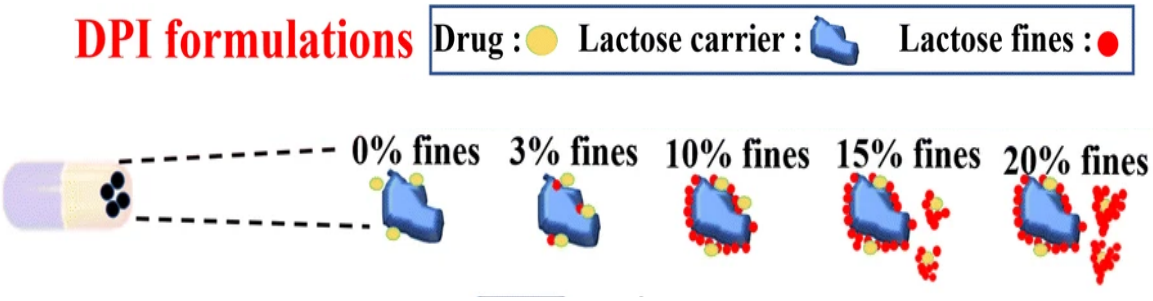

Figure 2. DPI formulations consist of drug, lactose carrier and different percentages of fine lactose (Sun et al., 2021)

2.2.2 Oral dosage forms

Previous research showed that drug particle size has a significant effect on drug dissolution and bioavailability. Nanosized active substances or excipients can improve the suspension uniformity of the powder to increase the delivery efficiency and the absorption rate in vivo. For water-insoluble drugs, when the particle size is reduced from 1000 nm to 400 nm, the oral bioavailability of the drug will be increased by 2.5 times. (Rabinow, 2004)

Tablets are solid preparations that are compressed after mixing drugs and excipients, which is an important part of oral dosage forms. As usual, tablets with excipients of a particle size of 20-50 μm are chewable or fast-disintegrating tablets, and excipients with a size around 100-200 μm are used for direct compressed ordinary tablets. The particle size and PSD of the drug and excipients will determine the compaction behavior and powder flow properties of the tablet. Smaller particle size, larger specific surface area and irregular particles have better compression formability because particles with these properties facilitate the reduction in the volume of the powder during the compaction process and the tight bonding between the particles, thereby increasing the bonding area and bonding strength of the powder and making the particles easier to compress and form. However, small particle size and irregular particles will also increase the friction and adhesion, reduce the fluidity between particles, and thus affect the quality of the tablet. (Chaudhary et al., 2018)

2.2.3 Ophthalmic drug delivery

Ophthalmic drug delivery is directly used in the eye to play a local therapeutic role or to be transferred into the systemic circulation through the eye to play a systemic therapeutic role. The particle size of ophthalmic drugs mainly affects the bioavailability of the drug, as well as the comfort and convenience of patients. Liposomes are a kind of carrier of the ocular drug made of phospholipid bilayers, which have high penetrability with biological membranes. The particle size of the prepared liposome ophthalmic drug is usually between 0.02 and 0.20 μm, and there is no foreign body sensation with high trans-corneal transport efficiency when instilled into the eye. (Ebrahim et al., 2005) Microparticles and nanoparticles are two other ophthalmic drug carriers with particle sizes in the micrometer and nanoscale ranges, respectively. Their drug delivery mechanism is different from liposomes, which cannot fuse with cells and penetrate the cornea, but the ingestion or phagocytosis of the particles completes the drug release. Nanoparticles (diameter < 1μm) mostly use bioadhesive and biodegradable polymers. Microparticles (diameter 1-10μm) can encapsulate the drug into polymer particles to form a suspension achieving sustained or controlled release, but particles larger than 25μm will cause eye discomfort and eye irritation as well as reduced tolerance. Therefore, an ocular dosage form with suitable particle size should be developed, which will have a certain sustained release effect, longer ocular retention time and lower irritation. (Kompella et al., 2010)

2.2.4 Transdermal drug delivery

Transdermal drug delivery refers to drug administration on the surface of the skin, where the drug penetrates all layers of the skin at a certain speed, and enters the human body's systemic blood circulation from capillaries to reach an effective blood drug concentration to achieve systemic or local therapeutic effects. (Shekunov et al., 2007) The drug with small particle size has a high enrichment, which is beneficial to the percutaneous penetration of the drug. However, due to the dense brick and mortar model of skin (**Figure 3**), the particle size of drugs will affect the skin penetration pathway (Prow et al., 2011). For example, particles larger than 10 μm are difficult to pass through the stratum corneum by passive diffusion into the deep layers of the skin, and can only stay on the surface of skin; particles between 3-10 μm can be enriched in the hair follicles of the skin; particles smaller than 3 μm can penetrate the hair follicle and stratum corneum, but due to their small particle size, quite small drug loading, they cannot achieve therapeutic levels of the drug (Rolland, 1993).Transdermally absorbed nanoparticles can penetrate into the deep skin tissue from the porous pathways of

the skin as their particle size decreases. When the amount of drugs penetrated into the skin increases, the therapeutic level of the drug should also be affected or improved. (Williams, 2003)

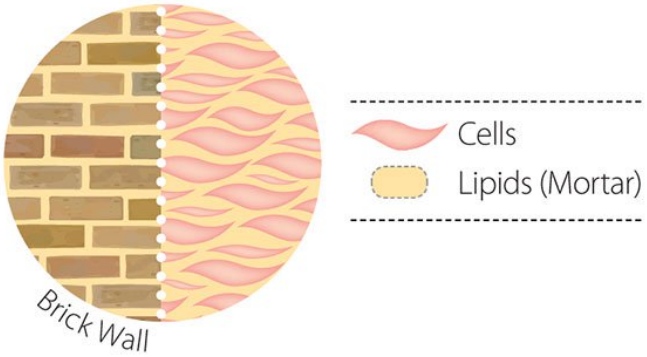

Figure 3. "Brick and mortar" model of the stratum corneum as the skin barrier ("The Miracle of the Skins Lipid Layer!," 2019)

2.2.5 Injection drug delivery

Injections are clear and transparent sterile liquid preparations made of active substances and excipients for injection into the body, including solutions, emulsions or suspensions, which can be used for subcutaneous injection, intradermal injection, intramuscular injection, intravenous injection, etc. The particle size in the reconstituted infusion solution is usually less than 2 μm. When it is mixed with visible particulate impurities or invisible insoluble substances, these substances will flow with the blood but cannot be metabolized and then cause allergic reactions, vascular embolism, arteriosclerosis and other adverse reactions that are harmful to the human body. In the process of preparing the solution of injections, a liquid filter with a suitable aperture should be used to retain bacteria and particles as well as eliminate air bubbles in the liquid, so that the particle size of the injection can be controlled to achieve the purpose of safe infusion. (Hung, 2002)

2.3 Particle sizing using laser diffraction

Laser diffraction can be used to measure the particle size distribution of dry powder, which is also a good way to measure equivalent sphere diameters for irregularly shaped particles. The Fourier lens focuses the scattered light emitted by the He-Ne laser with a wavelength of around 633 nm into a single parallel light with a diameter of about 8 mm. Particles at the proper concentration in liquid deflect the monochromatic light to cause diffraction in different angles. The angle of diffracted light is inversely proportional to the particle diameter, and its light intensity decays logarithmically with the increase of the angle. After passing a Fourier lens, the scattered light hits multiple detectors arranged on the focal plane (**Figure 4**). The particle size distribution will be calculated through different intensity of the scattering light. (Shekunov et al., 2007)

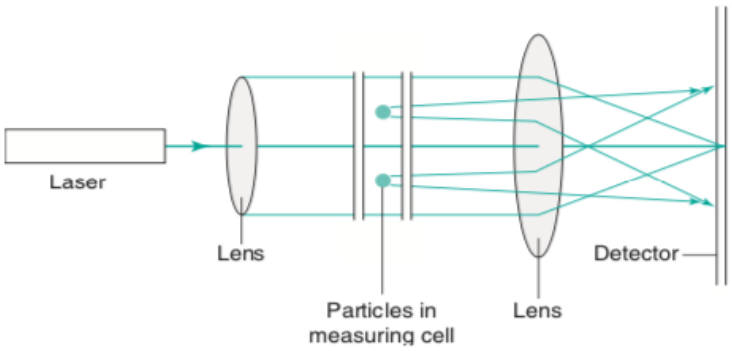

Figure 4. The principle of laser diffraction for particle sizer (Shekunov et al., 2007)

Prior research has applied Fraunhofer diffraction and Mie theory into the light scattering for particle size. In the Fraunhofer diffraction theory, the measured results are only affected by the particle size; it is assumed that the particles are not light-transmitting and therefore the effect of the dispersion medium is

not considered. When the particle size is much larger than the wavelength of the light, the light undergoes forward diffraction and is subjected to light and dark light intensity patterns that appear at certain angular intervals. (**Figure 5**) In the Mie theory, the effect of the refractive index of the dispersion medium is considered as well. When the particle size is close to the wavelength of light, part of the light will undergo forward diffraction, and the other part will undergo directional diffraction under the polarization of different wavelengths. Therefore, it is necessary to take into account the characteristics of the dispersion medium, and Mie theory will predict more accurately the size of the smaller particles and their distribution.

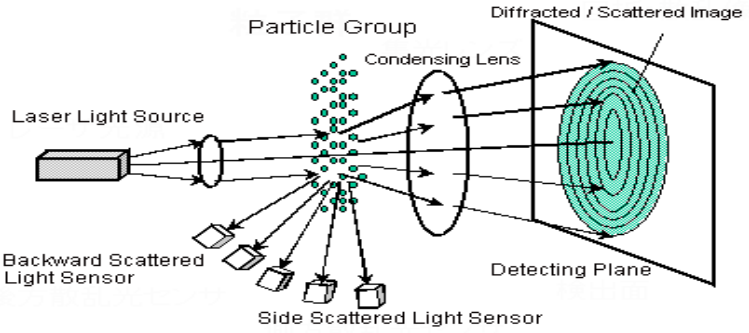

Figure 5. The Schematic of laser diffraction method forming Fraunhofer patterns ("Particle Size Distribution Calculation Method," 2022)

2.4 Particle sizing using microscope methods

Different microscope methods are suitable for different ranges when particle sizing shown in **Figure 6**. Among them, a light microscope and scanning electron microscope are applied to measure particle size in this report, and are explained in detail below.

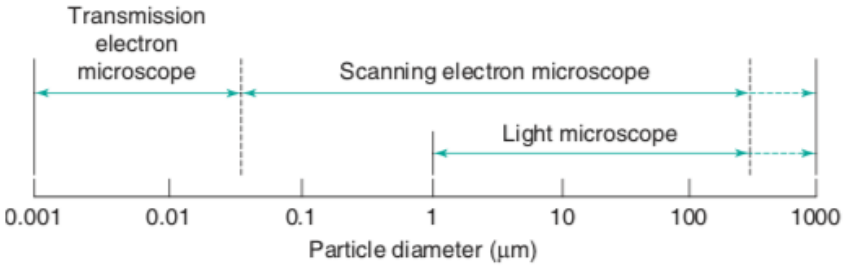

Figure 6. Different ranges of particle size analysis (Shekunov et al., 2007)

2.4.1 Light microscopy

Light microscopy enables simple and fast characterization of 2D images of particles. The principle of measurement is to use a point light source with high luminous efficiency to emit a certain wavelength of light through the color filter system as the excitation light. Then according to the principle of convex lens magnification and imaging, the tiny objects are magnified to the size that the human eye can distinguish: the convex lens of the objective lens forms an enlarged inverted real image, and then an enlarged virtual image is formed through the eyepiece. A lower-resolution image of the sample or blurred image is given by the light microscopy due to the scattered refracted light.

2.4.2 Scanning Electron Microscope

Scanning electron microscope (SEM) is used to check the surface morphology, shape and aggregation of the drug powder with high magnification, greater depth field and three-dimensional imaging. According to its scale, the average particle size of the drug powder can also be measured. The working principle is that the electron beam with a diameter of 20 nm-30 nm emitted from the anode of the electron gun is accelerated by the condenser lens as well as the objective lens and then focused on the surface of the sample. Under the excitation of the electron beam, the sample will emit a series of signals that reflect the information of the sample, such as backscattered

electrons, Auger electrons, X-rays and secondary electrons with lower energy. Due to the lower energy of the secondary electrons, most of the secondary electrons will be reabsorbed by the sample, and only the secondary electrons emitted from the surface have the opportunity to escape. Under the action of the scanning coil on the end lens, the electron beam raster scans from the upper left to the lower right of the sample surface, so that the excited secondary electrons can accurately image the surface topography of the sample.

In addition, elemental analysis can be performed in SEM by using energy dispersive spectroscopy (EDS). When the electron hits the sample, the inner layer electrons are excited to a higher energy level. At this time, the electrons in the outer orbit fill the inner layer vacancies and the excess energy is released in the form of X-rays. While electrons fill the vacancies in the inner layer based on the selection rules, the X-rays released by different elements have specific energies, and the content of different elements can be analyzed by analyzing the intensities of X-rays with different energies. (Williams et al., 1996)

2.5 Particle sizing using optical imaging

Qicpic is an instrument for direct dynamic image analysis of particle size and particle shape testing numerous fast-moving particles, whose testing principle is based on the optical imaging, as shown in **Figure 7.** When measuring, the pulsed light emitted from the high-frequency pulsed light source passes through the beam expander to form parallel pulsed light, and then the pulsed light in the test area is irradiated on the dispersed single particles. Through an optical imaging system, a clear image of each particle in an orthogonal orientation to the projection direction is obtained. After a number of image data obtained from the detection is processed by computer, it can not only give a close-up image of a single particle, but also get the particle shape characteristic information and particle size distribution of all particle groups after statistics. (Yu et al., 2008)

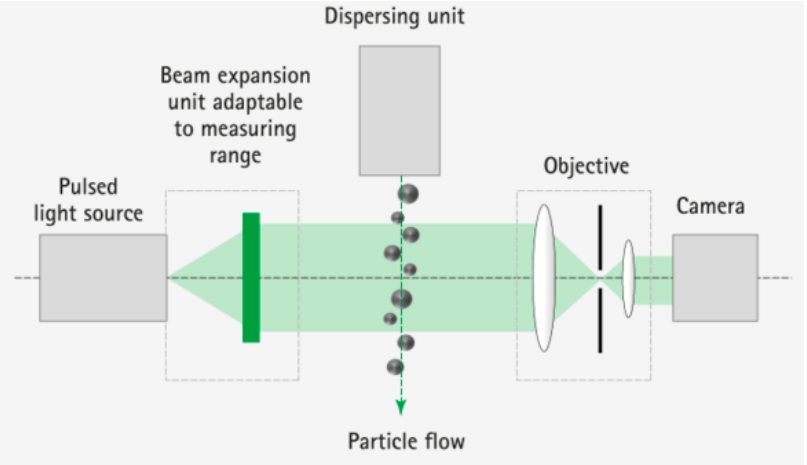

Figure 7. Schematic of the Qicpic measurement system (https://www.sympatec.com/en/particle-measurement/sensors/dynamic-image-analysis/)

3. Material & method

3.1 Materials

The specifications of materials from the supplier websites are shown in **Table 1** and full names and abbreviations of all materials are shown in **Table 2.**

Table 1. Specifications of all selected materials

Material	Product name	Supplier	Batch number	Particle Size Distribution		
				D10(μm)	D50(μm)	D90(μm)
Lactose	Lactohale 100	DFE	107CH5G	45-65	125-145	200-250
Lactose	Lactohale 300	DFE	1083C67	-	≦5	≦10
Lactose	Respitose SV001	DFE	105282C	120-160	210-250	290-350
Lactose	Respitose SV003	DFE	105SX25	19-43	53-66	75-106
Lactose	InhaLac 500	Meggle	L104424500137426A990	-	≦5	≦10
Cellets*	Cellets 100	Harke	20F1036	85% within 100-200		
Cellets	Cellets 200	Harke	18N1033	85% within 200-355		
Cellets	Cellets 350	Harke	29C1017	85% within 350-500		
Cellulose Microcrystalline	Cellulose Microcrystalline for Column Chromatography	Merck KGaA	K44173131	＜20		
Sodium Bicarbonate	Fine Sodium Bicarbonate	Brunner Mond & Company	-	median size around 140		
Sodium Bicarbonate	Standard Sodium Bicarbonate	Brunner Mond & Company	-	median size around 105		
Sodium Bicarbonate	Ultra Coarse Sodium Bicarbonate	Brunner Mond & Company	-	median size around 285		

* Cellets are microcrystalline cellulose pellets.

Table 2. The full names and corresponding abbreviations of products.

Full name of products	Abbreviation
Lactose Lactohale 100	LH100
Lactose Lactohale 300	LH300
LH300 with sonication and Span20	LH300-Span20
LH300 with sonication and double Span20	LH300-dSpan20
Lactose InhaLac 500	Inhalac500
Inhalac500 with sonication and Span20	Inhalac500-Span20
Inhalac500 with sonication and double Span20	Inhalac500-dSpan20
Lactose Respitose SV001	SV001
Lactose Respitose SV003	SV003
Fine Sodium Bicarbonate	SBF

Full name of products	Abbreviation
Standard Sodium Bicarbonate	SBS
Ultra Coarse Sodium Bicarbonate	SBC
Cellulose Microcrystalline	CM
Cellets 100	C100
Cellets 200	C200
Cellets 350	C350
95% LH100+5% Inhalac500	LI
95% SV003+5% Inhalac500	SI
50% C350+50% C100	CSCB
50% CM+50% C200	CMMCC

3.2 Manufacture:

3.2.1 Ultrasonication

a) Instrument

Branson Sonifier B-12 Ultrasonic Tip

b) Method

The lamp oil was added to the half volume of the plastic tube. If Span20 was used, it was applied to the inner wall of the tube with a dropper and shaked for 30s, then an amount of sample was poured and shaked for 30s.The prepared sample was ice-bathed in the beaker, followed by inserting the ultrasonic tip close to the bottom of the tube and making sure it does not touch the inner wall. Finally the powder was pressed with “on”, the output control was applied to more than setting 7 for 2 minutes of sonication.

3.2.2 Blending

a) Instrument

Turbula 3D mixer T2C, 0.710 mm mesh sieve and analytical balance

b) Method

Half of the first excipient, all of the second excipient and the rest of the first excipient were poured into a large glass jar in turn. Then all of the powders were mixed in the blender for 10 min. When finished, they were sieved through a 0.710 mm mesh sieve. The obtained powder was transferred to a small bottle and mixed again for 10 min. By comparing the state of mixed dry powder with naked eyes, the quality of the powder could be preliminarily judged.

3.3 Analytical method

3.3.1 Malvern wet analysis

a) Instrument

Malvern Mastersizer 2000 for wet analysis

b) Method

The small volume sample lamp oil dispersion unit was connected to the instrument, while the dispersion unit controller was adjusted at around 2000 rpm to remove air and bubbles.

The “measure” was selected in the software menu bar, and then following parameter were set under ”manual”: In the “option”, material properties corresponding applied theories were considered (In Fraunhofer diffraction, only the refractive index of the dispersion medium “liquid paraffin” was set to be 1.468; In Mie theory, lactose as a material was set in need and taken the refractive index and absorption index as 1.52 and 0.1); In the “result calculation model”, three options were set to “general purpose /single mode /multiple narrow modes”, “normal” and “spherical”. For background, the system was aligned to test the background until the scattered light energy was less than 150 and the laser intensity was above 70%. When measuring, the batch number of every sample was set in the “documentation”, then samples were added into the dispersion unit until the obscuration of the software reached around 5%, 10% and 15% for the test. After testing each batch of samples, the dispersion unit was cleaned three times with lamp oil until the background reached the requirements and then started the next measurement. Weighted Residues of the results refer to the difference between the actual light intensity curve and the theoretical light intensity curve based on least square fitting, usually within 1%, which means that the accuracy of the test is good.

3.3.2 Malvern dry analysis

a) Instrument

Malvern Mastersizer S for dry analysis

b) Method

The instrument, the computer, the vacuum inlet and the vacuum outlet were turned on while the knob of dry powder feeder was left to “AIRFLOW”. Then parameters in the software were set up: The “Measurement sequence” should be set 3 at first; In “Hardware”, the range, active beam length, set the range, sample unit and instrument port were chosen as 300F(0.5-900μm), 10mm, MS64-Dry Powder Feeder Unit and 1; Then the analysis model was set to Polydisperse; In “Experiment”, the measurement time, the range of concentration for sample were selected to 10s and 1-30%; In “Presentation”, the Standard-Dry (3RHA) was chosen as the system. For measurement, the batch number in the “Set sequence” was written, the system was aligned next, the background was tested and inspected ready to start. The powders were poured evenly on the tray of the feeder, then the desired feed rate and jet pressure could be set. After each batch was completed, the tray was removed to wash with water, wiped dry with paper, and then placed on the feeder to clean the interior of the tray again by adjusting the feed rate or jet pressure.

3.3.3 Sympatec Qicpic

a) Instrument

Sympatec QICPIC- LIXELL

b) Method

The instrument, computer was turned on, and then the database of the user in software Windox 5 could be opened. Then parameters were set up one by one: In the product control, the calculated diameter was set as as EQPC, the calculate shape values was chosen sphericity, aspect ratio as well as elongation and the adjustment curve was classified into a period of 30s; In the Trigger conditions control, frame rate, the stop and the repeat time were selected as 50 hz, 30s and 2; In the disperse method, the liquid was set as DEFAULT and cuvette with diameter of 1mm. Next, a small amount of samples were placed in a beaker on a magnetic stirrer and dissolved in isopropanol. “Execute auto focus” and signal test of the sample were clicked to see the live view of samples. Note: COPT value of the sample every time should be less than 0.2% to prevent the observed particles from overlapping. Sphericity and aspect ratio are parameters to describe the shape of particles. The former characterizes how close particles are to a sphere, the latter is the ratio of the particle's smallest and largest directional diameters.

3.3.4 SEM

a) Instrument

JEOL JSM-6700F scanning electron microscope

b) Method

Under 10kV accelerating voltage within 8 mm working distance, a small amount of sample powder was taken and distributed onto adhesive tabs. In a sub-vacuum environment, the tabs were placed with marked samples on the ion sputtering machine to sputter an approximately 15 nm Au/Pd layer for 200s reducing charge effects. Finally, prepared samples were put into the sample chamber, adjusting the sample position and the focal length of SEM through the computer as well as the detector in order to select the appropriate magnification to observe and photograph the sample.

3.3.5 Light microscopy

a) Instrument

Olympus System Microscope Model BX50

b) Method

The converter was turned to align the lowest magnification objective with the clear aperture and kept it 2 cm away from the stage. After proper treatment of LH100, prepared samples were dispersed on the slide and oriented directly to the center of the clear aperture. Then, the coarse focus screw was turned to make the lens barrel descend slowly until the objective lens was close to the sample. At this time, samples could be watched through the eyepiece. In order to make images more clear, the coarse focusing screw in the opposite direction and fine focus screw were adjusted in turn.

4. Results and discussion

4.1 Cellets

4.1.1 Figures obtained by Qicpic and SEM

C100 particles in the range of 140-170μm by Qicpic are given in **Figure 8**. The shape of most particles is close to rounded and a few artifacts (white areas) can be observed in some particles. Artifacts are in part because when several particles are overlapped in different directions, they will be regarded as one particle. (Yang & Chen, 2016) It is also because the light will be back-reflected at the interface between the scattering particles and the surrounding materials with different refractive index. (Markl et al., 2015)

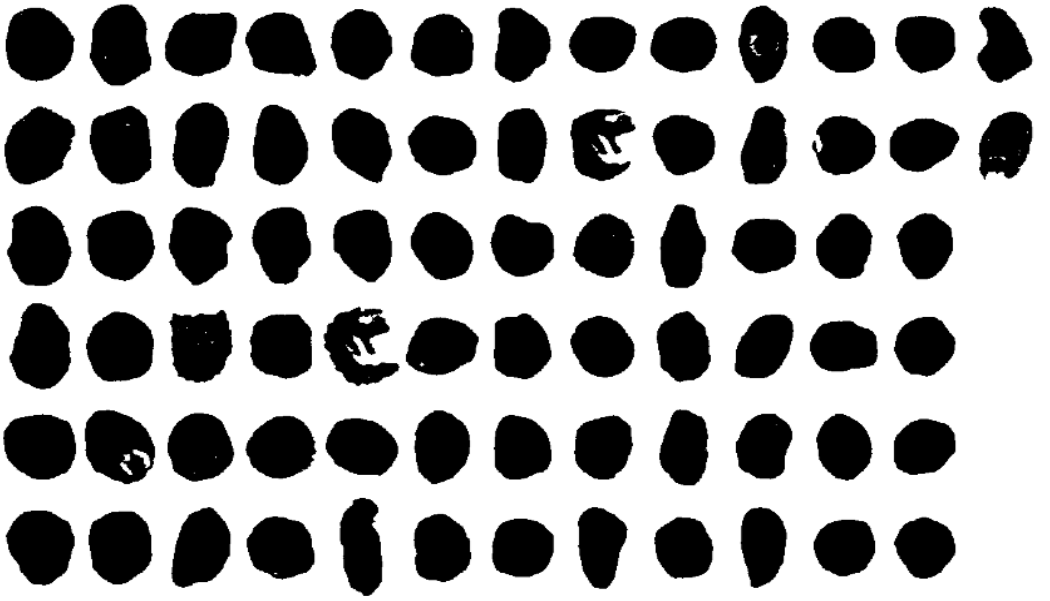

Figure 8. C100 from Qicpic measurement

At a magnification of 50, it is clear that the microphotograph of C200 is regular spherical and has a compact structure in the size range of 200-355 μm, shown on the left of **Figure 9**. From the right of **Figure 9**, the smooth spherical surface of C200 can be seen at higher magnification.

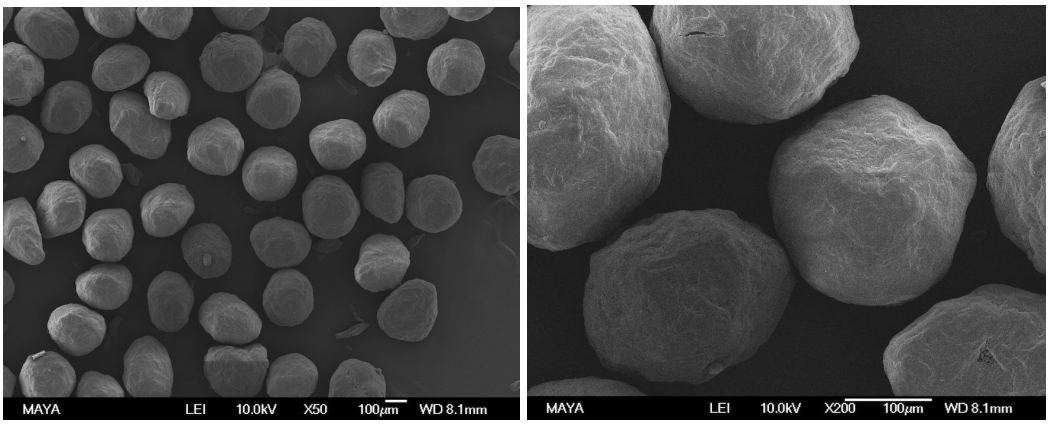

Figure 9. The image of C200 with a magnification of 50(left) and 200(right) by SEM

4.1.2 Comparison of the different laser diffraction methods

In the Malvern wet analysis, the obscuration represents the concentration of samples. Too low obscuration may give unstable particle size distribution due to lower signal-to-noise ratio. High obscuration may cause the multiple scattering. It can be also observed that 10% of obscuration has lowest weighted residues of three different obscurations in **Table 3**, indicating that the actual measured curve is more accurate and fits better with the theoretical curve. So obscuration of 10% is selected as the best for Cellets for further discussion.

Table 3. The data from Malvern wet analysis and dry analysis of C100, C200 and C350.

Sample	Obscuration (%)	D10 (μm)	D50 (μm)	D90 (μm)	Span	D [4,3] (μm)	Weighted residues
C100-01-5%-A (Wgp)	4.19	113.27	154.34	211.39	0.636	158.932	0.671
C100-01-10%-A (Wgp)	9.44	112.38	153.30	210.27	0.639	157.988	0.633
C100-01-15%-A (Wgp)	15.49	111.36	151.76	207.38	0.632	156.454	0.639
C100-01-5%-A (Wsm)	4.19	118.20	152.74	200.28	0.537	156.427	0.46
C100-01-10%-A (Wsm)	9.44	120.92	154.46	199.05	0.506	157.853	0.310
C100-01-15%-A (Wsm)	15.49	117.68	150.54	197.20	0.528	154.304	0.319
C100-A (D)	/	122.10	152.08	196.46	0.488	155.620	0.890
C200-01-5%-A (Wgp)	4.1	194.96	265.36	360.02	0.622	272.613	1.919
C200-01-10%-A (Wgp)	9.98	199.40	270.01	362.57	0.604	277.324	1.34
C200-01-15%-A (Wgp)	15.11	199.34	269.87	362.35	0.604	277.190	1.416
C200-01-5%-A (Wsm)	4.1	217.49	263.98	322.65	0.398	267.494	0.544
C200-01-10%-A (Wsm)	9.98	227.18	267.13	314.31	0.326	269.755	0.425
C200-01-15%-A (Wsm)	15.11	227.51	266.31	311.97	0.317	268.841	0.471
C200-A (D)	/	231.82	266.05	308.00	0.286	268.380	1.485
C350-01-5%-A (Wgp)	4.05	301.93	408.44	551.27	0.610	418.948	2.005
C350-01-10%-A (Wgp)	9.17	302.51	407.31	547.00	0.600	417.347	2.333
C350-01-15%-A (Wgp)	13.89	301.99	405.66	524.44	0.593	415.111	2.603
C350-01-5%-A (Wsm)	4.05	355.77	404.65	455.36	0.246	405.917	0.620
C350-01-10%-A (Wsm)	9.17	367.08	404.66	432.53	0.282	402.999	0.641
C350-01-15%-A (Wsm)	13.89	369.12	404.72	431.03	0.153	403.191	1.091
C350-A (D)	/	363.80	400.43	449.47	0.213	404.240	2.776

*A means average, Wgp means general purpose in Malvern wet analysis, Wsm means single mode in Malvern wet analysis and D means Malvern dry analysis.

In the Malvern wet software, there are three calculation models in the wet analysis: general purpose mode(gp mode), single narrow mode(sm mode) and multiple narrow modes(mn mode). Among them, the gp mode is suitable for most samples and is therefore the preferred choice for particles with unknown characteristics; the sm mode refers that there is one main peak with coarse and fine particles decreasing the percentage content on both sides; the mn mode is suitable for samples with known particle size distributions, for example mixed samples that have small differences in particle fraction. ("Zetasizer Nano Analysis Methods Explained," 2010) Gp mode and sm mode were applied in the measurement of C100, C200 and C350 in **Table 3**. C100 in 10% of obscuration could be taken as an example for comparing different methods in **Figure 10 and Figure 11**. From these two figures, it can be observed that the span was wider, the value of D10 was smaller, and the value D90 was larger in the gp mode. The sm mode and dry analysis are in excellent agreement and furthermore comply with the specification of C100, but the gp mode is not accurate enough.

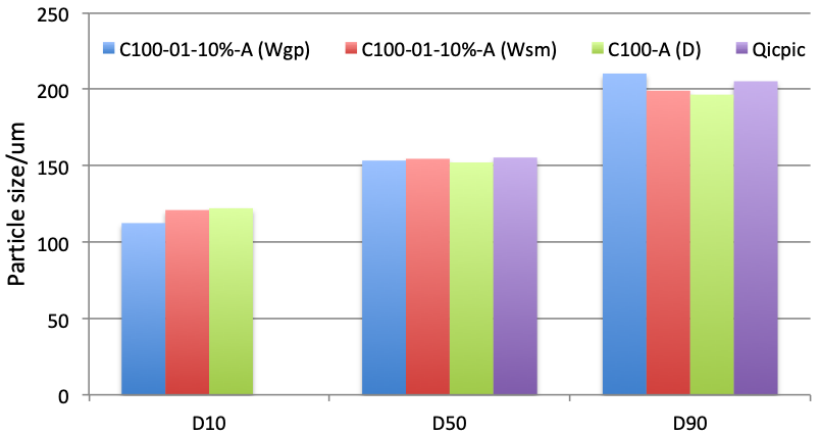

Figure 10. D10, D50, D90 of C100 from different methods

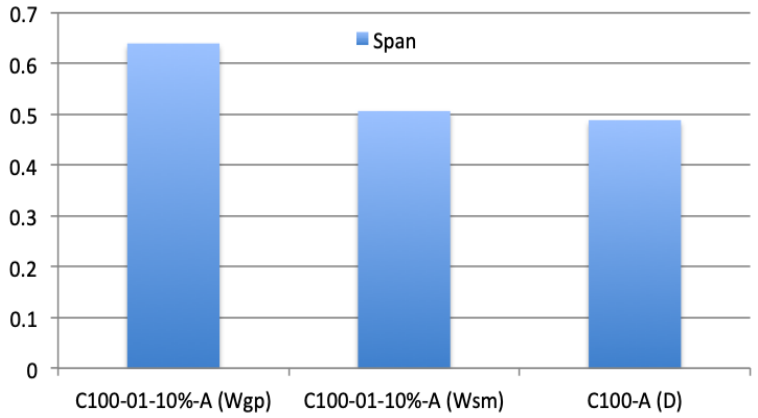

Figure 11. The span of C100 from different methods

Comparing C100, C200 and C350 at 10% obscuration in the sm mode of Malvern wet with the Malvern dry data in **Figure 12 and Figure 13**, there were slightly narrower spans with lower peaks of D50 in dry analysis, which could be caused by the powder was not sufficiently dispersed in the feeder in measurement and then some powders were left in the tray of the feeder. In the dry analysis, there were more losses in the powders of fine particles and large particles, so the obtained results are affected on D10 and D90 more, but D50 is more stable in the comparison of dry analysis and wet analysis. So Malvern wet with sm mode is the best method to measure the particle size of pure cellets but Malvern dry is also very good.

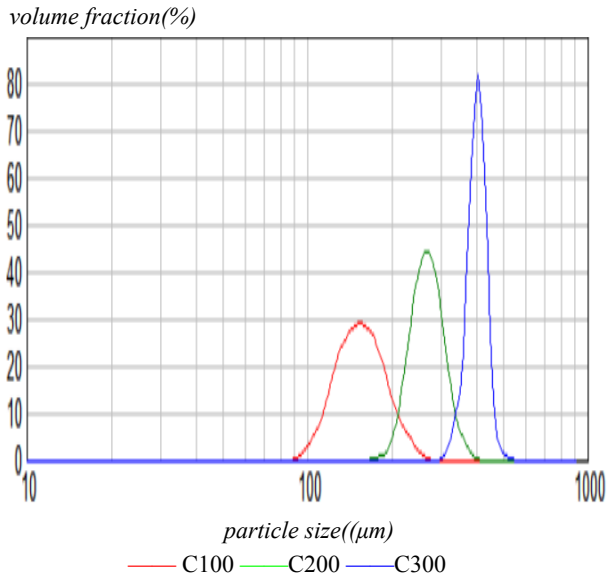

Figure 12. The Malvern wet measurement in sm mode of C100,C200 and C350

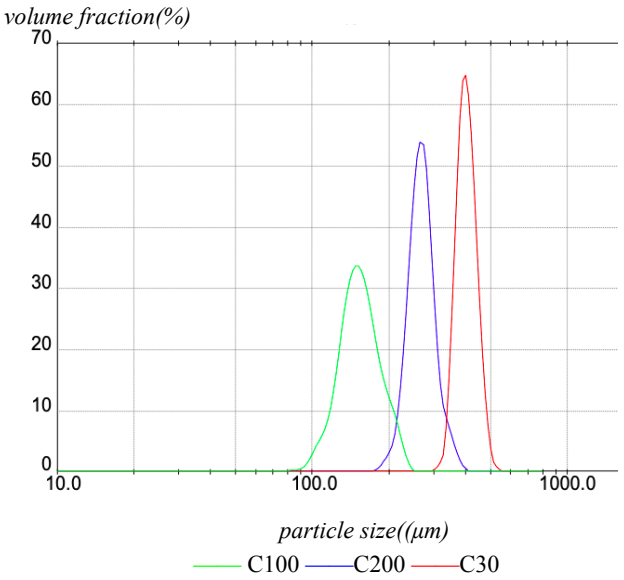

Figure 13. The Malvern dry measurement of C100,C200 and C350

4.1.3 Analysis of results from QicPic

Qicpic results of C100 are summarized in **Table 4**, D10 data from QicPic are disregarded because very fine particles can not be measured accurately with the principle of optical imaging. There were around 900 particles of different samples in the range of 10-230 μm detected by Qicpic. Comparing **Table 4** and **Figure 14**, C100 particles larger than 120 μm have a sphericity of 0.9, which means it is close to perfect spheres. The sphericity showed a declining trend with decreasing particle size. The aspect ratio of C100 supports this interpretation, confirming that the majority of C100 particles have a spherical shape.

Table 4. The data from Qicpic of C100

Sample	Copt (%)	D50 (μm)	D90 (μm)	VMD (μm)	Quantities and range
C100-1	0.08	157.92	218.40	166.17	837 with 10-230μm
C100-2	0.08	155.36	192.25	155.62	956 with 10-230μm
C100-3	0.07	152.59	205	156.16	929 with 10-230μm

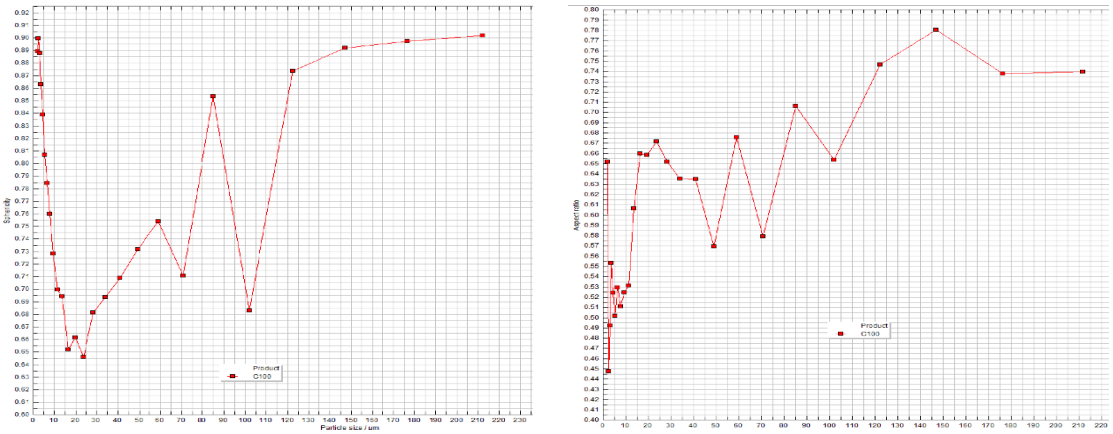

Figure 14. The curve of sphericity (left) and aspect ratio (right) of C100 given by Qicpic

The difference between D50 and D90 in Malvern wet analysis, Malvern dry analysis and Qicpic analysis is not significant in **Figure 10,** which means all three methods are accurate. That can be explained by the spherical shape of C100. In the Malvern analysis, the particles are regarded as equivalent spheres, then the particle size and distribution can be given, which is almost consistent with the results obtained from the Qicpic analysis. In addition, regardless of C100, C200, C350 in wet analysis, dry analysis or Qicpic all meet the specifications of the supplier in **Table 1**.

4.1.4 Comparison of methods for the CSCB blend

CSCB is a blend of C100 and C350 in a 1:1 ratio. Whether in the gp mode of wet analysis in **Figure 15** or multiple narrow(mn) mode in **Figure 16,** it is clear that the repeatability of CSCB in 5%, 10% and 15% of obscuration is good. As for **Figure 17**, it is obvious that mn mode is more suitable for CSCB, because it is easy to see two sharp peaks in one curve, one is at around 150 μm due to C100, another is at around 400 μm due to C350. In the dry analysis, it can be seen that the repeatability of every batch of CSCB is bad in **Figure 18**. Although there are two distinct peaks in each curve, the volume fraction of each peak is always different, which is because the mixed powder has segregated with poor uniformity. So the CSCB blend is best measured by the Malvern wet method with mn mode.

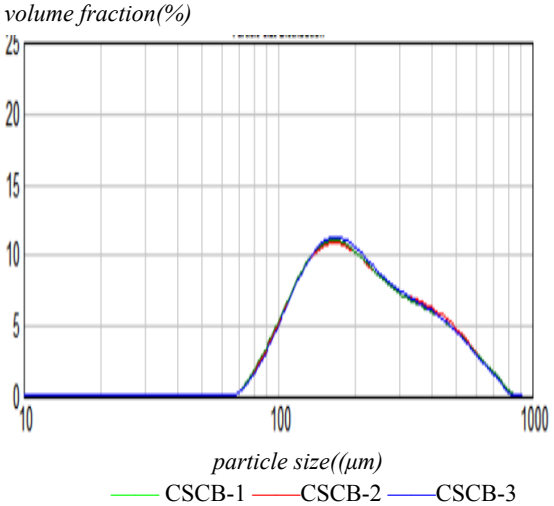

Figure 15. The Malvern wet analysis with gp mode of 5%,10% and 15% CSCB

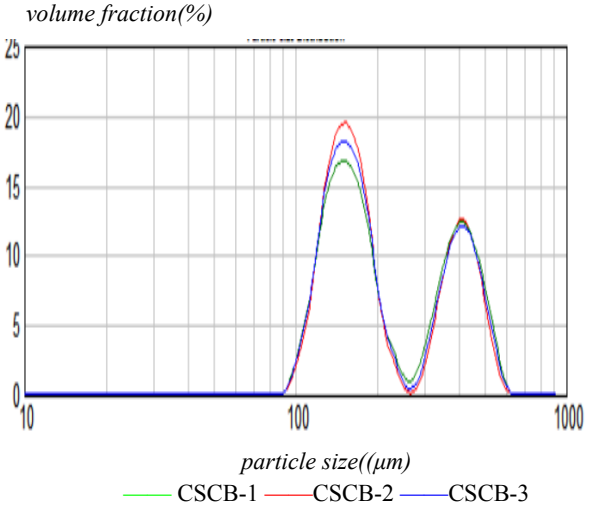

Figure 16. The Malvern wet analysis with mn mode of 5%, 10% and 15% CSCB

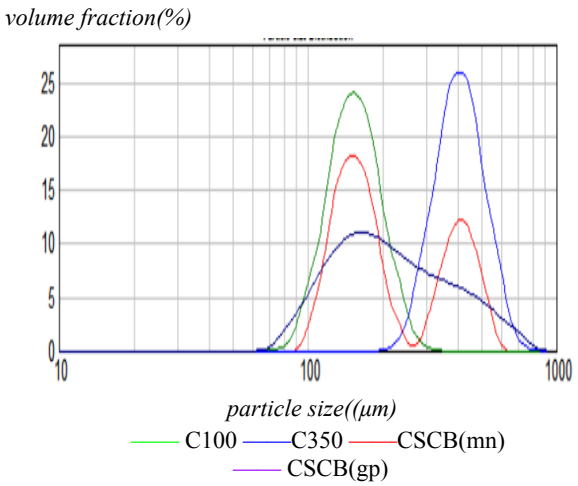

Figure 17. The Malvern wet analysis of C100,C350 and CSCB

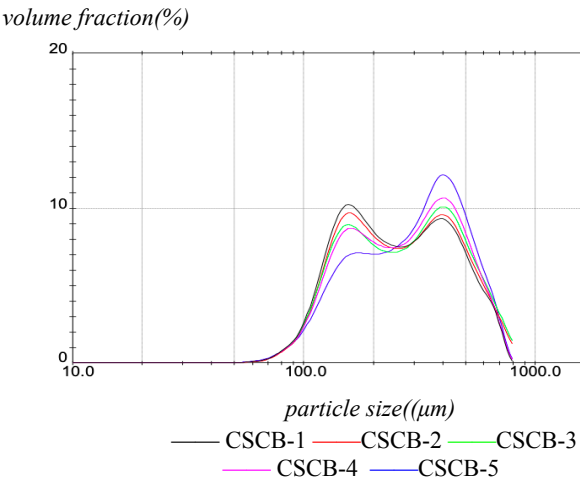

Figure 18. The Malvern dry analysis of 5 batches of CSCB

4.2 Cellulose microcrystalline

4.2.1 Figures of CM obtained by Qicpic and SEM

CM particles in the range of 61-65μm by Qicpic are given in **Figure 19**. Most of the particles are fibrillar or slender with some irregular aggregates or pellet formation.

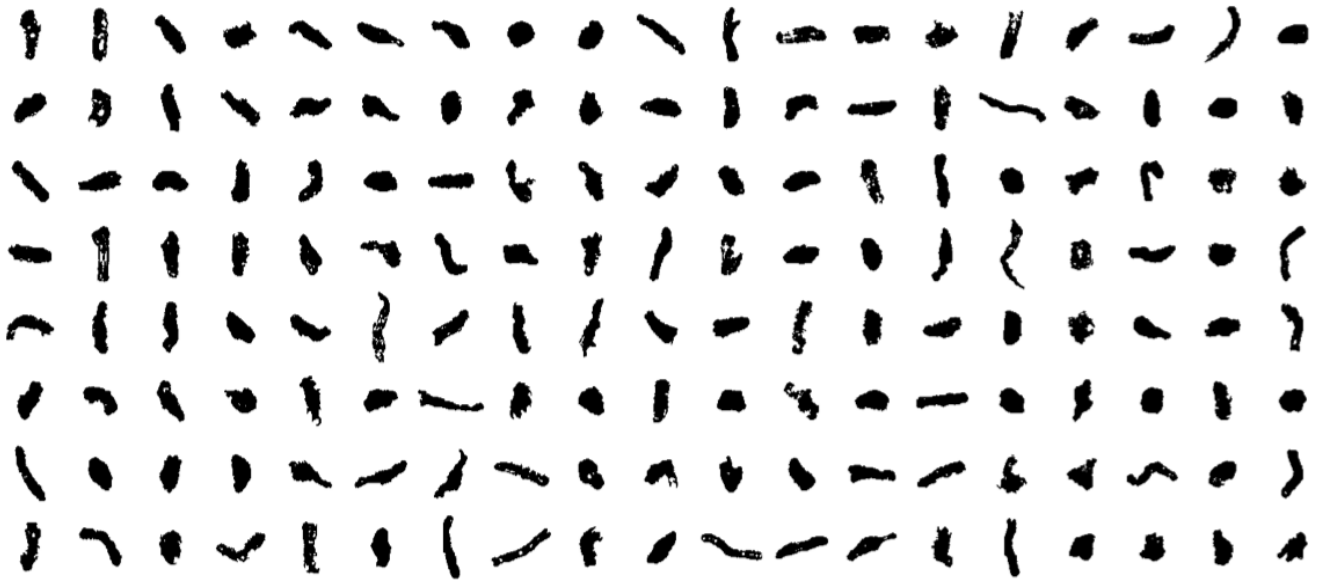

Figure 19. CM from Qicpic measurement

When viewed in SEM at a magnification of 50 on the left of **Figure 20**, it can be seen that the CM particles are not isometric and have an unequal distribution. The fibrous shape of smaller particles with a length of roughly 60μm is visible. Some agglomerations appear as numerous irregular lumps, which could be generated by the effect of high surface energy of CM. (Zhao et al., 2007) On the right of **Figure 20,** it is clear that particles are flat or like convoluted ribbons.

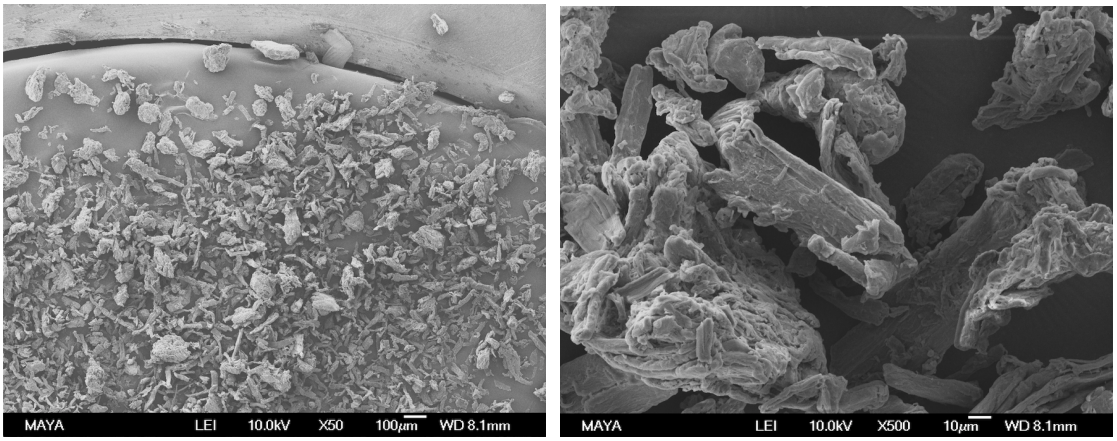

Figure 20. The image of CM with a magnification of 50(left) and 500(right) by SEM

4.2.2 Comparison of the different laser diffraction methods

Compare the weighted residues of different methods in **Table 5,** 15% of obscuration was selected as the reference obscuration in wet analysis of CM, because it has lowest weight residues. From **Figure 21 and 22**, it is clear that the span of sm mode in wet analysis and dry analysis is similar, which are both much lower than gp mode of wet analysis. So the sm mode and dry analysis is better in agreement with the CM.

Table 5. The data from Malvern wet analysis and dry analysis of CM.

Sample	Obscuration (%)	D10 (μm)	D50 (μm)	D90 (μm)	Span	D [4,3] (μm)	Weighted residues
CM-01-5%-A (Wgp)	4.39	15.40	57.60	133.97	2.058	67.000	2.508
CM-01-10%-A (Wgp)	10.31	16.09	59.51	135.78	2.011	68.525	1.613
CM-01-15%-A (Wgp)	15	16.81	61.85	138.98	1.975	70.669	1.125
CM-01-5%-A (Wsm)	4.39	18.20	58.73	121.72	1.763	66.135	2.107
CM-01-10%-A (Wsm)	10.31	17.26	60.84	127.80	1.816	68.552	1.416
CM-01-15%-A (Wsm)	15	17.12	63.02	132.55	1.831	70.929	1.024
CM-A (D)	/	20.65	65.73	139.04	1.801	73.630	0.504

* A means average, Wgp means general purpose in Malvern wet analysis, Wsm means single mode in Malvern wet analysis and D means Malvern dry analysis.

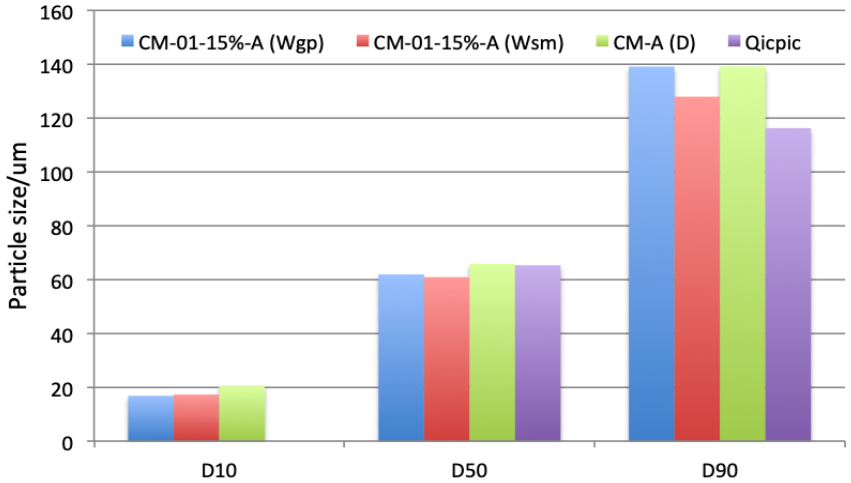

Figure 21. D10, D50, D90 of CM from different methods

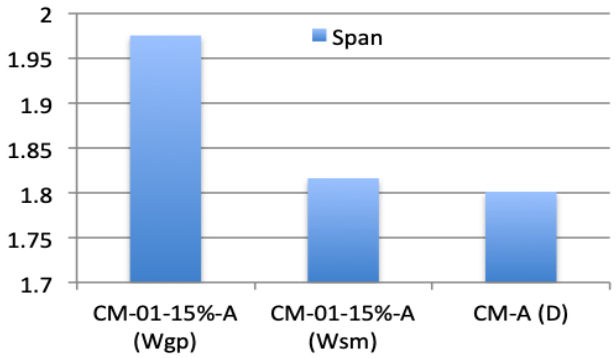

Figure 22. The span of CM from different methods

Figure 23 and 24 show that there is a difference in CM particle size curve between Malvern wet and Malvern dry. There are three peaks that can be identified in sm mode of **Figure 23**, 40µm, 100µm and 200µm, demonstrating that there are three particle sizes of CM: small CM particles, medium CM aggregates, and larger CM aggregates,which can also be seen in the SEM **Figure 20** of CM, where CMs of different particle sizes are present in the sample. In the dry analysis of **Figure 24**, its particle size curve has one distinct peak at 100µm with a skewed distribution towards the larger particle sizes.

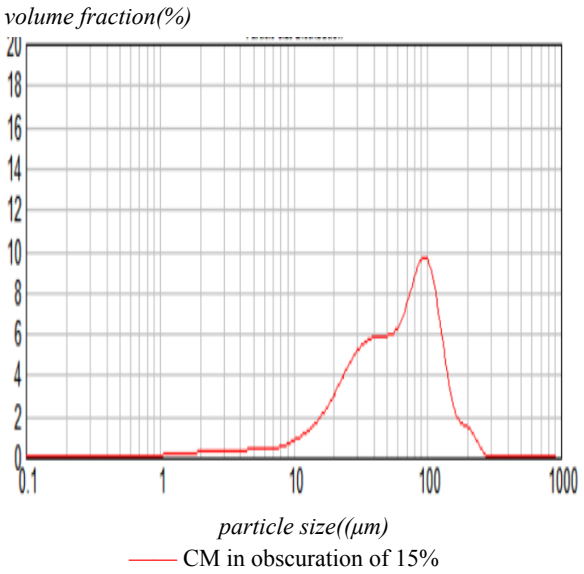

Figure 23. The Malvern wet measurement in sm mode of CM in obscuration of 15%

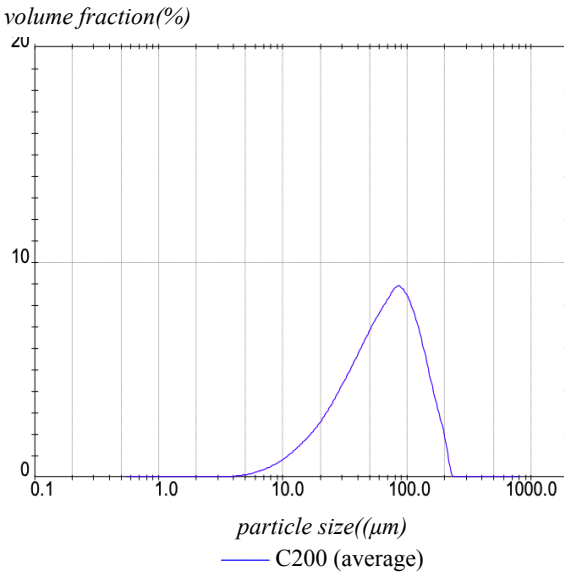

Figure 24. The Malvern dry measurement of CM (average)

4.2.3 Analysis of results from QicPic

More than 10000 CM particles in the range of 10-130 µm are measured by Qicpic seen in **Table 6**. The D90 of CM particles in the QicPic analysis is lower than in the Malvern analysis, which could be because CM is an elongated fibrillar shape. The left of **Figure 25** shows that particles of D50 have the lowest sphericity, around 0.65, while larger particles have an increasing sphericity up to 0.73 at D90 due to formation of aggregates. In terms of aspect ratio **in Figure 25**, aspect ratio increases from 0.47 to 0.54 when the particle size ranges from D50 to D90, again pointing to the aggregates.

Table 6. The data from Qicpic of CM

Sample	Copt (%)	D50 (µm)	D90 (µm)	VMD (µm)	Quantities and range
CM-1	0.19	64.74	114.71	69.52	more than 10000 with 10-130µm
CM-2	0.19	62.20	110.56	67.31	more than 10000 with 10-130µm
CM-3	0.15	68.73	123.13	73.24	more than 10000 with 10-130µm

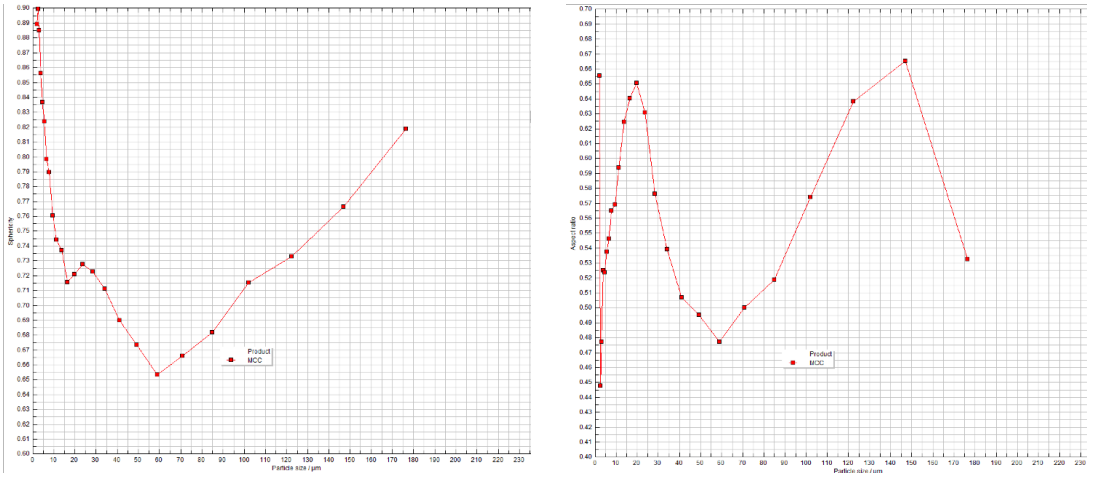

Figure 25. The curve of sphericity (left) and aspect ratio (right) of CM given by Qicpic
(Note: Particles larger than 150 μm could be caused by contamination and be disregarded in the analysis)

4.2.4 Comparison of methods for the CMMCC blend

CMMCC is a mixture of C200 and CM in a 1:1 ratio. Comparing gp mode in **Figure 26** and mn mode in **Figure 27** of Malvern wet analysis, the curves in each mode of the three batch mixtures are reasonably similar, indicating good reproducibility of the measurements.

In **Figure 28**, there are two noticeable peaks in gp mode: the first peak is about 70 μm and is caused by D50 of CM, and the second peak is around 250 μm and is caused by D50 of C200. In mn mode, however, there are four peaks that can be identified, at 40 μm, 100 μm, 250 μm and 900 μm. The initial peak is mostly affected by the smaller CM particles as shown in the sm mode, the second peak is created by the main peak of CM, the third peak can be identified by the D50 of C200 particles, and the last peak is probably an artifact due to the limitation of the software.

In **Figure 29**, the dry analysis of CMMCC shows two unique peaks at around 70 μm and 250 μm, which are caused by the quantity of CM and C200 particles in D50. In the dry analysis, the intensity of the first peak is lower, while the intensity of the second peak is higher, as compared to the wet analysis. Since CM and C200 are mixed in a 1:1 ratio, mn mode of wet analysis for CMMCC with the best resolution is preferred.

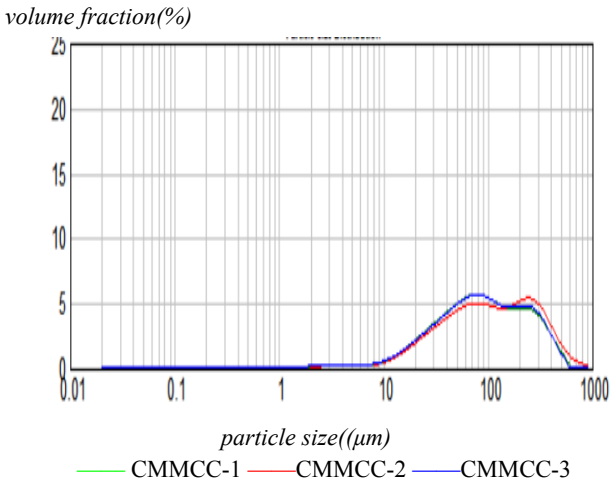

Figure 26. The Malvern wet analysis with general purpose(gp) of 5%,10% and 15% CMMCC

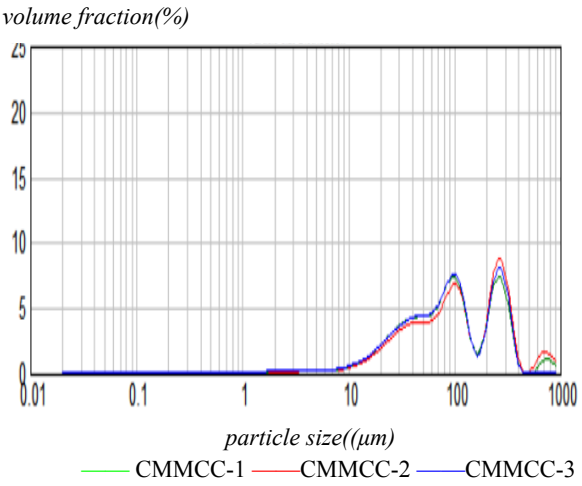

Figure 27. The Malvern wet analysis with multiple narrow modes(mn) of 5%, 10% and 15% CMMCC

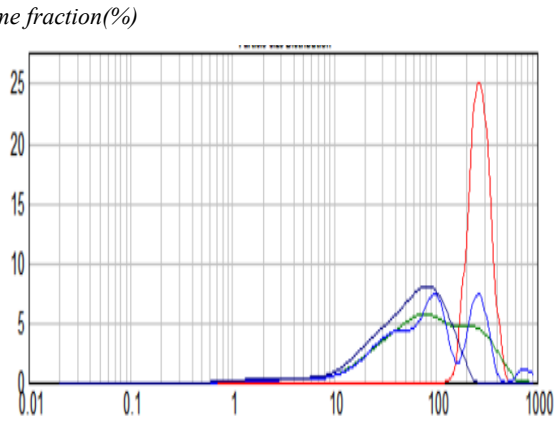

Figure 28. The Malvern wet analysis of C200,CM and CMMCC

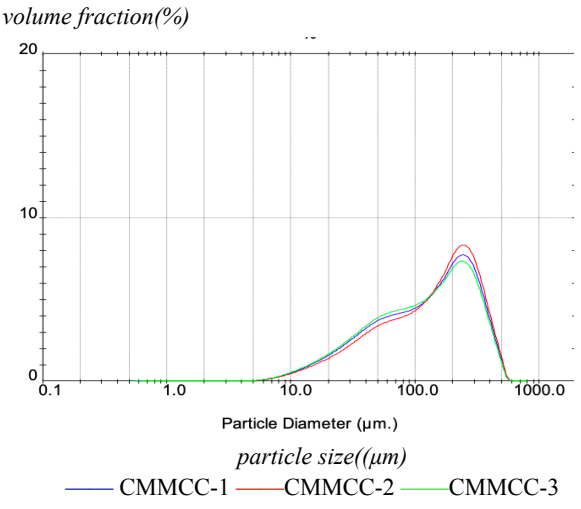

Figure 29. The Malvern dry analysis of 3 batches of CMMCC

4.3 Sodium bicarbonate

4.3.1 Figures of SBF obtained by Qicpic and SEM

SBF in the range of 90-110 μm are given by Qipic in **Figure 30**. It can be observed that most particles of SBF have an elongated, ovoid or spherical regular structure. ("EP2714591A1 - Sodium Bicarbonate Product with Excellent Flowability and Its Method of Manufacture - Google Patents," 2012)

Figure 30. SBF from Qicpic measurement

In SEM, SBF has a sheet-like structure covered with some spikes, having a flat and smooth surface, as seen at a smaller magnification in **Figure 31**, which can be seen more clearly at a bigger magnification. SBF particles with a length of about 120 μm are visible in the SEM figures.

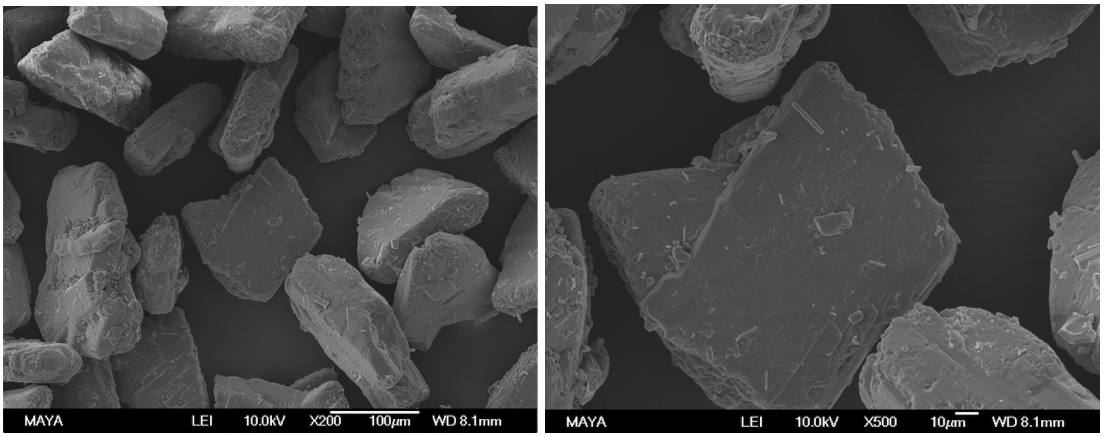

Figure 31. The image of SBF with a magnification of 200(left) and 500(right) by SEM

4.3.2 Comparison of the different laser diffraction methods

By comparing weight residues of SBF, SFC and SFS in **Table 7**, 10% of obscuration is chosen as the best for the following part. It is worth mentioning that the results in sm mode have much lower weight residues compared with the gp mode of wet analysis and dry analysis. So it is better to choose sm mode as the best mode in the wet analysis. In **Figure 33**, there is a decreasing trend in span of the gp mode of wet analysis, sm mode of wet analysis, and dry analysis, which could be explained by a decrease in the quantity of big particles (D90) in **Figure 32.** The explanation for this could be that the rotation speed of the dispersing unit is a little low in wet analysis, which does not suspend large particles in the lamp oil, resulting in a lower particle size measurement compared with dry analysis. **Figure 34** and **Figure 35** also show that more narrow spans of samples are given in the Malvern dry. So for large particles, dry analysis is more suitable for particle-sizing measurement.

Table 7. The data from Malvern wet analysis and dry analysis of SBF.

Sample	Obscuration (%)	D10 (µm)	D50 (µm)	D90 (µm)	Span	D [4,3] (µm)	Weighted residues
SBF-01-5%-A (Wgp)	6.01	86.93	135.46	205.17	0.873	140.732	0.645
SBF-01-10%-A (Wgp)	10	85.80	134.94	206.24	0.893	140.454	0.684
SBF-01-15%-A (Wgp)	14.76	84.66	134.22	206.63	0.909	139.811	0.717
SBF-01-5%-A (Wsm)	6.01	84.65	137.92	198.97	0.829	138.787	0.270
SBF-01-10%-A (Wsm)	10	84.17	138.25	198.74	0.829	138.588	0.168
SBF-01-15%-A (Wsm)	14.76	83.75	138.02	197.99	0.828	138.109	0.159
SBF-A (D)	/	83.70	127.90	180.77	0.759	129.59	0.537
SBS-01-5%-A (Wgp)	5.3	43.36	87.09	151.81	1.245	92.102	0.523
SBS-01-10%-A (Wgp)	10.24	42.17	86.19	150.77	1.260	91.108	0.497
SBS-01-15%-A (Wgp)	15.58	41.40	86.00	151.60	1.281	91.090	0.439
SBS-01-5%-A (Wsm)	5.3	41.09	88.59	144.22	1.153	91.455	0.238
SBS-01-10%-A (Wsm)	10.24	39.67	87.53	142.05	1.170	89.791	0.170
SBS-01-15%-A (Wsm)	15.58	38.95	87.44	143.88	1.200	90.399	0.161
SBS-A (D)	/	34.69	77.81	140.11	1.355	82.930	0.387
SBC-01-5%-A (Wgp)	4.49	232.27	382.84	608.04	0.982	402.349	0.993
SBC-01-10%-A (Wgp)	9.27	240.33	380.12	590.09	0.920	399.056	0.938
SBC-01-15%-A (Wgp)	15.51	223.39	385.61	614.94	0.989	405.870	0.953
SBC-01-5%-A (Wsm)	4.49	232.22	383.51	550.20	0.829	388.601	0.582
SBC-01-10%-A (Wsm)	9.27	242.69	386.79	548.39	0.790	391.915	0.582
SBC-01-15%-A (Wsm)	15.51	235.41	385.89	562.66	0.848	394.177	0.618
SBC-A (D)	/	213.95	374.73	585.53	0.990	387.360	1.027

*A means average, Wgp means general purpose in Malvern wet analysis, Wsm means single mode in Malvern wet analysis and D means Malvern dry analysis.

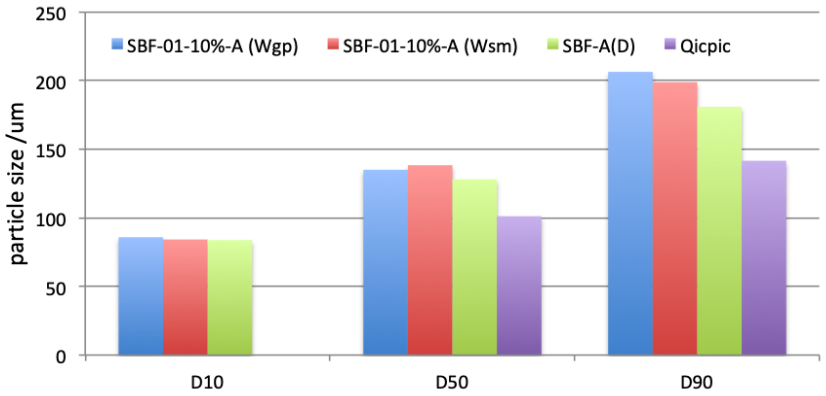

Figure 32. D10,D50, D90 of SBF from different methods

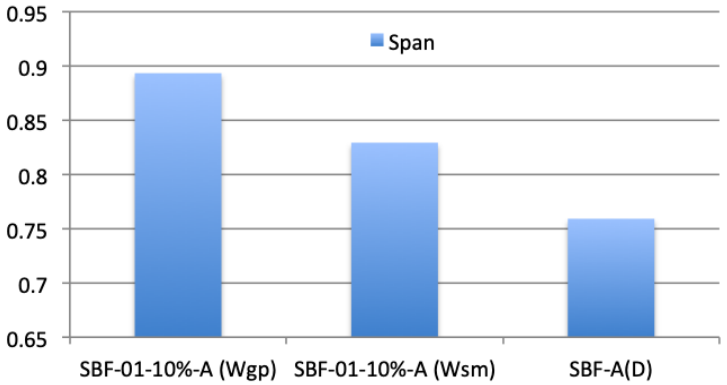

Figure 33. The span of SBF from different methods

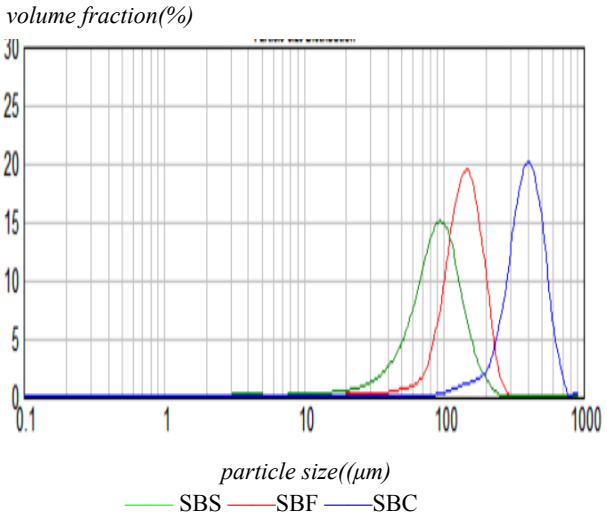

Figure 34. The Malvern wet measurement in sm mode of SBS,SBF and SBC-10%

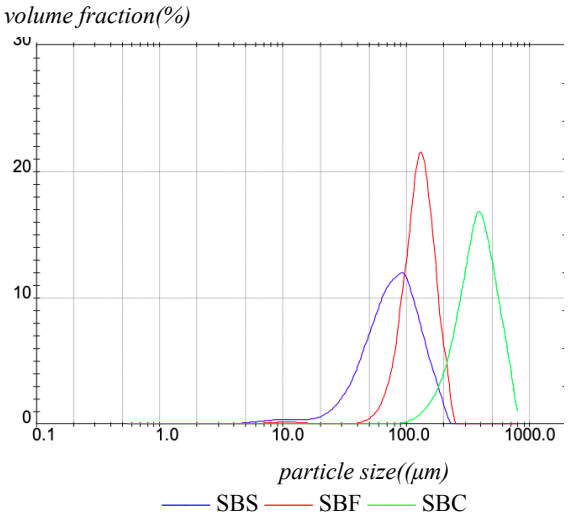

Figure 35. The Malvern dry measurement of SBS,SBF and SBC

4.3.3 Analysis of results from QicPic

SBF in the range of 10-170 μm are summarized in **Table 8**. The sphericity of SBF has only a slow rise in the range of D50 to D90 with 0.67 to 0.69. At the same time, the same trend can also be observed in aspect ratio in **Figure 36**, increasing from 0.55 to 0.6. From **Figure 32**, it can be seen that D50 and D90 in Qicpic are quite lower than from the other methods. Therefore, the shape of samples may have contributed to this difference, because most of the SBFs show a regular oval shape.

Table 8. The data from Qicpic of SBF

Sample	Copt (%)	D50 (µm)	D90 (µm)	VMD (µm)	Quantities and range
SBF-1	0.07	103.44	135.19	103.46	2019 with 10-170 µm
SBF-2	0.05	101.60	146.35	102.95	2008 with 10-170 µm
SBF-3	0.04	98.35	142.91	101.59	1953 with 10-170 µm

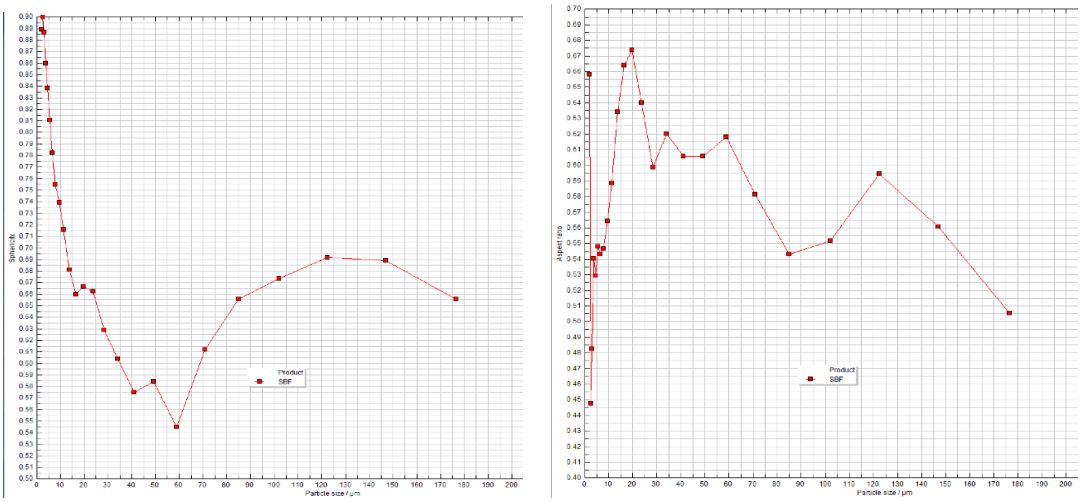

Figure 36. The curve of sphericity (left) and aspect ratio (right) of SBF given by Qicpic

4.4 Lactose carrier

4.4.1 Figures of LH100 and SV003 obtained by Qicpic

LH100 in the range of 95-110 µm and SV003 in the range of 66-70 µm measured by Qipic are shown in **Figure 37 and 38**. It is clear that most lactose carrier particles are characterized by a tomahawk or pyramidal shape.

Figure 37. LH100 from Qicpic measurement

Figure 38. SV003 from Qicpic measurement

4.4.2 Comparison of the different laser diffraction methods

Comparing the weighted residues in **Table 9**, 10% of obscuration can be selected for further analysis. The span of SV001 and SV003 is similar, and are both narrower than the span of LH100. The D50 of SV003, LH100 and SV001 has an increasing trend as shown clearly in **Figure 41**. The measured data (D50 and D90) of lactose carriers from Malvern wet and dry analysis are in excellent agreement with the specification in **Table 1**.

Table 9. The data from Malvern wet analysis and dry analysis of carrier lactose

Sample	Obscuration (%)	D10 (μm)	D50 (μm)	D90 (μm)	Span	D [4,3] (μm)	Weighted residues
LH100-01-5%-A (W)	4.75	72.15	143.82	249.97	1.236	152.128	0.506
LH100-01-10%-A (W)	9.81	70.38	141.91	246.94	1.244	149.956	0.526
LH100-01-15%-A (W)	15.13	69.61	140.97	244.73	1.242	148.683	0.587
LH100-A (D)	/	64.78	132.61	210.68	1.101	134.960	0.461
SV001-01-5%-A (W)	3.95	135.16	220.09	346.35	0.960	229.716	0.940
SV001-01-10%-A (W)	9.46	144.26	226.06	343.97	0.883	234.190	0.824
SV001-01-15%-A (W)	14.51	144.94	227.06	348.75	0.898	236.589	0.924
SV001-A (D)	/	155.49	231.61	319.55	0.706	232.860	0.830
SV003-01-5%-A (W)	5.55	37.56	63.35	97.92	0.953	64.953	1.221
SV003-01-10%-A (W)	9.94	37.56	63.32	96.66	0.933	64.363	1.137
SV003-01-15%-A (W)	16.06	34.93	61.98	98.25	1.022	63.575	0.950
SV003–P2-A(D)	/	36.06	65.27	99.44	0.971	66.030	0.436
SV003–P4-A (D)	/	31.60	62.98	98.36	1.060	63.690	0.384
SV003–P7-A (D)	/	24.79	59.67	98.82	1.240	65.960	0.402
SV003-P10-A (D)	/	17.76	58.09	108.15	1.556	84.930	0.443

*A means average, W means wet analysis, D means wet analysis and P2, P4, P7, P10 in dry analysis represent different feed rates and jet pressure (The details are shown in the Appendix)

When comparing **Figures 39 and 40**, it is clear that the results for LH100 are nearly same in wet and dry analysis, with the exception of D90 which is higher in the wet method, which may be due to larger particles being left in the feeder, resulting in a narrower span; Due to the loss of larger particles, SV001 exhibits the same situation as LH100, with a lower D90 and a narrower span of dry analysis than wet analysis. Also in **Figure 43**, it can be seen that LH100 and SV001 are performing triplicate dry analysis with excellent repeatability。

In **Figure 42**, SV003 was evaluated with settings 2, 4, 7, and 10 for the jet pressures to compare its effects on the particle size distribution in Malvern dry**.** It is shown that as jet pressure increases, D10

drops and D90 grows, indicating that there are more fine particles released from the carrier, and more larger particles agglomerated, resulting in an obvious increasing span of SV003 in **Figure 39 and 40**. As a result, it is difficult to determine the fine particle content of SV003 by the dry analysis due to changeable results. The best setting of jet pressure should be between 2 and 7 due to the highest pressure showing aggregates and having results outside the specification of D10 and D90.

Compare **Figure 41 and 44**, it is evident that LH100 and SV001 are suitable for wet analysis to measure its particle size and SV003 are acceptable for wet analysis or dry analysis with a range of 2-7 jet pressure.

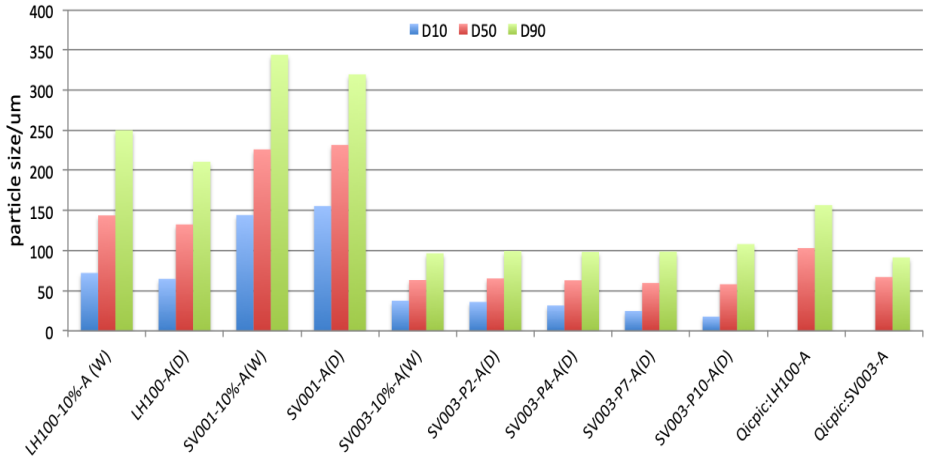

Figure 39. D10,D50, D90 of lactose carriers (LH100, SV001 and SV003) in different methods

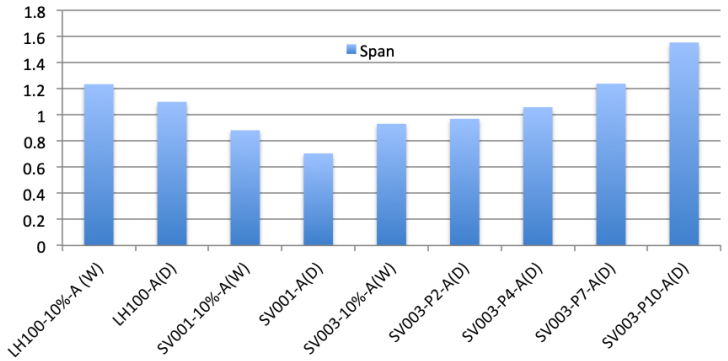

Figure 40. The span of lactose carriers (LH100, SV001 and SV003) in different methods

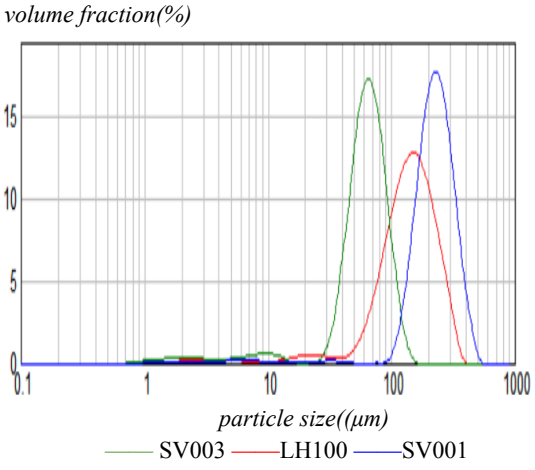

Figure 41. The Malvern wet measurement in gp mode of SV003, LH100 and SV001-10%

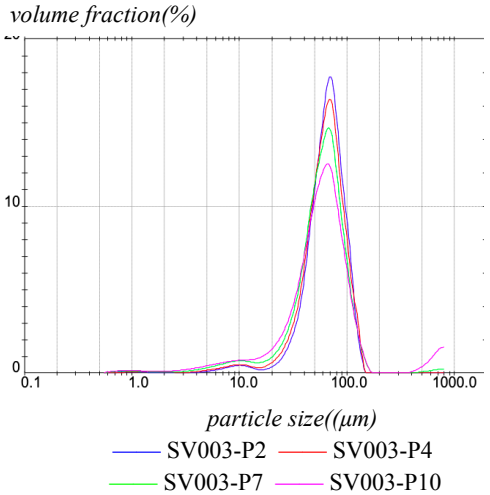

Figure 42. The Malvern dry measurement of SV003

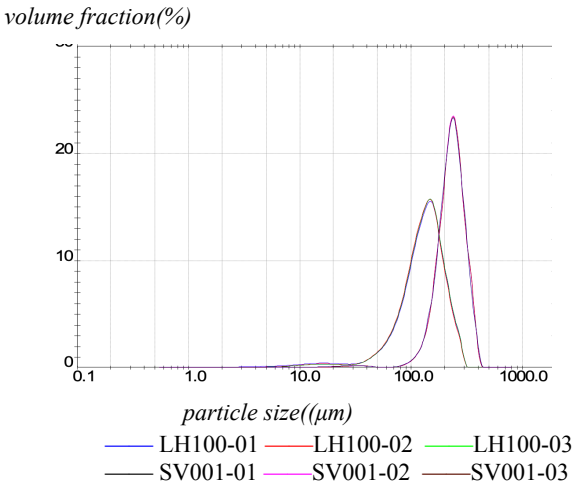

Figure 43. The Malvern dry measurement of LH100 and SV001

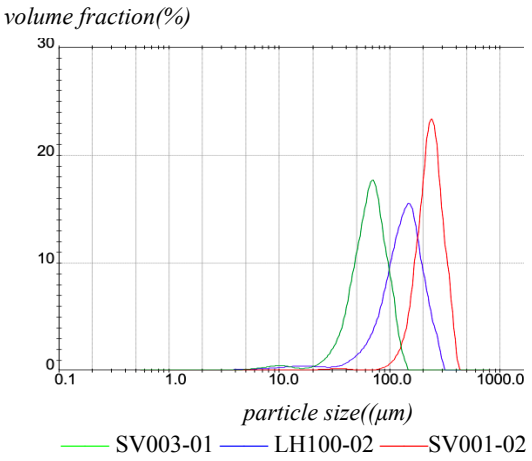

Figure 44. The Malvern dry measurement of SV003-P2, LH100, and SV001

4.4.3 Analysis of results from QicPic

Qicpic data for lactose carriers are summarized in **Table 10**. As indicated in 4.1.3,very fine particles should be ignored. **Figure 45** shows that the sphericity of LH100 drops from 0.79 to 0.71 in the range of 25-85 μm, then increases to 0.78 at D90 while the aspect ratio of LH100 follows a similar trend. As the particle size of SV003 increases in **Figure 46**, its sphericity declines with some fluctuations, reaching 0.75 at D90, as seen in the aspect ratio of SV003. It should be emphasized that the sphericity and aspect ratio of two lactose carriers appear to increase at the tail of the curves due to aggregation of larger particles.

The two lactose carriers are not perfect spheres because their sphericity and aspect ratio are not near to 1, which is also confirmed in 4.4.1. Comparing the results of Qicpic and other methods in **Figure 39**, it is clear that the results of LH100 are significantly different with lower D50 and D90 in Qicpic, which is probably caused by too large particles leading to segregation.

Table 10. The data from Qicpic of LH100 and SV003

Sample	Copt (%)	D50 (μm)	D90 (μm)	VMD (μm)	Quantities and range
LH100-1	0.17	107.90	174.81	121.73	4793 with 10-200um
LH100-2	0.16	101.95	149.56	103.16	5608 with 10-200um
LH100-3	0.16	99.50	145.64	100.23	6630 with 10-200um
SV003-1	0.13	66.94	90.76	69.44	5855 with 10-120um
SV003-2	0.13	67.16	91.47	68.03	5857 with 10-120um
SV003-3	0.13	67.09	92.26	68.93	5901 with 10-120um

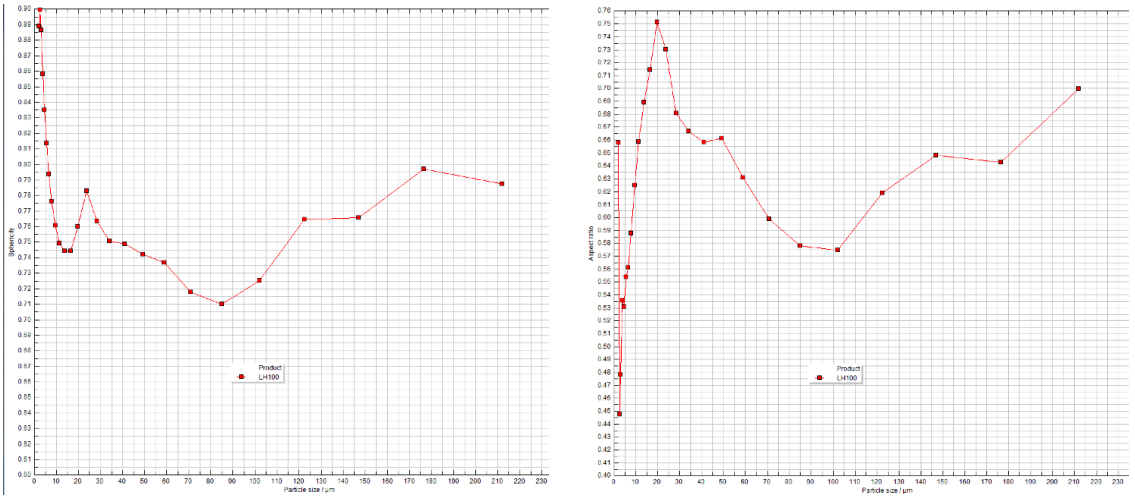

Figure 45. The curve of sphericity (left) and aspect ratio (right) of LH100 given by Qicpic

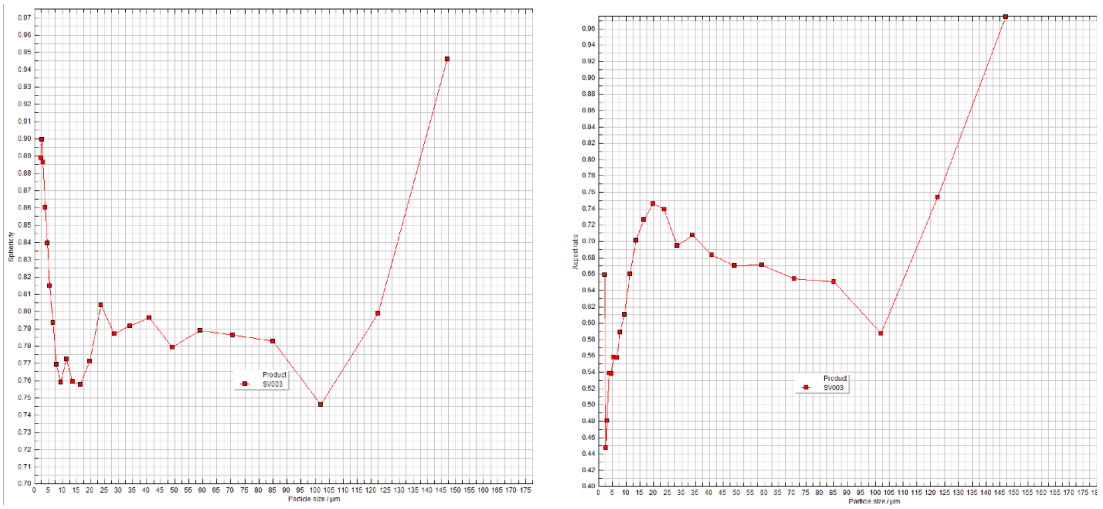

Figure 46. The curve of sphericity (left) and aspect ratio (right) of SV003 given by Qicpic

4.5 Lactose fines

4.5.1 Comparison of the different laser diffraction methods

10% of obscuration is selected as the reference for the lactose fines measurements shown in **Table 11.** In the following part, the effect of sonication and the choice of Fraunhofer or Mie theory in Malvern wet are explained, then the feasibility of fine powders in Malvern dry will be given.

a) Compare wet analysis without sonication and with sonication

The data in **Table 11** are summarized in **Figure 47 and 48.** It can be seen that when lactose fines (LH300 and Inhalac 500) were added with Span20 and sonicated, D10, D50, and D90 were greatly reduced and a wider span could be observed in **Figure 49 and 50**. Span20 can reduce particle surface tension and enhance its wettability, allowing particles to be better suspended in the liquid. As a result, better dispersibility and stability are obtained. Comparing the amount of Span20 added in LH100 and Inhalac 500 during sonication, it is clear the addition of double Span20 has a better effect, leading to particles with a VMD of less than 5µm, in agreement with the specification for these particles. Comparing the different ultrasonic intensity in **Table 11** and **Figure 47**, a slight decrease in fine particle size can be observed with increasing ultrasonic intensity from S4 to S7. But heat will be increased with growing intensity, therefore the ice bath is needed.

Table 11.The data in gp mode from Malvern wet analysis of lactose fines (LH300 and Inhalac500)

Sample	Obscuration (%)	D10 (μm)	D50 (μm)	D90 (μm)	Span	D [4,3] (μm)	Weighted residues
LH300-01-5%-A (W)	5.52	6.06	10.49	17.38	1.079	11.227	3.641
LH300-01-10%-A (W)	11.25	5.64	10.53	18.47	1.219	11.747	2.662
LH300-01-15%-A (W)	17.76	5.26	10.44	18.90	1.307	11.412	1.935
LH300-Span 20-S4-5%-A (W)	5.23	2.12	4.93	10.64	1.727	5.852	1.569
LH300-Span 20-S4-10%-A (W)	10.41	2.02	5.22	12.34	1.973	6.632	0.628
LH300-Span 20-S4-15%-A (W)	15.28	2.03	5.45	13.16	2.039	7.068	0.37
LH300-dSpan 20-S4-5%-A (W)	5.51	2.11	5.13	11.87	1.903	6.783	0.983
LH300-dSpan 20-S4-10%-A (W)	9.82	2.07	5.25	12.92	2.067	7.119	0.724
LH300-dSpan 20-S4-15%-A (W)	16.03	2.00	5.05	12.75	2.127	7.330	0.391
LH300-Span 20-S7-5%-A (W)	5.65	2.05	5.14	11.50	1.836	6.082	1.208
LH300-Span 20-S7-10%-A (W)	10.09	2.03	5.21	11.80	1.873	6.198	0.987
LH300-Span 20-S7-15%-A (W)	15.01	2.02	5.25	12.09	1.916	6.301	0.882
LH300-dSpan 20-S7-5%-A (W)	4.96	2.07	5.19	13.69	2.236	4.947	0.697
LH300-dSpan 20-S7-10%-A (W)	10.16	1.98	4.84	10.99	1.860	5.991	0.373
LH300-dSpan 20-S7-15%-A (W)	15.34	1.99	4.89	11.23	1.886	6.007	0.292
Inhalac 500-01-5%-A (W)	4.84	3.48	10.28	19.04	1.513	10.924	1.653
Inhalac 500-01-10%-A (W)	9.99	3.03	9.74	18.69	1.607	10.46	0.739
Inhalac 500-01-15%-A (W)	15.48	2.84	9.48	18.53	1.655	10.243	0.522
Inhalac 500-Span 20-S4-5%-A (W)	6.01	1.88	4.02	7.75	1.460	4.469	1.962
Inhalac 500-Span 20-S4-10%-A (W)	10.46	1.95	4.05	7.70	1.419	4.493	1.349
Inhalac 500-Span 20-S4-15%-A (W)	15.08	1.92	4.01	7.67	1.433	4.459	0.971
Inhalac 500-dSpan 20-S4-5%-A (W)	6.01	1.88	4.02	7.75	1.460	4.469	1.962
Inhalac 500-dSpan 20-S4-10%-A (W)	10.46	1.95	4.05	7.70	1.419	4.493	1.349
Inhalac 500-dSpan 20-S4-15%-A (W)	15.08	1.92	4.01	7.67	1.433	4.459	0.971
Inhalac 500-Span 20-S7-10%-A (W)	11.06	1.75	3.94	8.05	1.597	4.484	0.78
Inhalac 500-Span 20-S7-15%-A (W)	16.98	1.72	3.90	8.01	1.612	4.448	0.745
Inhalac 500-dSpan 20-S7-5%-A (W)	5.03	1.80	3.97	7.99	1.558	4.493	0.956
Inhalac 500-dSpan 20-S7-10%-A (W)	10.38	1.78	3.89	7.868	1.561	4.28	0.739
Inhalac 500-dSpan 20-S7-15%-A (W)	14.9	1.74	3.85	7.802	1.57	4.376	0.497

* W means wet analysis, dSpan20 means double span 20; In the sonication, “S4” stands for speed 4 and “S7” stands for speed 7.

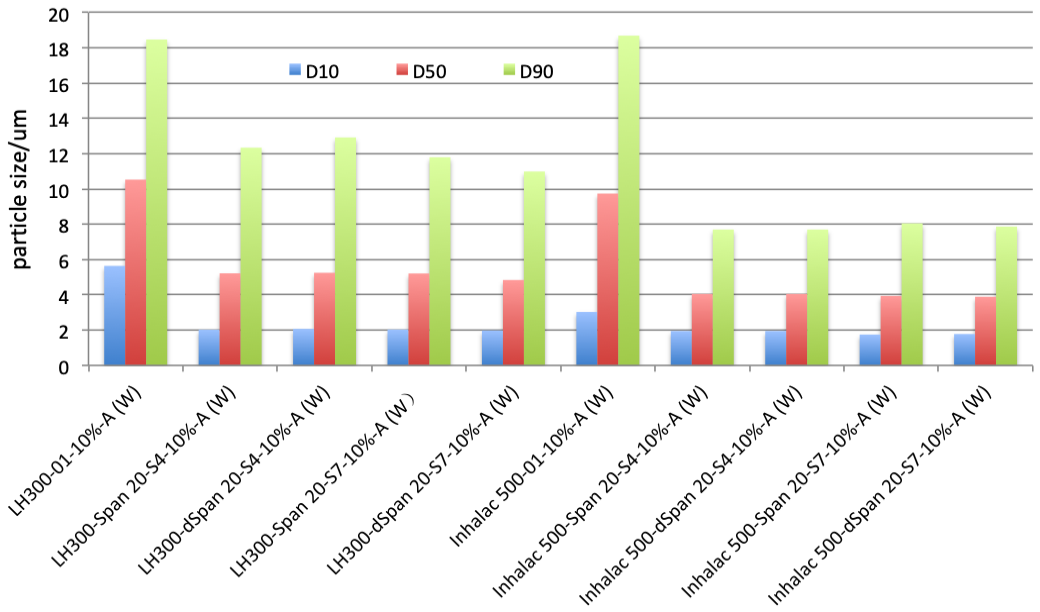

Figure 47. D10,D50, D90 of LH300 and Inhalac500 from wet analysis

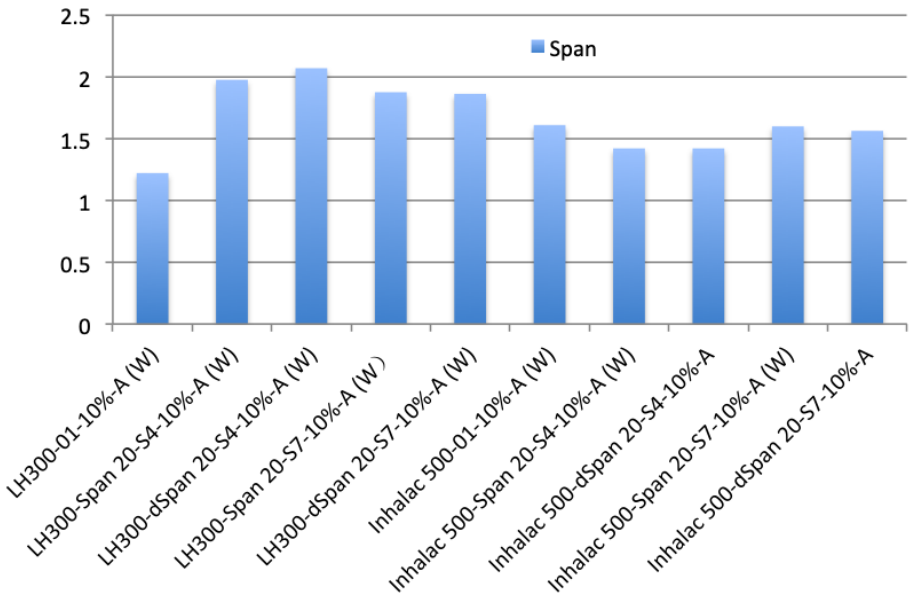

Figure 48. The span of LH300 and Inhalac500 from wet analysis

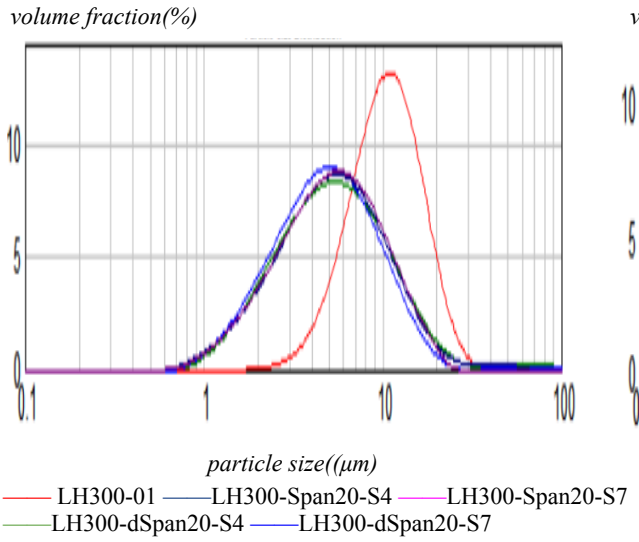

Figure 49. The Malvern wet measurement in gp mode of LH300-10%

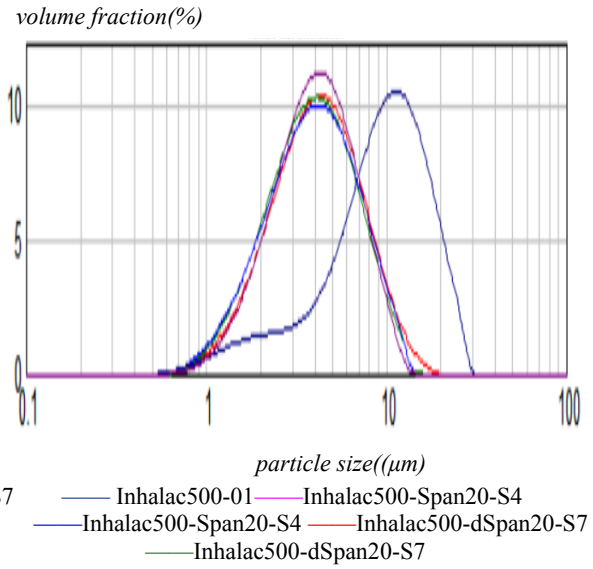

Figure 50. The Malvern wet measurement in gp mode of Inhalac 500-10%

b) Compare Fraunhofer and Mie theory in wet analysis

The data from **Table 12** are shown in **Figure 51 and 52**. When comparing Fraunhofer and Mie theory applied to the Malvern wet of lactose fines, it is clear that there were smaller particle sizes of D10, D50 and D90 in Mie theory in **Figure 51**; while the larger percentage of fine particles is given in **Figure 52**. Inhalac 500 has more fine particles than LH300 based on curves in **Figure 53**. Therefore, Mie theory is more suitable for fine particles less than 10μm in wet analysis, because the refractive index and absorptivity of material can be considered, which makes the analysis more accurate. But Mie theory gives bigger weighted residues, so it is hard to judge which theory is more acceptable because the two theories both work for fine lactoses in the wet analysis.

Table 12. The data in Fraunhofer and Mie theory from Malvern wet analysis of lactose fines(LH300 and Inhalac500)

Sample	Obscuration (%)	D10 (μm)	D50 (μm)	D90 (μm)	Span	D [4,3] (μm)	Percent <10 μm (%)	Weighted residues
LH300-dSpan 20-S7-5%-A (F)	4.96	2.07	5.20	13.69	2.236	4.95	81.64	0.697
LH300-dSpan 20-S7-10%-A (F)	10.16	1.99	4.85	11.00	1.860	5.99	86.88	0.373
LH300-dSpan 20-S7-15%-A (F)	15.34	1.99	4.90	11.23	1.886	6.01	86.13	0.292
LH300-dSpan 20-S7-5%-A (M)	4.96	1.67	4.56	10.05	2.037	24.03	87.44	1.953
LH300-dSpan 20-S7-10%-A (M)	10.16	1.60	4.32	9.83	1.905	5.13	90.52	1.94
LH300-dSpan 20-S7-15%-A (M)	15.34	1.76	4.40	8.57	1.777	5.14	91.35	2.007
Inhalac500-dSpan 20-S7-5%-A (F)	5.03	1.80	3.97	7.99	1.558	4.49	96.44	0.956
Inhalac500-dSpan 20-S7-10%-A (F)	10.38	1.79	3.90	7.87	1.561	4.28	96.60	0.739
Inhalac500-dSpan 20-S7-15%-A (F)	14.90	1.75	3.86	7.80	1.57	4.38	96.86	0.497
Inhalac500-dSpan 20-S7-5%-A (M)	5.03	1.46	3.50	6.88	1.549	3.89	98.34	2.282
Inhalac500-dSpan 20-S7-10%-A (M)	10.38	1.50	3.50	6.83	1.526	3.88	98.49	2.292
Inhalac500-dSpan 20-S7-15%-A (M)	14.90	1.33	3.41	6.77	1.596	3.78	98.53	2.486

*A means average, F means “Fraunhofer theory”, M means “Mie theory” and S7 means “speed 7 in sonication”

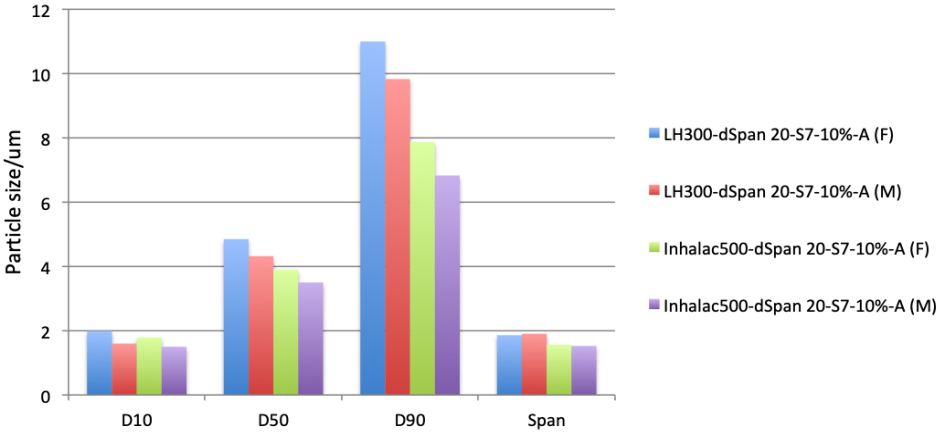

Figure 51. The span, D10, D50, D90 of fine lactoses compared Fraunhofer and Mie theory

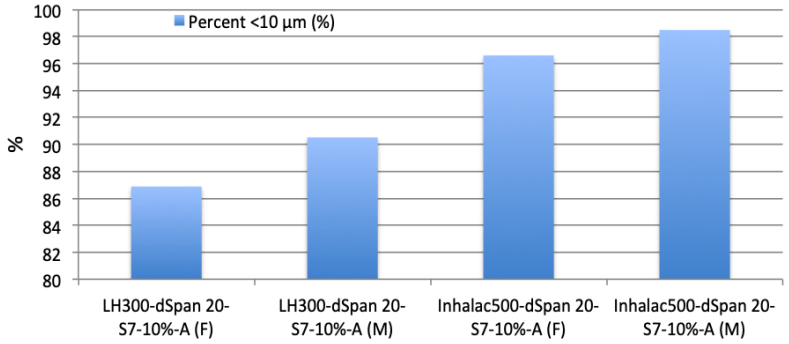

Figure 52. The percentage of particles smaller than 10μm of LH300 and Inhalac 500 compared Fraunhofer and Mie theory

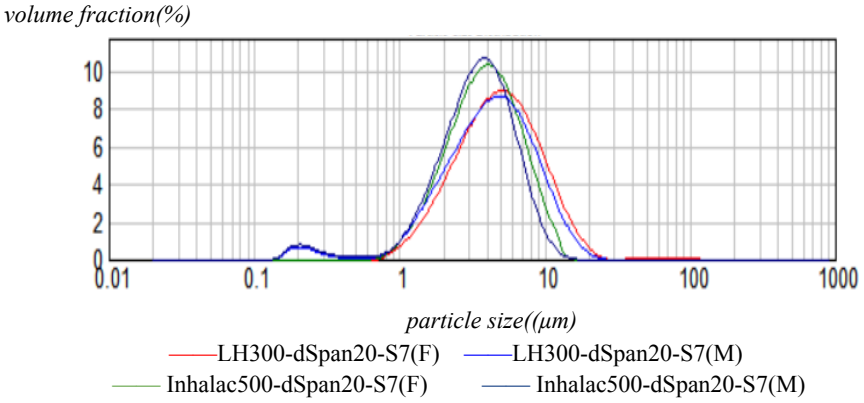

Figure 53. The Malvern wet measurement in Fraunhofer and Mie theory of LH300 and Inhalac500-10%

c) Dry analysis of lactose fines

From the dry analysis of lactose fines in **Table 13**, the curves at different jet pressures in **Figures 54 and 55** were obtained. Comparing **Figure 54 and Figure 55**, it can be seen that the first peak appears in the range 0.1-1 μm, which may be caused by the artifact of the instrument; the second peak in the range of 1-10 μm can be identified as fine lactose, but the curves of these peaks are random under different pressures. The third peak after 100 μm is due to the aggregation of fine powders. Therefore, fine lactose is not suitable for analysis by Malvern dry.

Table 13.The data from Malvern dry analysis of lactose fines(LH300 and Inhalac500)

Sample	Obscuration (%)	D10 (μm)	D50 (μm)	D90 (μm)	Span	D [4,3] (μm)	Weighted residues
LH300-P3-average (D)	/	2.22	7.63	24.18	2.863	35.880	0.248
LH300-P8-average (D)	/	1.84	6.92	572.96	82.413	121.98	0.560
LH300-P10-average (D)	/	1.87	7.33	686.43	93.400	178.71	0.724
Inhalac 500-P3-average (D)	/	1.38	6.65	18.64	2.5920	18.34	0.332
Inhalac 500-P8-average (D)	/	2.03	7.43	433.48	58.0533	91.26	0.314
Inhalac 500-P10-average (D)	/	1.75	7.16	676.12	94.26	172.79	0.781

"D"stand for dry analysis, "P3" stand for jet pressure 3, "P8" stand for jet pressure 8 and "P10" stands for jet pressure 10

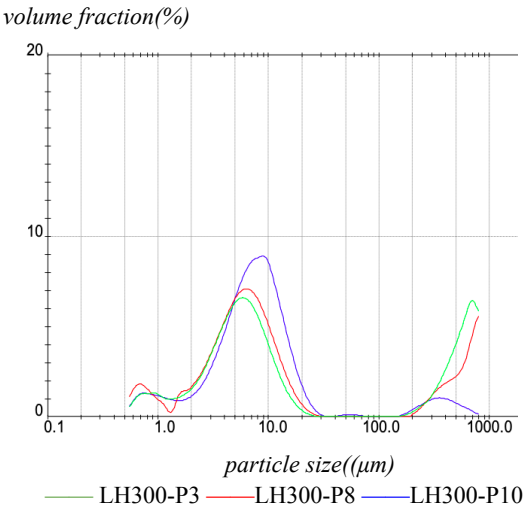

Figure 54. The Malvern dry measurement of LH300

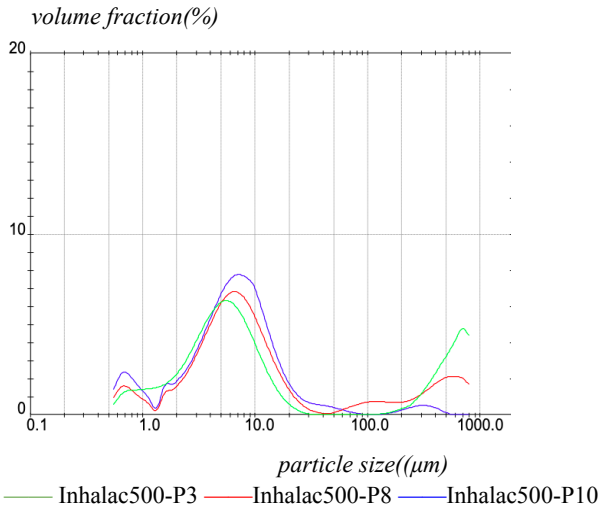

Figure 55. The Malvern dry measurement of Inhalac 500

4.6 Lactose blends

4.6.1 Pictures of LI and SI obtained by SEM

LI and SI are mixtures of LH100 or SV003 with Inhalac 500 in a 19:1 ratio, which means 5% of added fines. The blends were mixed in the Turbula mixer, see section 3.2. Mixtures LI and SI are shown by SEM in **Figure 56 and 57**. It can be seen that at the same magnification of 50, LI has larger particles than SI because of the larger carrier, and most particles of carrier lactoses (LH100 and SV003) are tomahawk-shaped. On the right of **Figure 56**, it can be seen that fine lactose with irregular shape accumulates in a recess on the surface of LH100, which are active sites caused by the heterogeneity of the carrier surface. (Pilcer et al., 2012) On the right of **Figure 57**, there are more fine particles or formed agglomerates adhering to the surface of the carrier SV003.

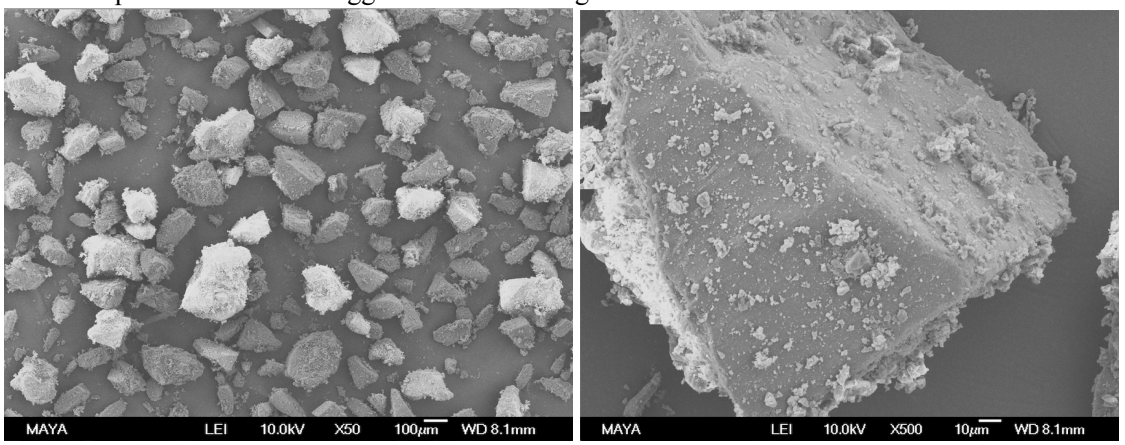

Figure 56. The image of LI with a magnification of 50(left) and 500(right) by SEM

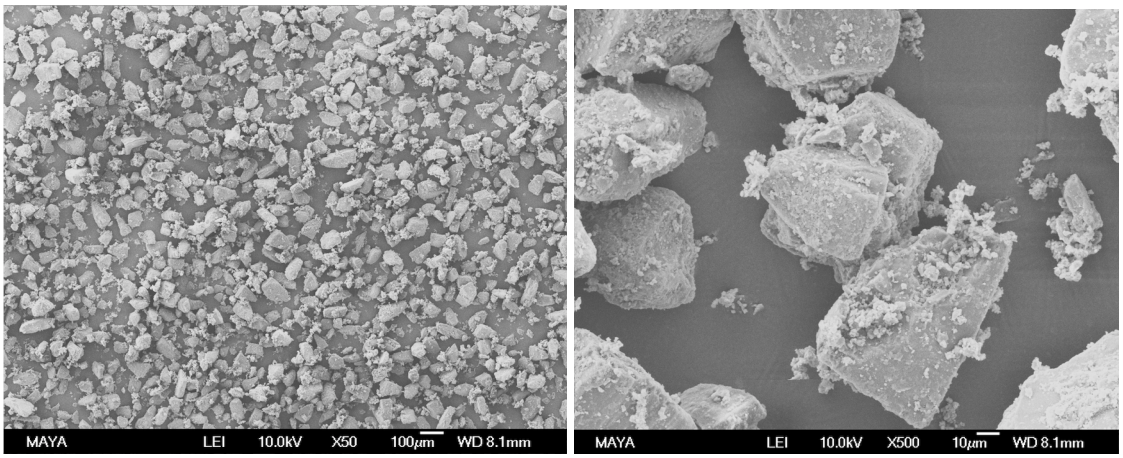

Figure 57. The image of SI with a magnification of 50 (left) and 500(right) by SEM

4.6.2 Comparison of the different methods for the blend

10% of Obscuration is selected for the further discussion of the blend powders. Compare **Figure 58 and 59,** it is more clear to distinguish two peaks of pure excipients in the mn mode. In **Figure 60 and 61**, there are two main peaks in the curve of blend powders, one is for lactose fine, another is for lactose carrier, and blend powders prepared with Span 20 and sonication showmore fine particles. In LI, it is noticeable that the peak of LH100 in LI is shifted compared to the wet analysis of the lactose carrier only. The further control experiment of LH100 in double span20 and sonication will be presented in section 4.6.3. In SI, there is an additional peak larger than 100µm due to powders aggregated. Compare LI/SI and LI/SI prepared with dSpan20 and sonication in **Table 14**, the percentage of particles less than 10µm are at around 30% in LI-dSpan20-S4 and 18% in SI-dSpan20-S4. However, fine particles were only 5% of the blended powders. The discrepancy is probably caused by a non-linear relationship between added fine lactose and measured fine particles of the blended powder. (Thalberg et al., 2012)

Referring to the dry analysis in **Figure 62 and 63**, it can be seen that there are two peaks in the

curve of blend powder, one is for fine lactose and another is for lactose carrier. But the repeatability of three batches is bad due to different jet pressure, which could be because higher pressure can release more fines but also lead to aggregates. Therefore, the best setting of jet pressure of the blends should be between 3 and 7.

Table 14. The data from Malvern wet analysis of LI and SI

Sample	Obscuration (%)	D10 (µm)	D50 (µm)	D90 (µm)	Span	D [4,3] (µm)	Weighted residues	Percentage less than 10 µm(%)
LI-01-10%-A(Wgp)	9.90	55.37	140.29	247.92	1.373	145.97	0.551	5.3
LI-01-10%-A(Wmn)	9.90	45.71	142.59	227.74	1.277	142.03	0.157	5.48
LI-dspan20-S4-10% (Wgp)	10.34	2.89	58.31	141.43	2.376	62.48	3.565	30.8
LI-dspan20-S4-10% (Wmn)	10.34	2.96	61.61	151.41	2.411	67.30	3.77	29.75
SI-01-10%-A(Wgp)	10.20	16.87	68.35	161.40	2.115	96.38	0.534	7.96
SI-01-10%-A(Wmn)	10.20	16.42	68.98	211.49	2.828	101.30	0.248	7.54
SI-dspan20-S4-10% (Wgp)	9.96	4.42	64.63	138.49	2.074	68.99	1.825	17.33
SI-dspan20-S4-10% (Wmn)	9.96	4.05	63.13	148.89	2.295	69.54	2.034	18.88

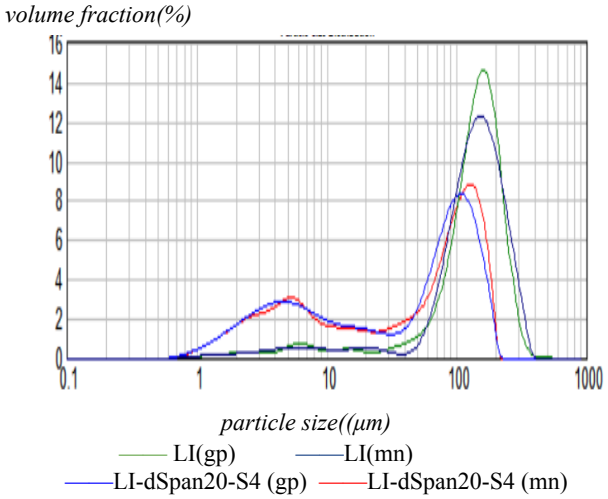

Figure 58. The Malvern wet analysis for 10% obscuration of LI and LI-dSpan20

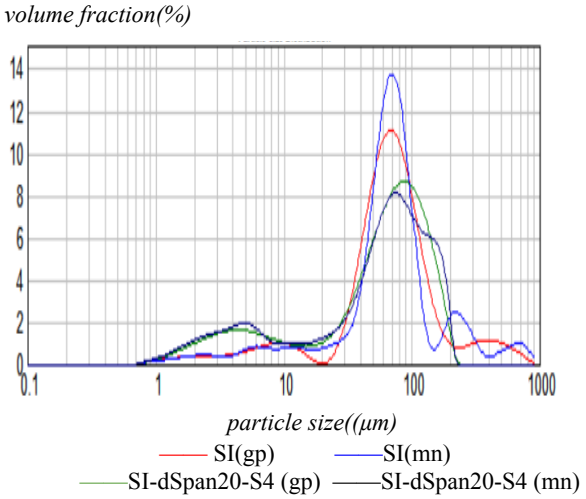

Figure 59. The Malvern wet analysis for 10% obscuration of SI and SI-dSpan20

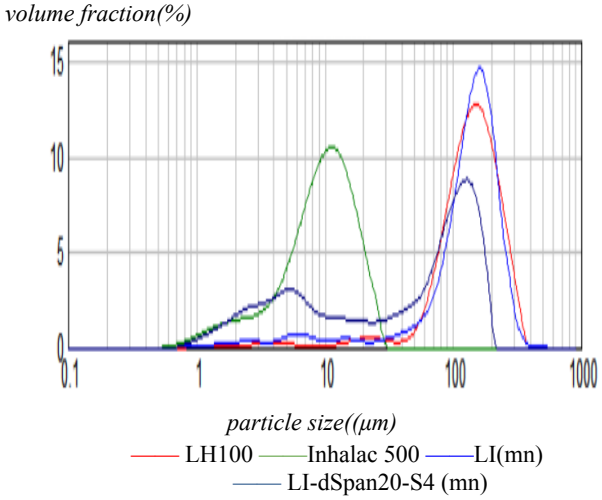

Figure 60. The Malvern wet analysis in mn mode of LH100, Inhalac500,LI and LI-dSpan20

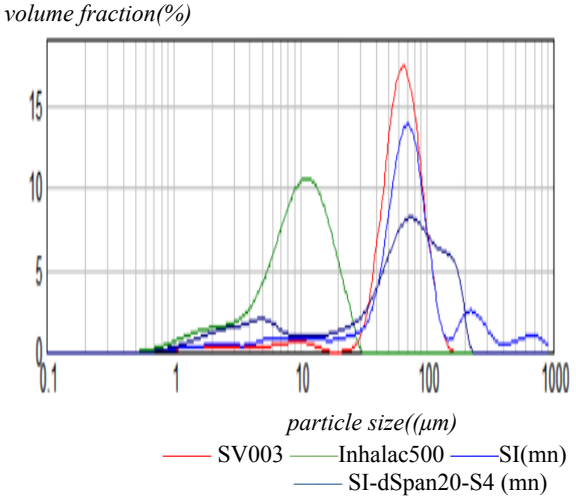

Figure 61. The Malvern wet analysis in mn mode of SV003, Inhalac500, SI and SI-dSpan20

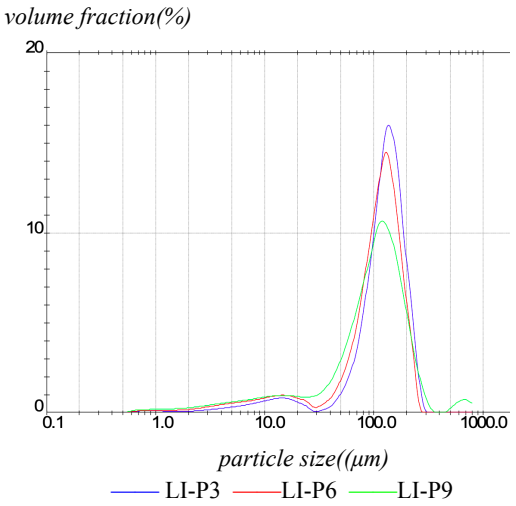

Figure 62. The Malvern dry measurement of LI

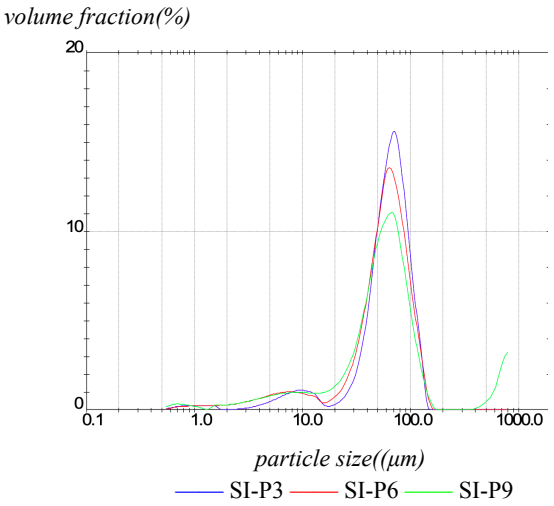

Figure 63. The Malvern dry measurement of SI

4.6.3 Control experiment: Sonication of different lactose carriers with dSpan

Compare **Table 9** and **Table 15** of lactose carriers, it can be seen that there is no big difference between SV001/SV003 and SV001/SV003 conditioned with double Span20 and sonication, but it is clear that the particle size of LH100 in blend powder is lower than its pure LH100 in wet analysis in **Figure 60**. In order to check what happened to the particles of LH100 in this process, light microscopy was used to collect pictures of the pure excipient, with Span20 addition, and after sonication in **Figure 64, 65 and 66**. Compare **Figure 64 and 65** at the magnification of 2, 5 and 10, it can be observed that LH100 particles added with Span20 have little change in particle size and density of particles compared to its pure excipient. However, in **Figure 66**, it is obvious that the LH100 particles were completely destroyed or broken after sonication, and formed a lot of fine particles, which was not the desired result.The other reason for the shifted LH100 could be the presence of line voids or cracks with different orientations on the surface of LH100 as shown in **Figure 67**, which could explain the fracture of the particles in diffraction.(Gajjar et al., 2020) Therefore, LH100 is not suitable for sonication.

Table 15. The control experiment with sonication for carrier lactose

Sample	Obscuration (%)	D10 (μm)	D50 (μm)	D90 (μm)	Span	D [4,3] (μm)	Weighted residues
SV001-dspan20-5%-A (W)	4.24	125.34	229.08	352.80	0.993	230.06	0.661
SV001-dspan20-10%-A (W)	10.58	125.80	228.78	362.46	1.034	232.84	0.725
SV001-dspan20-15%-A (W)	14.26	117.86	221.21	348.54	1.044	223.55	0.744
SV003-dSpan20-02-5%-A (W)	5.17	35.57	67.12	111.20	1.121	69.55	0.801
SV003-dSpan20-02-10%-A (W)	10.61	34.20	75.26	147.34	1.500	83.92	0.495
SV003-dSpan20-02-15%-A (W)	14.88	35.19	83.01	178.67	1.720	96.64	0.440

*A means average, W means wet analysis.

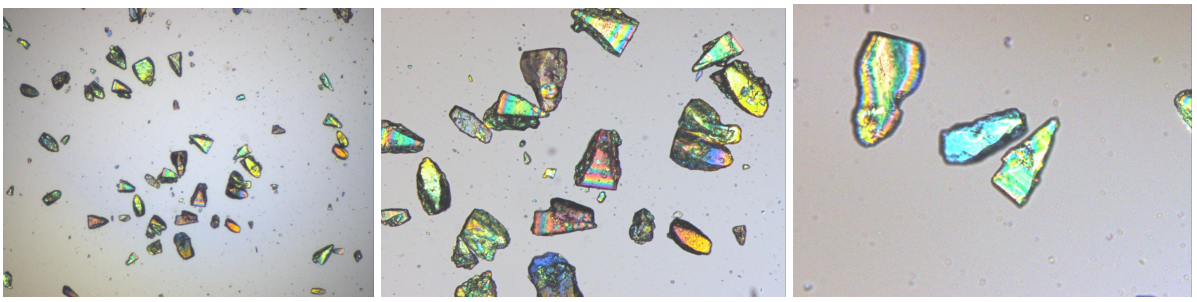

Figure 64. The images of LH100 at a magnification of 2(left), 5(middle) and 10(right) by light microscopy

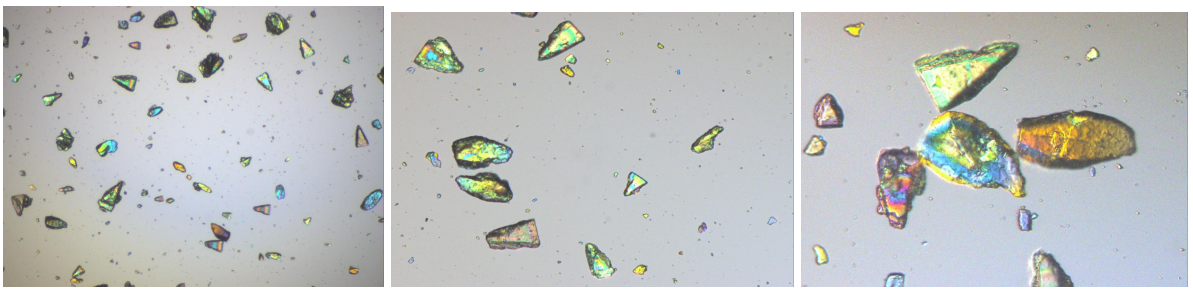

Figure 65. The images of LH100 with Span20 at a magnification of 2(left), 5(middle) and 10(right) by light microscopy

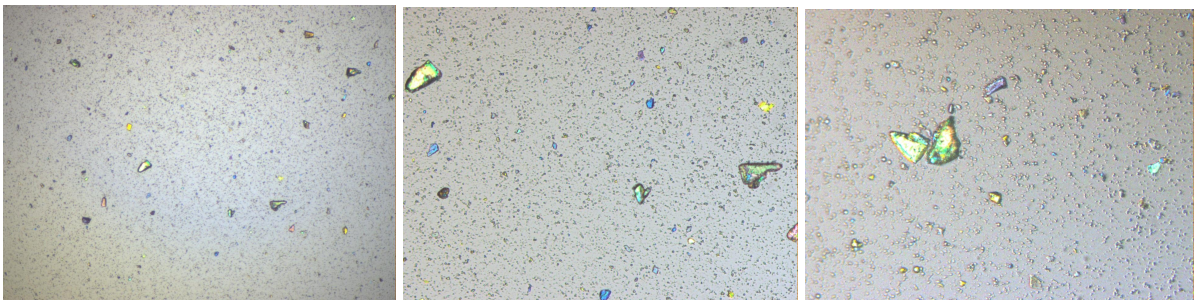

Figure 66. The images of LH100 with Span20 and Sonication at a magnification of 2(left), 5(middle) and 10(right) by light microscopy

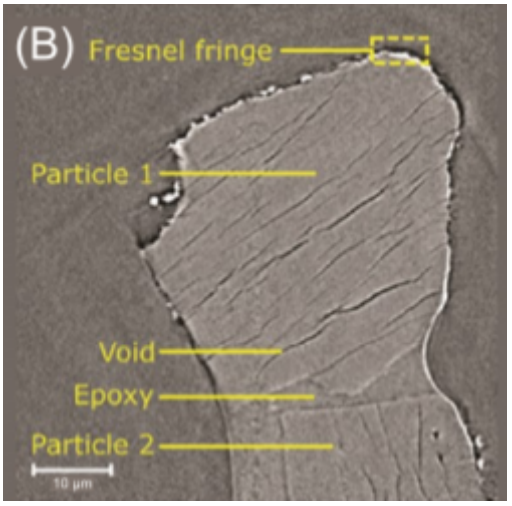

Figure 67. The the surface of lactose carrier scanned by the nano-XRM (Gajjar et al., 2020)

5. Conclusion

In conclusion, the following results are obtained through measuring the particle size of pure excipients and mixtures with different particle-sizing analysis methods :

1) In Malvern wet:
    a) Obscuration: the obscuration with lower weighted residues needs to be selected due to better accuracy.
    b) Sonication: wet analysis cannot accurately detect the dispersion of fine particles (LH300 and Inhalac 500), hence a higher intensity of sonication and a surfactant like Span 20 are required to enhance the fraction of fine particles. Whether sonication will destroy or disintegrate the particles depends on the presence of internal cracks or line voids in the particles, as was the case for LH100.
    c) Light scattering theory: determining whether the Fraunhofer and Mie theories are superior is difficult because two theories are both good based on the obtained data.
    d) Different modes: single mode is preferred for pure excipients to give the main peak with narrower span and in great agreement with the specification. Multiple narrow modes can identify blended powders better with the peaks of original excipients on a mixture curve.
    e) Blended powders: The ratio of original excipients needs to be considered to find an optimum condition assessing the particle size of a mixture. Furthermore, a non-linear relationship between added fine particles and measured fine particles of the lactoses blend was found by the Malvern method. A non-linear relation was also found for the CSCB and CMMCC blends. It seems that the lower particle size excipient in the blend powders is always overestimated in Malvern wet analysis.
2) In Malvern dry, there would be a loss of powders due to the fact that fine powder is difficult to be delivered to the detector and large particles remain on the feeder tray. The loss of fines has a bigger impact, thus it is not suitable for measuring very fine particles. Referring to the setting of jet pressure, too much pressure may cause particle aggregation, therefore pressure in the range of 2-7 is reasonable. Overall, in Malvern analysis, precision is both high in wet and dry analysis.
3) Comparing the Qicpic and Malvern method in **Figure 68,** D50 values from Qicpic are very consistent with the Malvern method (wet and dry). The closer the shape of the particle is to the sphere, the closer the results of the two methods are. D50 shows essentially the same trend in Qicpic and Malvern method, which could be that the sphericity of the selected excipient particle sizes is almost always above 0.65, which makes the relatively small errors of the methods based on different principles. In **Figure 68**, although CM has the lowest sphericity, the Qicpic and Malvern analysis are in good agreement. The reason could be that its broader particle size distribution makes the effect of shape changes insignificant. However, regardless of the sphericity, elongated particles (SBF) would get lower qicpic results.

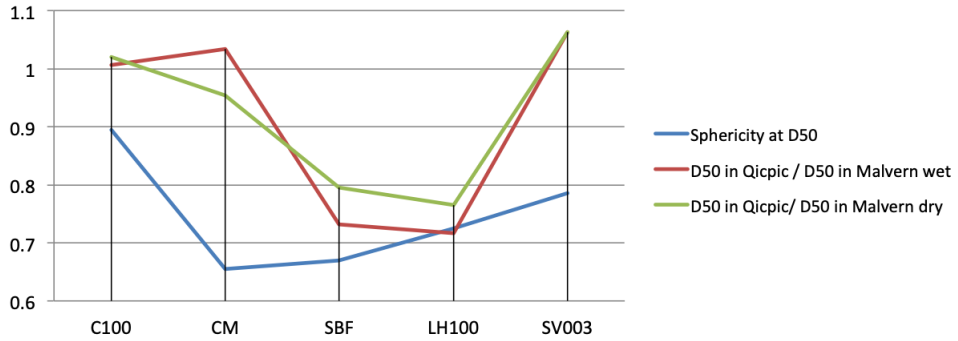

Figure 68. Correlation between the sphericity of excipients and the ratio of D50 under different methods

4) The principle of Qicpic is closer to the real definition of particle size compared with other particle-sizing methods, as obtained 2D images are very consistent with real particles. The measured sphericity and aspect ratio curves show the relationship with particle size. Furthermore, Qicpic is not suitable for measuring fine particles as they are not in the test range or larger particles due to segregation and some white artifacts need to be ignored during the measurement. The obtained 3D images from SEM can assist the interpretation of the particle size data, surface morphology and its shape. It also has a greater adjustable magnification than Qicpic, allowing it to more accurately reflect the structure of the particle.

6. References

Chaudhary, R. S., Patel, C., Sevak, V., & Chan, M. (2018). Effect of Kollidon VA®64 particle size and morphology as directly compressible excipient on tablet compression properties. Drug development and industrial pharmacy, 44(1), 19–29. https://doi.org/10.1080/03639045.2017.1371735

Crowder, T. M., Rosati, J. A., Schroeter, J. D., Hickey, A. J., & Martonen, T. B. (2002). Fundamental effects of particle morphology on lung delivery: predictions of Stokes' law and the particular relevance to dry powder inhaler formulation and development. Pharmaceutical research, 19(3), 239–245. https://doi.org/10.1023/a:1014426530935

Ebrahim, S., Peyman, G. A., & Lee, P. J. (2005). Applications of liposomes in ophthalmology. Survey of ophthalmology, 50(2), 167–182. https://doi.org/10.1016/j.survophthal.2004.12.006

Edwards, D. A., Hanes, J., Caponetti, G., Hrkach, J., Ben-Jebria, A., Eskew, M. L., Mintzes, J., Deaver, D., Lotan, N., & Langer, R. (1997). Large porous particles for pulmonary drug delivery. Science (New York, N.Y.), 276(5320), 1868–1871. https://doi.org/10.1126/science.276.5320.1868

EP2714591A1 - Sodium bicarbonate product with excellent flowability and its method of manufacture - Google Patents. (2012, June). Retrieved May 22, 2022, from Google.com website: https://patents.google.com/patent/EP2714591A1/en

Gajjar, P., Bale, H., Burnett, T., Chen, X., Elliot, J. A., Gomez, H. V., … Murnane, D. (2020). Unlocking the Microstructure of Inhalation Blends using X-ray Microscopy. Herts.ac.uk. https://doi.org/PURE: 21505581

Hung, J. C. (2002). Comparison of various requirements of the quality assurance procedures for 18F-FDG injection. Journal of Nuclear Medicine, 43(11), 1495-1506. Retrieved May 10, 2022 from https://jnm.snmjournals.org/content/jnumed/43/11/1495.full.pdf

Kompella, U. B., Kadam, R. S., & Lee, V. H. (2010). Recent advances in ophthalmic drug delivery. Therapeutic delivery, 1(3), 435–456. https://doi.org/10.4155/TDE.10.40

Markl, D., Zettl, M., Hannesschläger, G., Sacher, S., Leitner, M., Buchsbaum, A., & Khinast, J. G. (2015). Calibration-free in-line monitoring of pellet coating processes via optical coherence tomography. Chemical Engineering Science, 125, 200–208. https://doi.org/10.1016/j.ces.2014.05.049

Merkus, H.G. (2009). Particle Size, Size Distributions and Shape. In: Particle Size Measurements. Particle Technology Series, vol 17. Springer, Dordrecht. https://doi.org/10.1007/978-1-4020-9016-5_2

Particle Size Distribution Calculation Method. (2022). Retrieved May 17, 2022, from Shimadzu.com website: https://www.shimadzu.com/an/service-support/technical-support/analysis-basics/lesson22.html

Pilcer, G., Wauthoz, N., & Amighi, K. (2012). Lactose characteristics and the generation of the aerosol. Advanced drug delivery reviews, 64(3), 233–256. https://doi.org/10.1016/j.addr.2011.05.003

Prow, T. W., Grice, J. E., Lin, L. L., Faye, R., Butler, M., Becker, W., Wurm, E. M., Yoong, C., Robertson, T. A., Soyer, H. P., & Roberts, M. S. (2011). Nanoparticles and microparticles for skin drug delivery. Advanced drug delivery reviews, 63(6), 470–491. https://doi.org/10.1016/j.addr.2011.01.012

Rabinow B. E. (2004). Nanosuspensions in drug delivery. Nature reviews. Drug discovery, 3(9), 785–796. https://doi.org/10.1038/nrd1494

Rolland, A.P. (1993). Particulate carriers in dermal and transdermal drug delivery: myth or reality? Drugs and the pharmaceutical sciences, 61, 367-421.

Sarkar, S., Liew, C.V. Moistening Liquid-Dependent De-aggregation of Microcrystalline Cellulose and Its Impact on Pellet Formation by Extrusion–Spheronization. AAPS PharmSciTech 15, 753–761 (2014). https://doi.org/10.1208/s12249-014-0098-7

Shekunov B. (2005). Nanoparticle technology for drug delivery: from nanoparticles to cutting-edge delivery strategies - part I. IDrugs : the investigational drugs journal, 8(5), 399–401.

Shekunov, B. Y., Chattopadhyay, P., Tong, H. H., & Chow, A. H. (2007). Particle size analysis in pharmaceutics: principles, methods and applications. Pharmaceutical research, 24(2), 203–227. https://doi.org/10.1007/s11095-006-9146-7

Shur, J., Harris, H., Jones, M. D., Kaerger, J. S., & Price, R. (2008). The role of fines in the modification of the fluidization and dispersion mechanism within dry powder inhaler formulations. Pharmaceutical research, 25(7), 1631–1640. https://doi.org/10.1007/s11095-008-9538-y

Sun, Y., Qin, L., Li, J., Su, J., Song, R., Zhang, X., Guan, J., & Mao, S. (2021). Elucidating the Effect of Fine Lactose Ratio on the Rheological Properties and Aerodynamic Behavior of Dry Powder for Inhalation. The AAPS journal, 23(3), 55. https://doi.org/10.1208/s12248-021-00582-0

Thalberg, K., Berg, E., & Fransson, M. (2012). Modeling dispersion of dry powders for inhalation. The concepts of total fines, cohesive energy and interaction parameters. International Journal of Pharmaceutics, 427(2), 224–233. https://doi.org/10.1016/j.ijpharm.2012.02.009

The miracle of the skins lipid layer! (2019). Retrieved May 17, 2022, from HealthPost NZ website: https://www.healthpost.co.nz/blog/the-miracle-of-the-skins-lipid-layer/

Williams, A. (2003). Transdermal and topical drug delivery from theory to clinical practice. Pharmaceutical press. Retrieved May 11, 2022 from https://webcache.googleusercontent.com/search?q=cache:TieEKFQ86TIJ:https://pharmacyeducation.fip.org/pharmacyeducation/article/download/62/45/108+&cd=4&hl=zh-CN&ct=clnk&gl=se

Williams, D. B., & Carter, C. B. (1996). The transmission electron microscope. In Transmission electron microscopy (pp. 3-17). Springer, Boston, MA. Retrieved May 11, 2022 from http://dl.iran-mavad.com/pdf95/TEM-Williams%20&%20Carter_iran-mavad.com.pdf

Yang, J., & Chen, S. (2016). An online detection system for aggregate sizes and shapes based on digital image processing. Mineralogy and Petrology, 111(1), 135–144. https://doi.org/10.1007/s00710-016-0458-y

Yu, W., & Hancock, B. C. (2008). Evaluation of dynamic image analysis for characterizing pharmaceutical excipient particles. International journal of pharmaceutics, 361(1-2), 150-157. https://doi.org/10.1016/j.ijpharm.2008.05.025

Zetasizer Nano Analysis Methods Explained (2010, November 24) Retrieved May 15, 2022 from https://www.malvernpanalytical.com/en/learn/knowledge-center/technical-notes/tn101124zetasizernanoanalysismethodsexplained

Zhao, H., Kwak, J. H., Zhang, Z. C., Brown, H. M., Arey, B. W., & Holladay, J. E. (2007). Studying cellulose fiber structure by SEM, XRD, NMR and acid hydrolysis. Carbohydrate polymers, 68(2), 235-241. https://doi.org/10.1016/j.carbpol.2006.12.013

Appendix A:
The raw data of pure excipients in gp mode and sm mode from wet analysis without sonication

Sample	Obscuration (%)	D10 (μm)	D50 (μm)	D90 (μm)	Span	D [4,3] (μm)	Weighted residues
LH100-01-5% (Wgp)	4.74	72.243	142.818	246.879	1.223	150.869	/
LH100-01-5% (Wgp)	4.74	72.19	144.593	252.52	1.247	153.195	/
LH100-01-5% (Wgp)	4.77	72.042	144.083	250.457	1.238	152.319	/
LH100-01-5%-A (Wgp)	4.75	72.159	143.824	249.973	1.236	152.128	0.506
LH100-01-10% (Wgp)	9.79	70.615	141.951	246.846	1.241	150.004	/
LH100-01-10% (Wgp)	9.8	70.082	141.674	246.614	1.246	149.69	/
LH100-01-10% (Wgp)	9.83	70.475	142.109	247.375	1.245	150.175	/
LH100-01-10%-A (Wgp)	9.81	70.389	141.911	246.946	1.244	149.956	0.526
LH100-01-15% (Wgp)	15.21	69.931	141.485	246.874	1.251	149.615	/
LH100-01-15% (Wgp)	15.05	69.233	140.056	242.081	1.234	147.423	/
LH100-01-15% (Wgp)	15.14	69.686	141.393	245.235	1.242	149.011	/
LH100-01-15%-A (Wgp)	15.13	69.619	140.974	244.732	1.242	148.683	0.587
SV001-01-5% (Wgp)	4.28	135.989	220.291	348.932	0.967	231.428	/
SV001-01-5% (Wgp)	3.96	136.636	221.913	350.781	0.965	232.642	/
SV001-01-5% (Wgp)	3.63	132.336	218.173	339.107	0.948	225.078	/
SV001-01-5%-A (Wgp)	3.95	135.116	220.094	346.352	0.96	229.716	0.94
SV001-01-10% (Wgp)	9.81	144.812	226.278	347.282	0.895	235.992	/
SV001-01-10% (Wgp)	9.54	144.46	225.955	346.303	0.893	235.401	/
SV001-01-10% (Wgp)	9.05	142.682	225.957	339.613	0.872	231.178	/
SV001-01-10%-A (Wgp)	9.46	144.266	226.063	343.976	0.883	234.19	0.824
SV001-01-15% (Wgp)	14.48	144.746	226.459	347.452	0.895	235.932	/
SV001-01-15% (Wgp)	14.52	145.176	227.672	349.832	0.899	237.22	/
SV001-01-15% (Wgp)	14.53	144.914	227.064	348.963	0.899	236.615	/
SV001-01-15%-A (Wgp)	14.51	144.949	22.063	348.756	0.898	236.589	0.924
SV003-01-5% (Wgp)	5.56	37.33	64.627	101.942	1	66.36	/
SV003-01-5% (Wgp)	5.55	38.193	63.926	97.285	0.927	64.903	/
SV003-01-5% (Wgp)	5.55	36.899	61.855	97.205	0.926	62.997	/
SV003-01-5%-A (Wgp)	5.55	37.563	63.359	97.929	0.953	64.953	1.221
SV003-01-10% (Wgp)	9.85	37.727	63.397	96.657	0.93	64.442	/
SV003-01-10% (Wgp)	9.94	37.596	63.426	96.853	0.934	64.465	/
SV003-01-10% (Wgp)	10.04	37.366	63.166	96.477	0.936	64.181	/
SV003-01-10%-A (Wgp)	9.94	37.562	63.329	96.663	0.933	64.363	1.137
SV003-01-15% (Wgp)	15.92	35.157	62.178	98.564	1.02	63.807	/
SV003-01-15% (Wgp)	16.07	34.891	61.868	98.03	1.021	63.446	/
SV003-01-15% (Wgp)	16.2	34.774	61.911	98.178	1.024	63.472	/
SV003-01-15%-A (Wgp)	16.06	34.939	61.986	98.259	1.022	63.575	0.95
CM-01-5% (Wgp)	4.42	15.521	58.001	134.51	2.051	67.376	/
CM-01-5% (Wgp)	4.39	15.408	57.518	132.192	2.03	66.436	/
CM-01-5% (Wgp)	4.37	15.295	57.307	135.289	2.094	67.188	/
CM-01-5%-A (Wgp)	4.39	15.408	57.609	133.977	2.058	67	2.508
CM-01-10% (Wgp)	10.05	16.603	60.345	136.439	1.986	69.215	/
CM-01-10% (Wgp)	10.31	16.633	60.592	137.684	1.998	69.693	/

CM-01-10% (Wgp)	10.36	15.089	57.585	133.17	2.051	66.668	/
CM-01-10%-A (Wgp)	10.31	16.091	59.511	135.784	2.011	68.525	1.613
CM-01-15% (Wgp)	14.85	16.791	61.731	138.864	1.978	70.577	/
CM-01-15% (Wgp)	15	16.773	61.839	138.912	1.975	70.626	/
CM-01-15% (Wgp)	15.16	16.885	62.002	139.186	1.973	70.804	/
CM-01-15%-A (Wgp)	15	16.816	61.857	138.988	1.975	70.669	1.125
CM-01-5%-A (Wsm)	4.39	18.203	58.736	121.721	1.763	66.135	2.107
CM-01-10%-A (Wsm)	10.31	17.262	60.844	127.807	1.816	68.552	1.416
CM-01-15%-A (Wsm)	15	17.127	63.028	132.556	1.831	70.929	1.024
C100-01-5% (Wgp)	4.27	113.438	154.651	212.112	0.638	159.286	/
C100-01-5% (Wgp)	4.17	113.193	154.176	210.968	0.634	158.73	/
C100-01-5% (Wgp)	4.14	113.203	154.194	211.113	0.635	158.779	/
C100-01-5%-A (Wgp)	4.19	113.277	154.34	211.397	0.636	158.932	0.671
C100-01-10% (Wgp)	9.42	112.508	153.413	210.386	0.638	158.088	/
C100-01-10% (Wgp)	9.46	112.507	153.505	210.76	0.64	158.223	/
C100-01-10% (Wgp)	9.43	112.154	152.995	209.673	0.637	157.653	/
C100-01-10%-A (Wgp)	9.44	112.388	153.304	210.277	0.639	157.988	0.633
C100-01-15% (Wgp)	15.43	111.521	152.226	208.071	0.634	156.791	/
C100-01-15% (Wgp)	15.5	111.22	151.974	206.835	0.63	156.183	/
C100-01-15% (Wgp)	15.55	111.345	151.933	207.247	0.631	156.388	/
C100-01-15%-A (Wgp)	15.49	111.361	151.767	207.388	0.632	156.454	0.639
C100-01-5%-A (Wsm)	4.19	118.202	152.747	200.284	0.537	156.427	0.46
C100-01-10%-A (Wsm)	9.44	120.925	154.467	199.051	0.506	157.853	0.310
C100-01-15%-A (Wsm)	15.49	117.686	150.545	197.204	0.528	154.304	0.319
C200-01-5% (Wgp)	4.13	192.92	262.277	356.474	0.624	269.605	/
C200-01-5% (Wgp)	4.17	196.07	266.964	362.153	0.622	274.233	/
C200-01-5% (Wgp)	3.99	196.122	266.863	261.496	0.62	273.999	/
C200-01-5%-A (Wgp)	4.1	194.964	265.361	360.026	0.622	272.613	1.919
C200-01-10% (Wgp)	9.9	199.099	269.891	362.986	0.607	277.302	/
C200-01-10% (Wgp)	10.06	199.449	269.849	361.877	0.602	277.079	/
C200-01-10% (Wgp)	9.9	199.681	270.309	362.842	0.604	277.592	/
C200-01-10%-A (Wgp)	9.98	199.409	270.016	362.57	0.604	277.324	1.34
C200-01-15% (Wgp)	15.38	199.363	269.883	362.236	0.603	277.164	/
C200-01-15% (Wgp)	15.15	199.522	270.241	363.276	0.606	277.641	/
C200-01-15% (Wgp)	14.8	199.158	269.513	361.529	0.602	276.765	/
C200-01-15%-A (Wgp)	15.11	199.347	269.878	262.351	0.604	277.19	1.416
C200-01-5%-A (Wsm)	4.1	217.492	263.985	322.659	0.398	267.494	0.544
C200-01-10%-A (Wsm)	9.98	227.184	267.139	314.311	0.326	269.755	0.425
C200-01-15%-A (Wsm)	15.11	227.515	266.313	311.977	0.317	268.841	0.471
C350-01-5% (Wgp)	3.9	301.553	407.306	548.795	0.607	417.587	/
C350-01-5% (Wgp)	4.18	302.453	409.332	552.524	0.611	419.863	/
C350-01-5% (Wgp)	4.07	301.798	408.712	552.461	0.613	419.393	/
C350-01-5%-A (Wgp)	4.05	301.931	408.446	551.27	0.61	418.948	2.005
C350-01-10% (Wgp)	9.23	302.384	407.177	546.808	0.6	417.18	/
C350-01-10% (Wgp)	9.06	302.863	407.678	546.751	0.598	417.496	/
C350-01-10% (Wgp)	9.23	302.301	407.168	547.469	0.602	417.366	/
C350-01-10%-A (Wgp)	9.17	302.515	407.314	547.008	0.6	417.347	2.333

C350-01-15% (Wgp)	13.99	301.197	404.419	540.749	0.592	413.874	/
C350-01-15% (Wgp)	13.75	302.501	406.47	543.708	0.593	415.97	/
C350-01-15% (Wgp)	13.94	302.3	406.107	542.826	0.592	415.489	/
C350-01-15%-A (Wgp)	13.89	301.999	405.664	524.442	0.593	415.111	2.603
C350-01-5%-A (Wsm)	4.05	355.777	404.650	455.367	0.246	405.917	0.620
C350-01-10%-A (Wsm)	9.17	367.084	404.663	432.537	0.282	402.999	0.641
C350-01-15%-A (Wsm)	13.89	369.129	404.720	431.033	0.153	403.191	1.091
SBF-01-5% (Wgp)	6.3	88.592	136.748	205.178	0.853	141.822	/
SBF-01-5% (Wgp)	6	84.863	134.587	207.693	0.913	140.349	/
SBF-01-5% (Wgp)	5.72	87.549	134.994	202.541	0.852	140.025	/
SBF-01-5%-A (Wgp)	6.01	86.939	135.462	205.172	0.873	140.732	0.645
SBF-01-10% (Wgp)	9.93	84.803	134.754	208.729	0.92	140.775	/
SBF-01-10% (Wgp)	10.09	88.179	135.933	203.407	0.848	140.853	/
SBF-01-10% (Wgp)	9.98	84.631	134.064	206.6	0.91	139.735	/
SBF-01-10%-A (Wgp)	10	85.803	134.944	206.248	0.893	140.454	0.684
SBF-01-15% (Wgp)	14.88	84.651	134.176	206.439	0.908	139.729	/
SBF-01-15% (Wgp)	14.72	84.846	134.506	206.949	0.908	140.062	/
SBF-01-15% (Wgp)	14.68	84.511	133.993	206.522	0.911	139.639	/
SBF-01-15%-A (Wgp)	14.76	84.668	134.225	206.637	0.909	139.81	0.717
SBF-01-5%-A (Wsm)	6.01	84.65	137.92	198.97	0.829	138.787	0.270
SBF-01-10%-A (Wsm)	10	84.17	138.25	198.74	0.829	138.588	0.168
SBF-01-15%-A (Wsm)	14.76	83.75	138.02	197.99	0.828	138.109	0.159
SBS-01-5% (Wgp)	5.35	44.132	88.847	155.886	1.258	94.238	/
SBS-01-5% (Wgp)	5.33	43.273	86.757	150.675	1.238	91.587	/
SBS-01-5% (Wgp)	5.23	42.729	85.749	148.865	1.238	90.481	/
SBS-01-5%-A (Wgp)	5.3	43.364	87.099	151.812	1.245	92.102	0.523
SBS-01-10% (Wgp)	10.26	42.362	86.346	151.166	1.26	91.332	/
SBS-01-10% (Wgp)	10.29	42.223	86.286	150.506	1.255	91.085	/
SBS-01-10% (Wgp)	10.17	41.917	85.962	150.641	1.265	90.905	/
SBS-01-10%-A (Wgp)	10.24	42.172	86.198	150.771	1.26	91.108	0.497
SBS-01-15% (Wgp)	15.61	41.763	86.73	153.066	1.283	91.921	/
SBS-01-15% (Wgp)	15.7	41.411	86.147	151.958	1.283	91.258	/
SBS-01-15% (Wgp)	15.44	41.067	85.159	149.782	1.277	90.089	/
SBS-01-15%-A (Wgp)	15.58	41.407	86.008	151.609	1.281	91.09	0.439
SBS-01-5%-A (Wsm)	5.3	41.09	88.59	144.22	1.153	91.455	0.238
SBS-01-10%-A (Wsm)	10.24	39.67	87.53	142.05	1.170	89.791	0.170
SBS-01-15%-A (Wsm)	15.58	38.95	87.44	143.88	1.200	90.399	0.161
SBC-01-5% (Wgp)	4.86	236.786	390.723	619.117	0.979	410.093	/
SBC-01-5% (Wgp)	4.42	232.634	384.058	609.976	0.983	403.527	/
SBC-01-5% (Wgp)	4.19	227.903	373.995	594.242	0.98	393.429	/
SBC-01-5%-A (Wgp)	4.49	232.278	382.846	608.044	0.982	402.349	0.993
SBC-01-10% (Wgp)	9.55	240.354	379.304	584.58	0.908	396.626	/
SBC-01-10% (Wgp)	9.06	240.677	380.111	586.291	0.909	397.557	/
SBC-01-10% (Wgp)	9.21	239.987	380.994	599.406	0.943	402.983	/
SBC-01-10%-A (Wgp)	9.27	240.337	380.122	590.095	0.92	399.056	0.938
SBC-01-15% (Wgp)	15.72	235.469	389.986	622.953	0.994	410.582	/
SBC-01-15% (Wgp)	15.44	237.321	392.144	622.042	0.981	411.743	/

SBC-01-15% (Wgp)	15.36	227.938	374.979	598.887	0.989	395.287	/
SBC-01-15%-A (Wgp)	15.51	223.398	385.612	614.946	0.989	405.87	0.953
SBC-01-5%-A (Wsm)	4.49	232.22	383.51	550.20	0.829	388.601	0.582
SBC-01-10%-A (Wsm)	9.27	242.69	386.79	548.39	0.790	391.915	0.582
SBC-01-15%-A (Wsm)	15.51	235.41	385.89	562.66	0.848	394.177	0.618

* A means average, Wsm means single mode in wet analysis, Wgp means general purpose mode.

Appendix B:
The raw data of pure excipients in gp mode from wet analysis with sonication

Sample	Obscuration (%)	D10 (μm)	D50 (μm)	D90 (μm)	Span	D [4,3] (μm)	Weighted residues
LH300-S4-5%	5.34	2.665	8.947	18.063	1.721	9.794	/
LH300-S4-5%	5.34	2.639	8.743	17.667	1.719	9.584	/
LH300-S4-5%	5.36	2.626	8.64	17.388	1.716	9.439	/
LH300-S4-5%-A	5.35	2.643	8.764	17.709	1.719	9.606	1.593
LH300-S4-10%	11.65	2.768	10.208	21.015	1.788	11.219	/
LH300-S4-10%	11.76	2.693	9.621	19.63	1.761	10.55	/
LH300-S4-10%	11.84	2.654	9.289	18.893	1.748	10.175	/
LH300-S4-10%-A	11.75	2.704	9.692	19.855	1.77	10.648	0.623
LH300-S4-15%	15.56	2.647	9.551	19.595	1.775	10.492	/
LH300-S4-15%	15.66	2.607	9.21	18.778	1.756	10.09	/
LH300-S4-15%	15.73	2.581	8.969	18.28	1.751	9.836	/
LH300-S4-15%-A	15.65	2.611	9.237	18.89	1.762	10.14	0.506
LH300-S7-5%	4.89	3.513	12.933	24.37	1.613	13.699	/
LH300-S7-5%	4.97	3.379	12.263	22.986	1.599	12.945	/
LH300-S7-5%	4.99	3.338	11.953	22.454	1.599	12.639	/
LH300-S7-5%-A	4.95	3.407	12.372	23.284	1.607	13.094	1.766
LH300-S7-10%	10.72	3.475	12.783	23.77	1.588	13.468	/
LH300-S7-10%	10.8	3.391	12.387	22.94	1.578	13.017	/
LH300-S7-10%	10.83	3.351	12.159	22.585	1.582	12.799	/
LH300-S7-10%-A	10.78	3.404	12.439	23.012	1.584	13.095	1.408
LH300-S7-15%	15.45	3.354	12.479	23.228	1.593	13.14	/
LH300-S7-15%	15.52	3.297	12.231	22.726	1.588	12.864	/
LH300-S7-15%	15.56	3.275	12.089	22.5	1.598	12.764	/
LH300-S7-15%-A	15.51	3.308	12.265	22.853	1.594	12.923	1.039
LH300-S2-5%	5.47	6.257	10.931	18.146	1.088	11.68	/
LH300-S2-5%	5.51	5.914	10.428	17.813	1.112	11.191	/
LH300-S2-5%	5.59	6.041	10.165	17.439	1.023	10.809	/
LH300-S2-5%-A	5.52	6.064	10.495	17.384	1.079	11.227	3.641
LH300-S2-10%	11.06	5.914	11.018	19.367	1.221	12.517	/
LH300-S2-10%	11.27	5.615	10.453	18.287	1.212	11.626	/
LH300-S2-10%	11.43	5.437	10.14	17.74	1.213	11.098	/
LH300-S2-10%-A	11.25	5.642	10.53	18.478	1.219	11.747	2.662
LH300-S2-15%	17.38	5.453	10.776	19.492	1.305	11.773	/
LH300-S2-15%	17.81	5.246	10.415	18.864	1.308	11.383	/
LH300-S2-15%	18.09	5.117	10.15	18.344	1.303	11.08	/
LH300-S2-15%-A	17.76	5.26	10.443	18.908	1.307	11.412	1.935
LH300-Span 20-S4-5%	5.23	2.121	4.923	10.619	1.726	5.838	/
LH300-Span 20-S4-5%	5.23	2.121	4.923	10.628	1.728	5.84	/
LH300-Span 20-S4-5%	5.23	2.131	4.951	10.676	1.726	5.879	/
LH300-Span 20-S4-5%-A	5.23	2.125	4.932	10.641	1.727	5.852	1.569
LH300-Span 20-S4-10%	10.42	2.024	5.184	12.242	1.971	6.593	/

LH300-Span 20-S4-10%	10.42	2.03	5.23	12.367	1.976	6.649	/
LH300-Span 20-S4-10%	10.4	2.033	5.271	12.424	1.971	6.653	/
LH300-Span 20-S4-10%-A	10.41	2.029	5.228	12.346	1.973	6.632	0.628
LH300-Span 20-S4-15%	15.28	2.036	5.48	13.224	2.042	7.11	/
LH300-Span 20-S4-15%	15.25	2.047	5.572	13.461	2.049	7.224	/
LH300-Span 20-S4-15%-A	15.28	2.033	5.458	13.164	2.039	7.068	0.37
LH300-dSpan 20-S4-5%	5.52	2.168	5.109	11.492	1.825	6.583	/
LH300-dSpan 20-S4-5%	5.50	2.164	5.118	11.481	1.821	6.5S4	/
LH300-dSpan 20-S4-5%	5.50	2.022	5.167	12.744	2.075	7.267	/
LH300-dSpan 20-S4-5%-A	5.51	2.117	5.130	11.879	1.903	6.783	0.983
LH300-dSpan 20-S4-10%	9.87	2.061	5.221	12.878	2.072	7.139	/
LH300-dSpan 20-S4-10%	9.82	2.074	5.250	12.914	2.065	7.158	/
LH300-dSpan 20-S4-10%	9.78	2.085	5.280	12.975	2.063	7.06	/
LH300-dSpan 20-S4-10%-A	9.82	2.073	5.250	12.923	2.067	7.119	0.724
LH300-dSpan 20-S4-15%	16.27	1.994	5.033	12.746	2.136	7.4	/
LH300-dSpan 20-S4-15%	16.01	2.006	5.056	12.793	2.133	7.389	/
LH300-dSpan 20-S4-15%	15.82	2.014	5.067	12.71	2.111	7.2	/
LH300-dSpan 20-S4-15%-A	16.03	2.005	5.052	12.75	2.127	7.33	0.391
LH300-Span 20-S7-5%	5.65	2.051	5.123	11.43	1.831	6.05	/
LH300-Span 20-S7-5%	5.65	2.049	5.142	11.494	1.837	6.079	/
LH300-Span 20-S7-5%	5.64	2.055	5.173	11.575	1.84	6.117	/
LH300-Span 20-S7-5%-A	5.65	2.052	5.146	11.5	1.836	6.082	1.208
LH300-Span 20-S7-10%	10.09	2.027	5.171	11.653	1.862	6.131	/
LH300-Span 20-S7-10%	10.09	2.034	5.21	11.77	1.869	6.182	/
LH300-Span 20-S7-10%	10.09	2.044	5.263	11.977	1.887	6.28	/
LH300-Span 20-S7-10%-A	10.09	2.035	5.214	11.8	1.873	6.198	0.987
LH300-Span 20-S7-15%	15.01	2.015	5.22	11.99	1.911	6.255	/
LH300-Span 20-S7-15%	15.02	2.024	5.254	12.089	1.916	6.299	/
LH300-Span 20-S7-15%	15.01	2.034	5.292	12.2	1.921	6.349	/
LH300-Span 20-S7-15%-A	15.01	2.024	5.255	12.094	1.916	6.301	0.882
LH300-dSpan 20-S7-5%	4.97	2.103	5.357	18.426	3.047	76.651	/
LH300-dSpan 20-S7-5%	4.97	2.068	5.172	13.344	2.180	28.893	/
LH300-dSpan 20-S7-5%	4.96	2.052	5.096	12.324	2.016	25.765	/
LH300-dSpan 20-S7-5%-A	4.96	2.072	5.196	13.693	2.236	41.947	0.697
LH300-dSpan 20-S7-10%	10.15	1.988	4.858	11.178	1.892	6.399	/
LH300-dSpan 20-S7-10%	10.16	1.983	4.831	10.88	1.842	5.773	/
LH300-dSpan 20-S7-10%	10.16	1.988	4.850	10.949	1.847	5.802	/
LH300-dSpan 20-S7-10%-A	10.16	1.986	4.846	10.998	1.86	5.991	0.373
LH300-dSpan 20-S7-15%	15.44	1.982	4.878	11.265	1.903	6.221	/
LH300-dSpan 20-S7-15%	15.34	1.992	4.886	11.152	1.875	5.871	/
LH300-dSpan 20-S7-15%	15.24	2.005	4.928	11.275	1.881	5.927	/
LH300-dSpan 20-S7-15%-A	15.34	1.993	4.897	11.231	1.886	6.007	0.292
Inhalac 500-S4-5%	4.8	3.65	10.697	19.627	1.494	11.314	/
Inhalac 500-S4-5%	4.85	4.479	10.25	19.016	1.516	10.898	/
Inhalac 500-S4-5%	4.88	3.357	9.923	18.447	1.521	10.562	/
Inhalac 500-S4-5%-A	4.84	3.485	10.286	19.044	1.513	10.924	1.653
Inhalac 500-S4-10%	9.91	3.103	10.12	19.332	1.604	10.827	/

Inhalac 500-S4-10%	9.99	3.023	9.71	18.627	1.607	10.425	/
Inhalac 500-S4-10%	10.06	2.972	9.422	18.08	1.603	10.127	/
Inhalac 500-S4-10%-A	9.99	3.03	9.745	18.691	1.607	10.46	0.739
Inhalac 500-S4-15%	15.37	2.897	9.835	19.218	1.66	10.607	/
Inhalac 500-S4-15%	15.49	2.844	9.448	18.452	1.652	10.203	/
Inhalac 500-S4-15%	15.57	2.972	9.179	17.914	1.647	9.917	/
Inhalac 500-S4-15%-A	15.48	2.843	9.481	18.539	1.655	10.243	0.522
Inhalac 500-S7-5%	5.54	2.807	9.799	19.139	1.667	10.534	/
Inhalac 500-S7-5%	5.63	2.692	8.986	17.626	1.662	9.714	/
Inhalac 500-S7-5%	5.68	2.633	8.579	16.822	1.654	9.277	/
Inhalac 500-S7-5%-A	5.62	2.706	9.1	17.89	1.669	9.842	1.44
Inhalac 500-S7-10%	10.16	2.633	8.769	17.482	1.693	9.551	/
Inhalac 500-S7-10%	10.22	2.588	8.437	16.756	1.679	9.179	/
Inhalac 500-S7-10%	10.25	2.557	8.213	16.278	1.671	8.929	/
Inhalac 500-S7-10%-A	10.21	2.592	8.467	16.843	1.683	9.22	1.156
Inhalac 500-S7-15%	14.89	2.55	8.542	17.289	1.725	9.367	/
Inhalac 500-S7-15%	14.96	2.515	8.264	16.609	1.705	9.037	/
Inhalac 500-S7-15%	15.01	2.489	8.071	16.17	1.695	8.813	/
Inhalac 500-S7-15%-A	14.95	2.518	8.288	16.692	1.71	9.072	0..885
Inhalac500-Span 20-S4-5%	6.01	1.978	4.049	7.584	1.385	4.463	/
Inhalac500-Span 20-S4-5%	6.02	1.84	4.002	7.841	1.499	4.47	/
Inhalac500-Span 20-S4-5%	6.02	1.843	4.007	7.844	1.498	4.474	/
Inhalac500-Span-S4-5%-A	6.01	1.886	4.02	7.755	1.46	4.469	1.962
Inhalac500-Span 20-S4-10%	10.46	1.953	4.045	7.697	1.42	4.487	/
Inhalac500-Span 20-S4-10%	10.46	1.956	4.052	7.708	1.419	4.494	/
Inhalac500-Span 20-S4-10%	10.47	1.957	4.055	7.711	1.419	4.496	/
Inhalac500-Span 20-S4-10%-A	10.46	1.955	4.051	7.705	1.419	4.493	1.349
Inhalac500-Span 20-S4-15%	15.08	1.922	4.007	7.662	1.432	4.452	/
Inhalac500-Span 20-S4-15%	15.08	1.927	4.016	7.681	1.433	4.463	/
Inhalac500-Span 20-S4-15%	15.08	1.926	4.015	7.682	1.434	4.462	/
Inhalac500-Span 20-S4-15%-A	15.08	1.925	4.013	7.675	1.433	4.459	0.971
Inhalac500-dSpan 20-S4-5%	4.89	1.962	4.280	9.14	1.677	5.778	/
Inhalac500-dSpan 20-S4-5%	4.88	1.949	4.218	8.611	1.579	4.856	/
Inhalac500-dSpan 20-S4-5%	4.87	1.945	4.211	8.601	1.581	4.851	/
Inhalac500-dSpan-S4-5%-A	4.88	1.952	4.236	8.77	1.61	5.162	0.88
Inhalac500-dSpan 20-S4-10%	10.12	1.899	4.148	8.437	1.576	4.751	/
Inhalac500-dSpan 20-S4-10%	10.14	1.898	4.145	8.426	1.575	4.746	/
Inhalac500-dSpan 20-S4-10%	10.12	1.895	4.141	8.419	1.576	4.742	/
Inhalac500-dSpan 20-S4-10%-A	10.13	1.897	4.145	8.427	1.576	4.746	0.571
Inhalac500-dSpan 20-S4-15%	14.86	1.867	4.107	8.413	1.594	4.717	/
Inhalac500-dSpan 20-S4-15%	14.84	1.865	4.103	8.403	1.593	4.712	/
Inhalac500-dSpan 20-S4-15%	14.83	1.866	4.105	8.398	1.591	4.711	/
Inhalac500-dSpan 20-S4-15%-A	14.84	1.866	4.105	8.404	1.593	4.713	0.466
Inhalac500-Span 20-S7-5%	4.85	1.8	4.014	8.138	1.579	4.55	/
Inhalac500-Span 20-S7-5%	4.87	1.796	4.007	8.141	1.584	4.546	/
Inhalac500-Span 20-S7-5%	4.88	1.799	4.011	8.132	1.579	4.547	/
Inhalac500-Span 20-S7-5%-A	4.87	1.799	4.011	8.137	1.58	4.548	0..945

Inhalac500-Span 20-S7-10%	11.07	1.752	3.947	8.052	1.596	4.484	/
Inhalac500-Span 20-S7-10%	11.07	1.752	3.949	8.06	1.597	4.487	/
Inhalac500-Span 20-S7-10%	11.05	1.75	3.943	8.05	1.598	4.481	/
Inhalac500-Span 20-S7-10%-A	11.06	1.751	3.946	8.054	1.597	4.484	0.78
Inhalac500-Span 20-S7-15%	16.99	1.719	3.902	8.011	1.612	4.444	/
Inhalac500-Span 20-S7-15%	16.97	1.718	3.877	8.002	1.612	4.44	/
Inhalac500-Span 20-S7-15%	16.99	1.727	3.918	8.039	1.611	4.46	/
Inhalac500-Span 20-S7-15%-A	16.98	1.721	3.906	8.018	1.612	4.448	0.745
Inhalac500-dSpan 20-S7-5%	4.98	1.801	3.943	7.919	1.552	4.461	/
Inhalac500-dSpan 20-S7-5%	5.05	1.803	3.971	7.989	1.558	4.493	/
Inhalac500-dSpan 20-S7-5%	5.06	1.808	3.998	8.061	1.564	4.525	/
Inhalac500-dSpan 20-S7-5%-A	5.03	1.804	3.971	7.99	1.558	4.493	0..956
Inhalac500-dSpan 20-S7-10%	10.52	1.778	3.896	7.843	1.557	4.413	/
Inhalac500-dSpan 20-S7-10%	10.38	1.79	3.901	7.89	1.564	4.439	/
Inhalac500-dSpan 20-S7-10%	10.23	1.792	3.894	7.873	1.562	4.432	/
Inhalac500-dSpan 20-S7-10%-A	10.38	1.786	3.897	7.868	1.561	4.28	0.739
Inhalac500-dSpan 20-S7-15%	15.04	1.742	3.855	7.798	1.571	4.373	/
Inhalac500-dSpan 20-S7-15%	14.86	1.746	3.858	7.801	1.57	4.376	/
Inhalac500-dSpan 20-S7-15%	14.78	1.748	3.86	7.805	1.569	4.379	/
Inhalac500-dSpan 20-S7-15%-A	14.9	1.745	3.857	7.802	1.57	4.376	0.497
SV003-dSpan20-S7-5%	4.90	13.664	72.327	180.764	2.310	89.057	/
SV003-dSpan20-S7-5%	4.90	12.469	67.729	142.865	1.925	75.750	/
SV003-dSpan20-S7-5%	4.85	12.222	66.306	136.426	1.873	73.380	/
SV003-dSpan20-S7-5%-A	4.88	12.740	68.581	151.548	2.024	79.395	0.227
SV003-dSpan20-S7-10%	9.71	10.315	73.890	179.287	2.287	87.904	/
SV003-dSpan20-S7-10%	9.58	10.369	72.356	167.265	2.168	83.672	/
SV003-dSpan20-S7-10%	9.45	10.325	71.077	161.235	2.123	81.316	/
SV003-dSpan20-S7-10%-A	9.58	10.336	72.404	169.036	2.192	84.297	0.138
SV003-dSpan20-S7-15%	14.84	30.678	129.288	280.056	1.929	144.158	/
SV003-dSpan20-S7-15%	14.80	30.204	124.288	265.231	1.894	137.834	/
SV003-dSpan20-S7-15%	14.77	30.334	118.759	249.040	1.853	130.618	/
SV003-dSpan20-S7-15%-A	14.80	30.071	123.755	264.852	1.897	137.537	0.260

* “A” means average, “dSpan” stands for double span 20, “S2” stands for speed 2, “S4” stands for speed 4 and “S7” stands for speed 7.

Appendix C:
The raw data of pure excipients from dry analysis

Sample	Obscuration (%)	D10 (μm)	D50 (μm)	D90 (μm)	Span	D [4,3] (μm)	Weighted residues	Feed rate	Jet pressure	RSD of D50
LH100-01	3.1	66.90	133.44	211.75	1.0880	136.18	0.462	3	2	/
LH100-02	3.3	61.65	132.48	210.98	1.1270	134.15	0.436	3	2	/
LH100-03	3.1	65.79	131.91	209.31	1.0880	134.56	0.484	3	2	/
LH100-A	/	64.78	132.61	210.68	1.1010	134.96	0.461	/	/	0.583
SV001-01	2.7	156.54	231.79	320.37	0.7068	233.28	0.818	3	2	/
SV001-02	2	156.09	232.08	321.00	0.7106	233.29	0.841	3	2	/
SV001-03	1.7	153.83	230.97	317.28	0.7007	232.00	0.830	3	2	/
SV001-A	/	155.49	231.61	319.55	0.7060	232.86	0.830	/	/	0.249
SV003-P2-01	2.3	35.84	65.15	99.45	0.9764	65.90	0.445	4	2	/
SV003-P2-02	4.9	36.28	65.43	99.43	0.9653	66.17	0.438	4	2	/
SV003-P2-03	3	36.06	65.22	99.45	0.9718	66.01	0.426	4	2	/
SV003-P2-A	/	36.06	65.27	99.44	0.9712	66.03	0.436	/	/	0.223
SV003-P4-01	5.1	31.43	62.86	97.31	1.048	63.23	0.411	4	4	/
SV003-P4-02	3.4	32.02	63.16	99.14	1.063	64.11	0.391	4	4	/
SV003-P4-03	4.0	31.36	62.92	98.63	1.069	63.72	0.351	4	4	/
SV003-P4-A	/	31.60	62.98	98.36	1.060	63.69	0.384	/	/	0.252
SV003-P7-01	5.8	24.77	59.64	98.44	1.235	64.91	0.387	5	7	/
SV003-P7-02	5.6	24.96	59.68	98.60	1.234	65.93	0.385	5	7	/
SV003-P7-03	5.3	24.65	59.68	99.42	1.253	67.04	0.435	5	7	/
SV003-P7-A	/	24.79	59.67	98.82	1.2407	65.96	0.402	/	/	0.039
SV003-P10-01	6.7	14.28	57.75	107.41	1.613	82.35	0.450	5	10	/
SV003-P10-02	4.2	19.39	58.24	108.67	1.533	87.01	0.452	5	10	/
SV003-P10-03	4.2	19.62	58.27	108.36	1.523	85.43	0.426	5	10	/
SV003-P10-A	/	17.764	58.09	108.15	1.556	84.93	0.443	/	/	0.503
CM-01	1.8	21.64	67.72	141.03	1.7630	75.32	0.564	4	2	/
CM-02	2.3	20.44	64.97	138.89	1.8230	73.19	0.533	4	2	/
CM-03	2	19.88	64.49	137.21	1.8190	72.37	0.415	4	2	/
CM-A	/	20.65	65.73	139.04	1.8017	73.63	0.504	/	/	2.652
C100-01	1.1	121.32	150.09	193.69	0.4796	154.04	0.875	3	2	/
C100-02	1.6	122.27	152.39	196.21	0.4852	155.60	0.897	3	2	/
C100-03	1.3	122.70	153.75	199.49	0.4994	157.23	0.897	3	2	/
C100-A	/	122.10	152.08	196.46	0.4881	155.62	0.890	/	/	1.216
C200-01	1.5	231.47	265.80	308.03	0.2880	268.17	1.497	3	2	/
C200-02	1	233.02	267.46	310.52	0.2898	269.81	1.472	3	2	/
C200-03	1.9	230.98	264.88	305.45	0.2811	267.17	1.486	3	2	
C200-A	/	231.82	266.05	308.00	0.2863	268.38	1.485	/	/	0.491
C350-01	1.5	363.77	401.00	450.35	0.2159	404.75	2.849	4	2	/
C350-02	1.8	363.82	399.92	448.54	0.2119	403.72	2.738	4	2	/
C350-03	2.1	363.82	400.37	449.52	0.2140	404.26	2.742	4	2	/

C350-A	/	363.80	400.43	449.47	0.2139	404.24	2.776	/	/	0.135
SBS-01	2.9	34.67	77.66	140.23	1.359	82.95	0.385	3	3	/
SBS-02	2.7	34.82	77.98	140.67	1.358	83.19	0.410	3	3	/
SBS-03	2.4	34.58	77.79	139.42	1.348	82.66	0.366	3	3	/
SBS-A	/	34.69	77.81	140.11	1.355	82.93	0.387	/	/	0.207
SBF-01	3.6	85.67	129.55	182.49	0.7474	131.32	0.545	4	2	/
SBF-02	1.8	83.12	127.32	179.52	0.7571	128.97	0.515	4	2	/
SBF-03	2	82.32	126.84	180.30	0.7724	128.47	0.552	4	2	/
SBF-A	/	83.70	127.90	180.77	0.7590	129.59	0.537	/	/	1.131
SBC-01	1.3	215.00	376.83	589.32	0.9934	389.92	1.000	3	2	/
SBC-02	1.7	215.22	376.24	588.43	0.9887	388.91	1.045	3	2	/
SBC-03	1.5	211.63	371.12	578.85	0.9890	383.24	1.036	3	2	/
SBC-A	/	213.95	374.73	585.53	0.9904	387.36	1.027	/	/	0.838
LH300-P3-01	12.1	2.42	7.93	31.93	3.7210	31.93	0.199	4	3	/
LH300-P3-02	9.9	2.09	7.45	19.91	2.3920	35.94	0.248	4	3	/
LH300-P3-03	10.6	2.15	7.50	20.71	2.4780	39.76	0.296	4	3	/
LH300-P3-A	/	2.22	7.63	24.18	2.8637	35.88	0.248	/	/	3.460
LH300-P8-01	10.1	1.86	6.99	545.50	77.78	116.64	0.556	4	8	/
LH300-P8-02	9.9	1.86	6.77	519.80	76.47	110.51	0.630	4	8	/
LH300-P8-02	7.8	1.81	7.01	653.59	92.99	138.79	0.493	4	8	/
LH300-P8-A	/	1.84	6.92	572.96	82.4133	121.98	0.560	/	/	1.923
LH300-P10-01	10	1.88	7.11	683.27	95.80	169.17	0.651	4	10	/
LH300-P10-02	7.1	1.94	7.42	681.98	91.61	184.61	0.867	4	10	/
LH300-P10-02	8.3	1.80	7.46	694.05	92.78	182.34	0.653	4	10	/
LH300-P10-A	/	1.87	7.33	686.43	93.40	178.71	0.724	/	/	2.614
Inhalac 500-P3-01	5.2	1.69	7.21	21.21	2.7080	22.55	0.320	4	3	/
Inhalac 500-P3-02	3.4	1.22	6.41	18.49	2.6960	17.58	0.323	4	3	/
Inhalac 500-P3-03	3.8	1.24	6.32	16.22	2.3720	14.88	0.354	4	3	/
Inhalac 500-P3-A	/	1.38	6.65	18.64	2.5920	18.34	0.332	/	/	7.371
Inhalac 500-P8-01	6.1	2.06	7.50	476.65	63.28	99.56	0.321	4	8	/
Inhalac 500-P8-02	8.3	2.01	7.48	406.90	54.10	89.14	0.328	4	8	/
Inhalac 500-P8-03	10.4	2.03	7.31	416.89	56.78	85.07	0.292	4	8	/
Inhalac 500-P8-A	/	2.03	7.43	433.48	58.0533	91.26	0.314	/	/	1.405
Inhalac 500-P10-01	9.8	1.83	7.18	690.20	95.82	168.80	0.656	4	10	/
Inhalac 500-P10-02	9.2	1.61	6.54	628.07	95.67	146.14	0.875	4	10	/
Inhalac 500-P10-03	6.8	1.82	7.76	710.10	91.29	203.42	0.813	4	10	/
Inhalac 500-P10-A	/	1.75	7.16	676.12	94.26	172.79	0.781	/	/	8.523

* D means wet analysis and P2, P3,P4, P7, P8, P10 in dry analysis represent jet pressure 2,3,4,7,8 and 10.

Appendix D:
The raw data of blender powders from wet analysis and dry analysis

Sample	Obscuration (%)	D10 (μm)	D50 (μm)	D90 (μm)	Span	D [4,3] (μm)	Weighted residues	Feed rate	Jet pressure	Percent <10 um
LI-P3-1 (D)	7.30	48.02	127.16	198.80	1.19	125.55	0.683	4	3	4.69
LI-P6-1(D)	5.30	17.15	112.72	183.01	1.47	110.32	0.653	4	6	6.89
LI-P9-1 (D)	2.60	13.64	103.44	202.97	1.83	118.04	0.763	4	9	8.35
LI-P6-02 (D)	5.70	18.34	108.81	183.43	1.52	107.89	0.553	4	6	6.89
LI-P6-03 (D)	2.20	18.83	112.64	204.83	1.65	122.91	0.651	4	6	6.91
LI-P6-A (D)	4.40	18.11	111.39	190.42	1.55	113.71	0.619	4	6	6.90
LI-01-5% (W)	4.64	60.67	143.10	253.77	1.35	149.69	/	/	/	/
LI-01-5% (W)	4.75	57.99	142.50	252.80	1.37	148.75	/	/	/	/
LI-01-5% (W)	4.80	56.15	142.49	253.98	1.39	148.77	/	/	/	/
LI-01-5%-A(W)	4.73	58.27	142.69	253.52	1.37	149.07	0.558	/	/	4.83
LI-01-10% (W)	9.73	56.64	139.95	246.93	1.36	145.70	/	/	/	/
LI-01-10% (W)	9.92	55.60	140.42	247.84	1.37	146.03	/	/	/	/
LI-01-10% (W)	10.06	53.86	140.50	249.00	1.39	146.19	/	/	/	/
LI-01-10%-A(W)	9.90	55.37	140.29	247.92	1.37	145.97	0.551	/	/	5.30
LI-01-15% (W)	14.97	51.50	139.10	246.25	1.40	144.52	/	/	/	/
LI-01-15% (W)	15.17	49.82	139.90	247.42	1.41	145.14	/	/	/	/
LI-01-15% (W)	15.38	50.22	139.58	247.20	1.41	144.91	/	/	/	/
LI-01-15%-A(W)	15.17	50.51	139.53	246.96	1.41	144.85	0.567	/	/	5.80
LI-dspan20-S4-5%	5.13	2.71	42.40	109.17	2.51	47.73	/	/	/	/
LI-dspan20-S4-5%	5.13	2.69	41.31	106.21	2.51	46.52	/	/	/	/
LI-dspan20-S4-5%	5.07	2.65	37.00	100.90	2.66	43.94	/	/	/	/
LI-dspan20-S4-5%-A	5.11	2.68	40.25	105.44	2.55	46.06	6.704	/	/	35.59
LI-dspan20-S4-10%	10.50	2.90	61.06	144.08	2.31	64.16	/	/	/	/
LI-dspan20-S4-10%	10.34	2.89	58.10	141.42	2.38	62.40	/	/	/	/
LI-dspan20-S4-10%	10.20	2.88	55.76	138.73	2.44	60.88	/	/	/	/
LI-dspan20-S4-10%-A	10.34	2.89	58.31	141.43	2.38	62.48	3.565	/	/	30.80
LI-dspan20-S4-15%	15.37	3.64	80.75	163.03	1.97	79.39	/	/	/	/
LI-dspan20-S4-15%	15.17	3.63	78.99	160.83	1.99	77.95	/	/	/	/
LI-dspan20-S4-15%	14.99	3.61	77.10	158.88	2.01	76.56	/	/	/	/
LI-dspan20-S4-15%-A	15.18	3.62	78.95	160.93	1.99	77.97	1.930	/	/	23.04
LI-dspan20-S7-5%	6.08	4.481	97.399	196.884	1.98	99.50	/	/	/	/
LI-dspan20-S7-5%	5.94	4.444	93.14	189.034	1.98	95.22	/	/	/	/
LI-dspan20-S7-5%	5.87	4.519	93.157	187.381	1.96	94.97	/	/	/	/
LI-dspan20-S7-5%-A	5.96	4.481	94.532	191.117	1.97	96.57	1.13	/	/	17.57

LI-dspan20-S7-10%	10.21	4.329	91.092	188.414	2.02	93.12	/	/	/	/
LI-dspan20-S7-10%	9.95	4.374	89.437	184.673	2.02	91.37	/	/	/	/
LI-dspan20-S7-10%	9.84	4.488	89.499	181.924	1.98	90.95	/	/	/	/
LI-dspan20-S7-10%-A	10	4.396	90	184.999	2.01	91.81	0.796	/	/	18.41
LI-dspan20-S7-15%	15.46	4.549	95.178	193.854	1.99	97.02	/	/	/	/
LI-dspan20-S7-15%	15.24	4.607	93.914	190.918	1.98	95.72	/	/	/	/
LI-dspan20-S7-15%	15.09	4.634	93.343	188.155	1.97	94.70	/	/	/	/
LI-dspan20-S7-15%-A	15.27	4.596	94.137	190.953	1.98	95.81	0.673	/	/	17.45
SI-P3-01(D)	3.80	18.97	63.65	100.37	1.28	61.13	0.619	5	3	7.43
SI-P6-01 (D)	3.60	10.18	58.55	99.32	1.52	58.76	0.682	5	6	10.18
SI-P9-01(D)	3.60	10.04	57.29	123.71	1.98	106.44	0.505	5	9	10.29
SI-P6-02 (D)	6.70	12.66	59.55	101.57	1.49	66.35	0.418	5	6	8.85
SI-P6-03 (D)	7.50	11.94	58.20	96.71	1.46	58.00	0.447	5	6	9.19
SI-P6-A (D)	5.93	11.59	58.77	99.20	1.49	61.04	0.516	5	6	9.41
SI-01-5% (W)	4.83	31.36	76.25	296.95	3.48	123.25	/	/	/	/
SI-01-5% (W)	4.95	29.61	75.82	292.38	3.47	123.05	/	/	/	/
SI-01-5% (W)	5.04	29.32	76.17	292.70	3.46	122.71	/	/	/	/
SI-01-5%-A(W)	4.94	30.10	76.08	294.01	3.47	123.00	0.618	/	/	6.36
SI-01-10% (W)	10.05	22.40	68.78	163.85	2.06	96.99	/	/	/	/
SI-01-10% (W)	10.24	14.63	68.27	160.25	2.13	96.07	/	/	/	/
SI-01-10% (W)	10.30	13.57	68.00	160.09	2.16	96.09	/	/	/	/
SI-01-10%-A(W)	10.20	16.87	68.35	161.40	2.12	96.38	0.534	/	/	7.96
SI-01-15% (W)	16.25	11.75	65.56	129.83	1.80	85.33	/	/	/	/
SI-01-15% (W)	16.37	11.21	65.10	126.74	1.78	82.48	/	/	/	/
SI-01-15% (W)	16.42	10.78	64.69	126.29	1.79	82.68	/	/	/	/
SI-01-15%-A(W)	16.35	11.25	65.12	127.62	1.79	83.50	0.515	/	/	9.20
SI-dspan20-S4-5%	5.05	3.97	62.77	128.26	1.98	65.31	/	/	/	/
SI-dspan20-S4-5%	5.04	4.06	63.23	126.17	1.93	65.02	/	/	/	/
SI-dspan20-S4-5%	5.02	4.13	62.63	122.76	1.89	63.96	/	/	/	/
SI-dspan20-S4-5%-A	5.03	4.05	62.88	125.71	1.94	64.77	5.137	/	/	18.00
SI-dspan20-S4-10%	10.18	4.28	64.54	142.63	2.14	69.95	/	/	/	/
SI-dspan20-S4-10%	9.92	4.41	64.23	137.07	2.07	68.33	/	/	/	/
SI-dspan20-S4-10%	9.80	4.59	65.10	136.04	2.02	68.69	/	/	/	/
SI-dspan20-S4-10%-A	9.96	4.42	64.63	138.49	2.07	68.99	1.825	/	/	17.33
SI-dspan20-S4-15%	15.17	5.08	84.18	203.99	2.36	96.67	/	/	/	/
SI-dspan20-S4-15%	15.01	5.12	83.01	194.36	2.28	93.38	/	/	/	/
SI-dspan20-S4-15%	14.92	5.16	81.70	184.33	2.19	90.11	/	/	/	/
SI-dspan20-S4-15%-A	15.03	5.12	82.93	193.98	2.28	93.39	0.422	/	/	14.94
SI-dspan20-S7-5%	5	5.98	65.51	106.94	1.54	65.29	/	/	/	/
SI-dspan20-S7-5%	4.96	6.16	65.08	104.98	1.51	64.62	/	/	/	/
SI-dspan20-S7-5%	4.95	6.31	64.87	101.11	1.46	63.72	/	/	/	/
SI-dspan20-S7-5%-A	4.97	6.15	65.14	104.22	1.5	64.54	1.104	/	/	11.66

SI-dspan20-S7-10%	10.11	7.7	79.76	175.57	2.1	90.64	/	/	/	/
SI-dspan20-S7-10%	10.1	7.56	75.65	152.76	1.91	82.58	/	/	/	/
SI-dspan20-S7-10%	10.06	7.39	72.95	140.07	1.81	77.62	/	/	/	/
SI-dspan20-S7-10%-A	10.09	7.54	75.9	155.47	1.94	83.62	0.549	/	/	11.11
SI-dspan20-S7-15%	15.21	10.14	89.59	197.17	2.08	101.58	/	/	/	/
SI-dspan20-S7-15%	15.18	9.59	85.96	181.65	2	95.67	/	/	/	/
SI-dspan20-S7-15%	15.19	9.41	84.05	171.03	1.92	91.57	/	/	/	/
SI-dspan20-S7-15%-A	15.19	9.69	86.41	183.04	2	96.27	0.443	/	/	10.09
CSCB-01 (D)	/	/	/	/	/	/	/	3	2	/
CSCB-02 (D)	/	/	/	/	/	/	/	3	2	/
CSCB-03 (D)	/	/	/	/	/	/	/	3	2	/
CSCB-A (D)	/	/	/	/	/	/	/	/	/	/
CSCB-01-5% (W)	4.38	113.77	211.65	479.34	1.73	258.57	/	/	/	/
CSCB-01-5% (W)	4.41	110.92	203.94	465.44	1.74	250.32	/	/	/	/
CSCB-01-5% (W)	4.25	110.98	206.23	474.75	1.76	253.96	/	/	/	/
CSCB-01-5%-A(W)	4.35	111.89	207.27	473.18	1.74	254.28	1.296	/	/	/
CSCB-01-10% (W)	9.12	107.17	199.47	472.21	1.83	248.85	/	/	/	/
CSCB-01-10% (W)	8.97	112.87	206.96	469.07	1.72	253.04	/	/	/	/
CSCB-01-10% (W)	8.92	112.93	205.80	471.70	1.74	254.31	/	/	/	/
CSCB-01-10%-A(W)	9.00	110.99	204.07	470.99	1.77	252.07	1.336	/	/	/
CSCB-01-15% (W)	14.59	112.96	205.32	463.35	1.71	250.71	/	/	/	/
CSCB-01-15% (W)	14.44	112.90	205.19	461.56	1.70	250.23	/	/	/	/
CSCB-01-15% (W)	14.59	113.07	206.52	469.26	1.73	252.96	/	/	/	/
CSCB-01-15%-A(W)	14.54	112.98	205.68	464.72	1.71	251.30	1.314	/	/	/
CMMCC-01 (D)	3.60	27.79	135.80	333.02	2.25	160.55	1.014	4	2	/
CMMCC-02 (D)	3.40	29.78	149.36	340.78	2.08	168.86	1.083	4	2	/
CMMCC-03 (D)	3.70	26.79	126.90	326.70	2.36	154.95	0.932	4	2	/
CMMCC-01-A (D)	/	28.12	137.35	333.50	2.23	161.45	1.010	/	/	/
CMMCC-01-5% (W)	5.33	23.52	104.64	316.60	3.23	158.23	/	/	/	/
CMMCC-01-5% (W)	5.33	23.25	102.00	352.17	3.23	152.97	/	/	/	/
CMMCC-01-5% (W)	5.33	23.16	101.28	350.28	3.22	151.91	/	/	/	/
CMMCC-01-5%-A(W)	5.33	23.31	102.64	339.68	3.23	154.37	0.500	/	/	/
CMMCC-01-10% (W)	9.96	20.98	85.16	304.11	3.33	128.70	/	/	/	/
CMMCC-01-10% (W)	10.02	21.19	86.27	304.73	3.29	128.54	/	/	/	/
CMMCC-01-10% (W)	10.07	21.24	86.79	307.97	3.30	129.58	/	/	/	/
CMMCC-01-10%-A(W)	10.02	21.13	86.07	305.60	3.31	128.94	0.404	/	/	/
CMMCC-01-15% (W)	16.26	20.81	85.38	297.49	3.24	125.92	/	/	/	/
CMMCC-01-15% (W)	16.32	21.00	87.05	301.29	3.22	127.92	/	/	/	/
CMMCC-01-15% (W)	16.33	21.20	88.57	309.00	3.25	131.01	/	/	/	/
CMMCC-01-15%-A(W)	16.30	21.00	87.00	302.60	3.24	128.28	0.442	/	/	/

*A means average, D means dry analysis, P3, P6 and P9 mean the jet pressure 3, 6 and 9 in dry analysis;
W means dry analysis, S4 and S7 mean the speed of 4 and 7 in the sonication.

Appendix E:
The raw data of blender powders in gp mode and mn mode from wet analysis

Sample	Obscuration (%)	D10 (μm)	D50 (μm)	D90 (μm)	Span	D [4,3] (μm)	Weighted residues	Percentage less than 10 um (%)
LI-01-5%-A(Wgp)	4.73	58.27	142.69	253.52	1.368	149.07	0.558	4.83
LI-01-10%-A(Wgp)	9.90	55.37	140.29	247.92	1.373	145.97	0.551	5.3
LI-01-15%-A(Wgp)	15.17	50.51	139.53	246.96	1.408	144.85	0.567	5.8
LI-01-5%-A(Wmn)	4.73	49.44	144.77	232.59	1.265	144.76	0.181	5.03
LI-01-10%-A(Wmn)	9.90	45.71	142.59	227.74	1.277	142.03	0.157	5.48
LI-01-15%-A(Wmn)	15.17	41.61	141.85	226.45	1.303	140.52	0.187	6
LI-dspan20-S4-5% (Wgp)	5.11	2.68	40.25	105.44	2.553	46.06	6.704	35.59
LI-dspan20-S4-10% (Wgp)	10.34	2.89	58.31	141.43	2.376	62.48	3.565	30.8
LI-dspan20-S4-15% (Wgp)	15.18	3.62	78.95	160.93	1.993	77.97	1.93	23.04
LI-dspan20-S4-5% (Wmn)	5.11	2.53	41.61	130.38	3.073	56.50	8.222	35.92
LI-dspan20-S4-10% (Wmn)	10.34	2.96	61.61	151.41	2.411	67.30	3.77	29.75
LI-dspan20-S4-15% (Wmn)	15.18	3.73	83.64	161.58	1.887	79.75	1.932	22.65
SI-01-5%-A(Wgp)	4.94	30.10	76.08	294.01	3.469	123.00	0.618	6.36
SI-01-10%-A(Wgp)	10.20	16.87	68.35	161.40	2.115	96.38	0.534	7.96
SI-01-15%-A(Wgp)	16.35	11.25	65.12	127.62	1.787	83.50	0.515	9.2
SI-01-5%-A(Wmn)	4.94	24.98	75.16	283.76	3.443	131.41	0.42	5.96
SI-01-10%-A(Wmn)	10.20	16.42	68.98	211.49	2.828	101.30	0.248	7.54
SI-01-15%-A(Wmn)	16.35	12.31	66.33	120.92	1.637	86.99	0.165	8.84
SI-dspan20-S4-5% (Wgp)	5.03	4.05	62.88	125.71	1.935	64.77	5.137	18
SI-dspan20-S4-10% (Wgp)	9.96	4.42	64.63	138.49	2.074	68.99	1.825	17.33
SI-dspan20-S4-15% (Wgp)	15.03	5.12	82.93	193.98	2.277	93.39	0.422	14.94
SI-dspan20-S4-5% (Wmn)	5.03	4.30	65.00	146.45	2.187	70.65	5.817	16.95
SI-dspan20-S4-10% (Wmn)	9.96	4.05	63.13	148.89	2.295	69.54	2.034	18.88
SI-dspan20-S4-15% (Wmn)	15.03	5.15	83.42	192.17	2.242	96.65	0.2	14.73
CSCB-01-5%-A(Wgp)	4.35	111.89	207.27	473.18	1.743	254.28	1.296	/
CSCB-01-10%-A(Wgp)	9.00	110.99	204.07	470.99	1.765	252.07	1.336	/
CSCB-01-15%-A(Wgp)	14.54	112.98	205.68	464.72	1.71	251.30	1.314	/
CSCB-01-5%-A(Wmn)	4.35	124.42	184.37	460.19	1.821	255.59	0.484	/
CSCB-01-10%-A(Wmn)	9.00	124.46	178.43	454.55	1.85	248.51	0.508	/
CSCB-01-15%-A(Wmn)	14.54	125.51	175.73	448.43	1.838	244.82	0.544	/
CMMCC-01-5%-A(Wgp)	5.33	23.31	102.64	339.68	3.226	154.37	0.5	/
CMMCC-01-10%-A(Wgp)	10.02	21.13	86.07	305.60	3.305	128.94	0.404	/
CMMCC-01-10%-A(Wgp)	10.02	21.13	86.07	305.60	3.305	128.94	0.404	/
CMMCC-01-5%-A(Wmn)	5.33	23.70	100.99	324.64	2.98	160.91	0.302	/

CMMCC-01-10%-A(Wmn)	10.02	21.59	88.82	298.56	3.118	137.08	0.221	/
CMMCC-01-10%-A(Wmn)	10.02	21.11	87.85	286.58	3.022	122.49	0.202	/

*A means average, gp means general purpose mode, mn means multiple narrow modes and S4 means the speed of 4 in the sonication of wet analysis

Appendix F:
The raw data of lactose fines, LI and SI in Fraunhofer and Mie theory from wet analysis

Sample	Obscuration (%)	D10 (μm)	D50 (μm)	D90 (μm)	Span	D [4,3] (μm)	Percent <10 μm (%)	Weighted residues
DFE LH300	/	/	＜5	≦10	/	/	/	/
LH300-dSpan 20-S7-5%-A (F)	4.96	2.07	5.20	13.69	2.236	41.95	81.64	0.697
LH300-dSpan 20-S7-10%-A (F)	10.16	1.99	4.85	11.00	1.86	5.99	86.88	0.373
LH300-dSpan 20-S7-15%-A (F)	15.34	1.99	4.90	11.23	1.886	6.01	86.13	0.292
LH300-dSpan 20-S7-5%-A (M)	4.96	1.67	4.56	10.05	2.037	24.03	87.44	1.953
LH300-dSpan 20-S7-10%-A (M)	10.16	1.60	4.32	9.83	1.905	5.13	90.52	1.94
LH300-dSpan 20-S7-15%-A (M)	15.34	1.76	4.40	8.57	1.777	5.14	91.35	2.007
Meggle InhaLac 500	/	/	≦5	≦10	/	/	/	/
Inhalac500-dSpan 20-S7-5%-A (F)	5.03	1.80	3.97	7.99	1.558	4.49	96.44	0.956
Inhalac500-dSpan 20-S7-10%-A (F)	10.38	1.79	3.90	7.87	1.561	4.28	96.60	0.739
Inhalac500-dSpan 20-S7-15%-A (F)	14.90	1.75	3.86	7.80	1.57	4.38	96.86	0.497
Inhalac500-dSpan 20-S7-5%-A (M)	5.03	1.46	3.50	6.88	1.549	3.89	98.34	2.282
Inhalac500-dSpan 20-S7-10%-A (M)	10.38	1.50	3.50	6.83	1.526	3.88	98.49	2.292
Inhalac500-dSpan 20-S7-15%-A (M)	14.90	1.33	3.41	6.77	1.596	3.78	98.53	2.486
LI-dSpan 20-S7-5%-A (F)	5.11	2.68	40.25	105.44	2.553	46.06	6.70	35.59
LI-dSpan 20-S7-10%-A (F)	10.34	2.89	58.31	141.43	2.376	62.48	3.57	30.8
LI-dSpan 20-S7-15%-A (F)	15.18	3.62	78.95	160.93	1.993	77.97	1.93	23.04
LI-dSpan 20-S7-5%-A (M)	5.11	1.67	19.41	102.87	5.215	41.37	6.18	42.48
LI-dSpan 20-S7-10%-A (M)	10.34	1.71	46.20	139.09	2.974	57.65	3.33	36.75
LI-dSpan 20-S7-15%-A (M)	15.18	2.56	72.94	158.81	2.146	73.18	1.82	28.07
SI-dSpan 20-S7-5%-A (F)	5.03	4.05	62.88	125.71	1.935	64.77	5.14	18
SI-dSpan 20-S7-10%-A (F)	9.96	4.42	64.63	138.49	2.074	68.99	1.83	17.33
SI-dSpan 20-S7-15%-A (F)	15.03	5.12	82.93	193.98	2.277	93.39	0.42	14.94
SI-dSpan 20-S7-5%-A (M)	5.03	2.77	61.32	125.52	2.002	62.92	4.98	21.07
SI-dSpan 20-S7-10%-A (M)	9.96	2.95	61.60	137.19	2.179	66.01	1.76	21.13
SI-dSpan 20-S7-15%-A (M)	15.03	3.53	80.18	192.91	2.362	90.72	0.41	17.7

*A means average, F means “Fraunhofer theory”, M means “Mie theory” and S7 means “speed 7 in sonication”